Alternative routes to methyl mercaptan from C$_1$-compounds

Christoph Rudolf Erwin Kaufmann

Vollständiger Abdruck der von der Fakultät für Chemie der Technischen Universität München zur Erlangung des akademisches Grades eines

Doktors der Naturwissenschaften (Dr. rer. nat.)

genehmigten Dissertation.

Vorsitzender: Univ.-Prof. Dr. K.-O. Hinrichsen

Prüfer der Dissertation:

1. Univ.-Prof. Dr. J. A. Lercher
2. Univ.-Prof. Dr. K. Köhler

Die Dissertation wurde am 18.09.2015 bei der Technischen Universität München eingereicht und durch die Fakultät für Chemie am 12.11.2015 angenommen.

Fortunato l'uom che prende

Ogni cosa pel buon verso

E tra i casi e le vicende

Da ragion guidar si fà.

Quel che suole altrui far piangere

Fia per lui cagion di riso

E del mondo in mezzo i turbini

Bella calma troverà.

(Glücklich preis ich, wer erfasset alles von der rechten Seite,

der bei Stürmen niemals erblasset, wählt Vernunft als Führerin.

Was im Leben andre weinen macht, ist für Ihn ein Grund zum Lachen,

drohn Gefahren noch so fürchterlich, wahrt er seinen heitren Sinn.)

Lorenzo da Ponte, Cosi fan tutte

Acknowledgements

First of all I would like to thank Johannes for giving me the opportunity to work on this interesting and challenging topic. Thank you for your trust in me, your guidance, patience and fruitful discussions. Thank you also for the opportunity to visit international conferences (Weimar, Milan).

Next I want to thank Oliver. Thank you for your help with the publications and for proofreading this thesis. I am very grateful for your continuous support, be it motivational or sharing your expertise.

Building the set up and dealing with operational problems would have been impossible without the help of Xaver, Andreas and Martin. Thank you, I learned a lot!

I want to thank Evonik for financial support and highly interesting discussions during project meetings. Special thanks to Jan-Olaf, who was always available to answer urgent questions in a very quick and helpful manner.

Heike, Steffi, Helen for helping me get things organized and thereby allowing me to fully concentrate on my scientific work.

Those four years at TC 2 would have been less cheerful and for sure less successful without my great colleagues:

Hendrik, Jürgen, Matteo, Florian, Andreas S., Andreas J., Roberta, Wolfgang, Phillip, Manuel, Ana, Aonsurang, Prado, Felix, Richard, Manuela, Rino, Krishna, Olga, Christian, Virginia, Elvira, Ben, Florencia, Lay-Hwa, Peter, Praveen, Carsten, Oliver, Stefan, Tobias, Frederik, Xuebing, Yongzhong, Chintan, Dechao.

Thank you for the great time we had, at laboratory and office as well as outside university.

I also would like to thank my diploma student Max and my internship students Linus, Astrid, Stephan, Bert and Ingrid for their great effort and the contribution to this work.

During my time at TC 2 my life changed in a very positive and fundamental way. Not only did I learn and develop a lot, but I also got to know Sandra. Thank you for sharing your time with me ever since, for you love, your support, your encouragement and your help to set things into the right perspective.

Last but not least I want to thank my parents for all the financial and non-financial support during my years at school and university. I am well aware that you offered me an ideal start into (working-) life and I am very grateful for that.

Mama, vielen Dank für Deine Liebe und Unterstützung. Papa, vielen Dank dafür, dass Du seit meiner frühesten Kindheit mein Interesse an Naturwissenschaften geweckt und gefördert hast. Es tut mir leid, dass diese Arbeit nicht mehr rechtzeitig fertig geworden ist, sodass Du sie hättest lesen können. Diese Arbeit sei Dir gewidmet, ich hoffe, sie hätte Dir gefallen.

Table of Contents

Chapter 1

General Introduction

This chapter provides an introduction to the subject of this thesis. First the target compound methyl mercaptan is introduced and its industrial relevance described. A short overview of the findings of academic and industrial research concerning the synthesis of methyl mercaptan from synthesis gas and other C_1-compounds is given. After a brief discussion of the relevant catalysts the chapter is finished by presenting the scope of this thesis.

1.1. Methyl mercaptan

1.1.1. Physical and Chemical Properties

Methyl mercaptan or methanethiol is an aliphatic thiol of the formula CH_3SH. Thiols or mercaptans, as they were originally called due to their affinity for mercury (latin: corpus *merc*urium *aptans*), can either be regarded as hydrogen sulfide derivatives or as thio analogues of alcohols. Since the S-H bond energy (339 kJ/mol) is substantially lower than that of the O-H bond (462 kJ/mol), mercaptans are significantly more acidic than their oxygen analogues. As hydrogen bonding to sulfur is consequently also weaker than to oxygen, mercaptans exhibit lower boiling points than their corresponding alcohols. Furthermore aliphatic thiols act as strong nucleophiles [1, 2]. Methyl mercaptan is a colorless, highly flammable gas at room temperature and atmospheric pressure and possesses a pungent odor resembling that of garlic or rotten cabbage. Some physical and chemical properties of methanethiol in comparison with its alcohol analogue methanol are compiled in Table 1.1.

Table 1.1: Some physical and chemical properties of methyl mercaptan and methanol.

Property	CH_3SH	CH_3OH
Molecular weight (g/mol)	48.1	32.04
Melting point (°C)	-123	-98
Boiling point (°C)	5.95	64.7
Solubility in H_2O (g/kg)	23.3	miscible
Density *d20/4* (g/ccm)	0.87	0.79
Bond energy (kJ/mol)	339 (S-H)	462 (O-H)
pKa	10.33	15.30

1.1.2. Applications of methyl mercaptan

Methyl mercaptan is a chemical feedstock employed in the synthesis of numerous products in the agricultural, plastics, rubber and chemical industries [3]. More specifically it is a raw material in the synthesis of the organo-sulfur compounds methionine, dimethyl sulfoxide and dimethyl sulfone [4], as well as in the production of herbicides [5], fungicides and jet fuel additives [6]. Methyl mercaptan itself is added to natural gas as odorant or tracer [6].

Oxidation of methanethiol leads to dimethyldisulfide and, when strong oxidizing reagents are applied, to the formation of methylsulfonic acid [1].

In 2013 the global market for methionine, the synthesis of which is depicted in Fig. 1.1, amounted to about 850.000 tons and a sales volume of 2.85 billion US$.
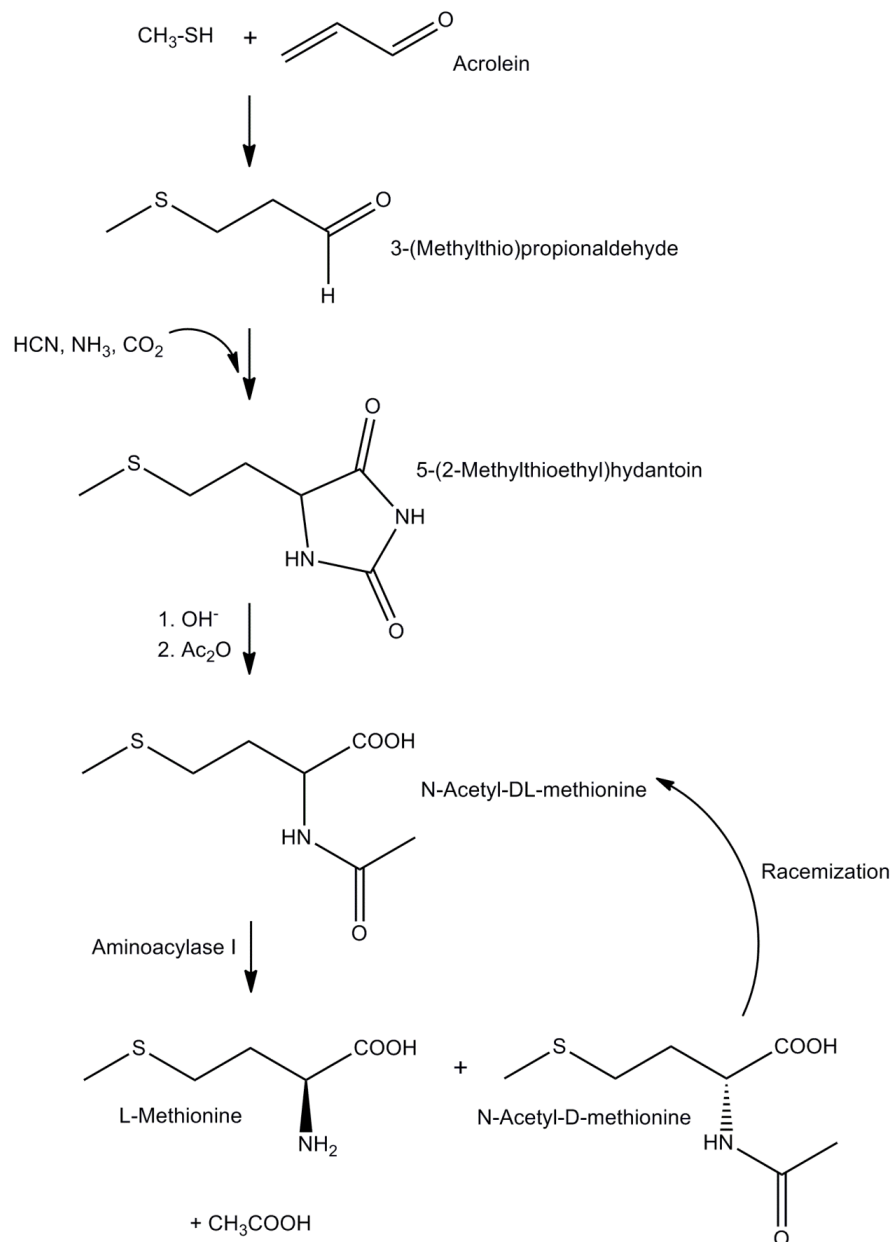
Figure 1.1: Process for the production of methionine [10].

Methionine is one of nine essential, proteinogenic amino acids mainly used as feed additive in livestock production [7]. It also plays an important role within the human body. Patients with a defective metabolism of methionine suffer from severe symptoms such as mental

retardation, skeletal abnormalities and hearing defects. Moreover, a methionine-deficient diet is considered a cause of depression and Parkinson's disease [8]. Synthetic methionine can be applied directly as racemic mixture in animal feed although D-methionine is not found in nature. This is due to the animals organisms being capable of converting D-methionine into L-methionine enzymatically [9].

The global market for methionine gives an indication of the industrial relevance of methyl mercaptan and of its annual production volume although it is employed in other processes and applications as well, as outlined above.

1.1.3. State of the art in the synthesis of methyl mercaptan

On an industrial scale methyl mercaptan is predominantly produced by the gas phase reaction of methanol with hydrogen sulfide over alkali tungstate modified alumina catalysts. The reaction is usually carried out at temperatures between 300 and 500 °C and pressures of 1 to 25 bar [11].

The heterogeneously catalysed reaction between aliphatic alcohols and hydrogen sulfide to form the corresponding mercaptan was discovered in 1910 by Sabatier, who had been working on dehydration catalysts. When passing alcohols and H_2S over thoria at elevated temperatures he observed the formation of mercaptans in addition to the desired olefins. In 1921 Kramer and Reid supported thoria on pumice and used this catalyst to produce methyl mercaptan from methanol and H_2S [12].

Yields of methyl mercaptan of more than 90% and selectivities of about 95% are achieved by the reaction of methanol with hydrogen sulfide over the nowadays conventional alkalitungstate/alumina catalysts. Besides the desired thiolation to yield methyl mercaptan

$$CH_3OH + H_2S \rightarrow CH_3SH + H_2O \qquad (I)$$

dimethyl sulfide is formed as a byproduct according to

$$2\ CH_3OH + H_2S \rightarrow (CH_3)_2S + 2\ H_2O \qquad (II)$$

$$2\ CH_3SH \rightleftharpoons (CH_3)_2S + H_2S \qquad (III)$$

$$CH_3SH + CH_3OH \rightarrow (CH_3)_2S + H_2O \qquad (IV).$$

Dehydration of methanol results in the formation of dimethyl ether

$$2\ CH_3OH \rightarrow (CH_3)_2O + H_2O \qquad (V)$$
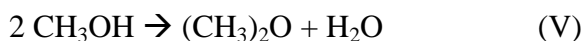
which can be further converted into the desired methyl mercaptan or into dimethyl sulfide by reaction with hydrogen sulfide

$$(CH_3)_2O + 2\ H_2S \rightarrow 2\ CH_3SH + H_2O \qquad (VI)$$
$$(CH_3)_2O + H_2S \rightarrow (CH_3)_2S + H_2O \qquad (VII)$$

The formation of both methanethiol and dimethyl sulfide is thermodynamically favorable over a wide temperature range. Although higher H_2S to methanol ratios allow for higher methyl mercaptan contents in the product mixture, dimethyl sulfide formation cannot be entirely suppressed. Thermodynamic calculations reveal that a large molar excess of H_2S would be required to shift the equilibrium of (III) towards methyl mercaptan. Thus catalysts that selectively increase the rate of methyl mercaptan formation without accelerating equilibrium reaction (III) are required in the thiolation of methanol [13].

1.2. Alternative routes towards methyl mercaptan

1.2.1. Synthesis from carbon oxides and H_2S

Pioneering work in the synthesis of methanethiol from carbon oxides and H_2S was done at Pennwalt Corporation. The idea to synthesize methyl mercaptan from synthesis gas was brought forward owing to the fact that methanol, which is up to nowadays the carbon source for the industrial production of methyl mercaptan, itself is produced from synthesis gas (Figure 1.2). That is, the cost- and energy intensive methanol production step could be omitted using a very basic, cheap and readily available reactant mixture comprising carbon oxides and hydrogen.

In 1962 Olin et al. proposed the synthesis of methyl mercaptan by reacting carbon oxides, i.e. carbon monoxide and carbon dioxide, with hydrogen sulfide in the presence of hydrogen over a sulfided catalyst. They described the process as reductive thiolation of the employed carbon oxides following the overall chemical equations

$$CO + H_2S + 2\ H_2 \rightarrow CH_3SH + H_2O \quad (VIII)$$

and

$$CO_2 + H_2S + 3\ H_2 \rightarrow CH_3SH + 2\ H_2O \quad (IX)$$

Sulfides of hydrogenating metals were suggested and employed as catalysts, since they are not poisoned in the presence of sulfur. A conversion of carbon monoxide to methyl mercaptan as high as 23.2% was reported for the reaction of CO with H_2S and H_2 ($CO:H_2S:H_2=1:2:4$) over an alumina supported NiS catalyst in presence of the organic base piperidine [14].

Hydrocarbons

Steam reforming

CO + H₂

(Synthesis gas)

H_2S

CH₃OH   **CH₃SH**

H_2S

CH₃SH
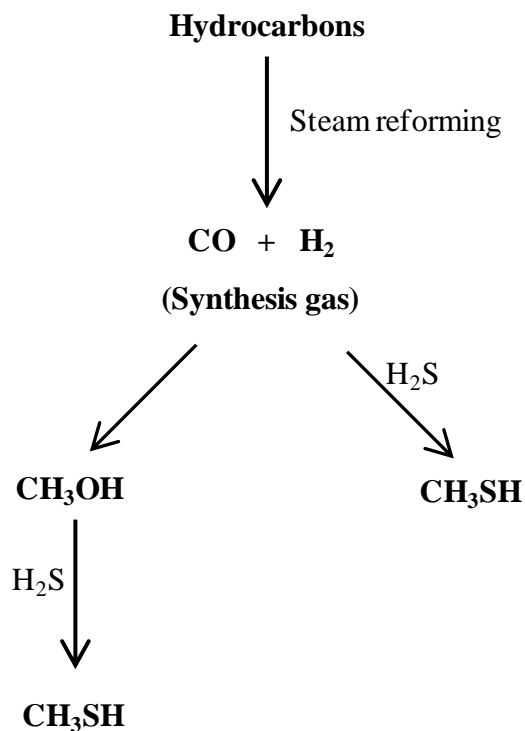
Figure 1.2: Routes to methanethiol starting from synthesis gas.

In 1983 Buchholz (Pennwalt Corporation) was granted a patent on an improved process for the manufacture of methyl mercaptan from carbon oxides. The main difference to the process patented in 1962 was the addition of an alkali metal sulfide, termed "promoter", to the catalyst composition. In addition, elemental sulfur was considered as sulfur source alternative to hydrogen sulfide and no organic base was employed in the process. The inventor set up the following overall chemical equations for the synthesis of methyl mercaptan from carbon oxides and elemental sulfur in the presence of hydrogen:

$$CO + S + 3\ H_2 \rightarrow CH_3SH + H_2O \quad (X)$$

and

$$CO_2 + S + 4\ H_2 \rightarrow CH_3SH + 2\ H_2O \quad (XI)$$

The overall chemical reactions (VIII) and (X) for the synthesis of methyl mercaptan from carbon monoxide were broken down into the following reaction sequence:

When starting from elemental sulfur H_2S is formed by the reaction between elemental sulfur and hydrogen

$$S + H_2 \rightarrow H_2S \qquad\qquad (XII)$$

H_2S, whether formed in situ according to (XII) or supplied as reactant (VIII) reacts with carbon monoxide to produce carbonyl sulfide

$$CO + H_2S \rightarrow COS + H_2 \qquad\qquad (XIII)$$

which is then hydrogenated to form methyl mercaptan

$$COS + 3\ H_2 \rightarrow CH_3SH + H_2O \qquad (XIV)$$

The highest conversion of carbon monoxide to methyl mercaptan was reported to be 90.2% for a reactant ratio of $CO:H_2S:H_2$ of 1:8:4 over a cesium promoted nickel sulfide catalyst. The highest conversion of carbon dioxide to methyl mercaptan was achieved under the same conditions and amounted to 52% [15].

Barrault et al. were the first ones to study the formation of methanethiol from carbon oxides and H_2S in the presence of hydrogen with respect to the reaction mechanism and the role of the catalyst [3]. They did so by reacting $CO(CO_2)/H_2S/H_2$ mixtures over potassium promoted, presulfided tungsten-alumina catalysts. For both, the reaction of CO and the reaction of CO_2, with hydrogen and hydrogen sulfide, the formation of COS was observed and it was concluded to be the main intermediate in the formation of methyl mercaptan according to

$$CO + H_2S \rightarrow COS + H_2 \qquad\qquad (XIII)$$

or

$$CO_2 + H_2S \rightarrow COS + H_2O \qquad\qquad (XV)$$

and

$$COS + 3\ H_2 \rightarrow CH_3SH + H_2O \qquad \text{(XIV)}$$
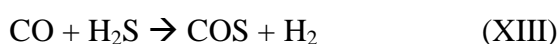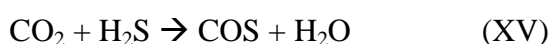
which is in agreement with the results of Buchholz.

Since COS and methyl mercaptan were observed in parallel, the hydrogenation of COS was identified as the rate determining step in the synthesis of methanethiol.

In the reaction starting from CO as carbon source, CO_2 was found as a reaction product in amounts similar to that of the formed methyl mercaptan, whereas H_2O could not be detected among the reaction products. This was interpreted in terms of CO_2 being formed either by the water-gas shift reaction

$$CO + H_2O \rightarrow CO_2 + H_2 \qquad \text{(XVI)}$$

or by hydrolysis of carbonyl sulfide

$$COS + H_2O \rightarrow CO_2 + H_2S \qquad \text{(XVII)}$$
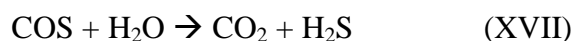
In the reaction starting from CO_2 substantial amounts of CO were formed, whereas the yields of COS and CH_3SH were much lower than in the reaction starting from carbon monoxide. CO was believed to be formed either by the inverse water-gas shift reaction

$$CO_2 + H_2 \rightarrow CO + H_2O \qquad \text{(XVIII)}$$

or by the inverse reaction of carbonyl sulfide formation

$$COS + H_2 \rightarrow CO + H_2S \qquad \text{(XIX).}$$

A reaction network summarizing the findings of Barrault et al. is depicted in Figure 1.3.

In the mid 1980's Exxon Research and Engineering filed several patents on the production of methyl mercaptan from H_2S and CO. In contrast to the processes claimed by Pennwalt, Exxon was not adding H_2 to the reactant mixture. Ratcliffe et al. reported the catalytic reduction of CO with H_2S, yielding methanethiol, over titania in its rutile phase [6] and over titania-supported vanadia catalysts [16].
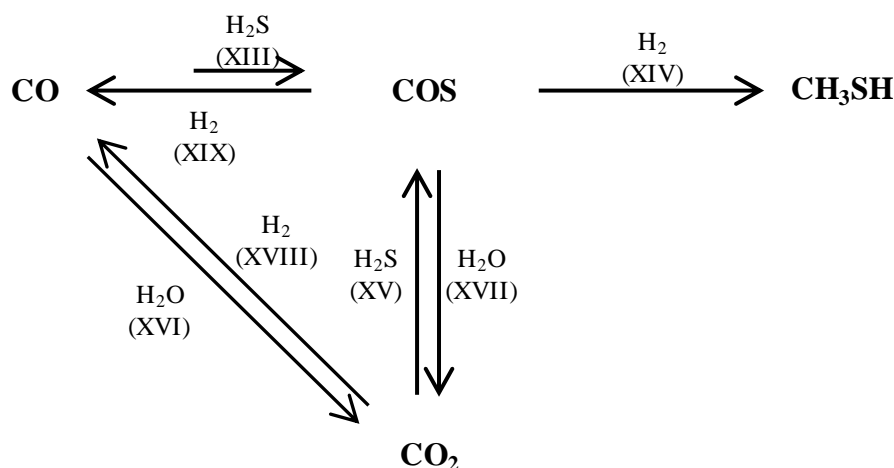
Fig. 1.3: Reaction network for the synthesis of methyl mercaptan from carbon oxides and H_2S in presence of hydrogen over potassium promoted tungsten-alumina catalysts.

The reaction over vanadia based catalysts was studied more closely by Mul et al. [17]. A reaction network for the synthesis of methyl mercaptan from reactant mixtures of CO and H_2S was established by reacting a 1:1 feed of H_2S and CO at 1 bar (Fig. 1.4). Based on their experimental findings the overall chemical equation is

$$3\,CO + 2\,H_2S \rightarrow CH_3SH + COS + CO_2 \quad (XX)$$

which means theoretical carbon selectivities of 33.3% for methyl mercaptan, COS and CO_2. However, the contribution of carbonyl sulfide to the overall amount of products decreases on an increase in CO conversion. This led to the conclusion that COS is the primary reaction product from which all other products are formed by secondary reactions.

The hydrogenation of COS according to (XIV), forming the target compound methyl mercaptan, was identified as rate determining step. Water formed in the hydrogenation of carbonyl sulfide was not detected in the reaction mixture which was attributed to it being consumed in the water-gas shift reaction (XVI) and the hydrolysis of COS (XVII).

CS_2 and CH_4 were detected as byproducts and concluded to result from the disproportionation of COS

$$2\,COS \rightarrow CO_2 + CS_2 \quad\quad\quad\quad (XXI)$$

and the hydrogenation of methyl mercaptan

$$CH_3SH + H_2 \rightarrow CH_4 + H_2S \qquad (XXII)$$
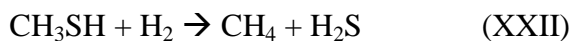
respectively.
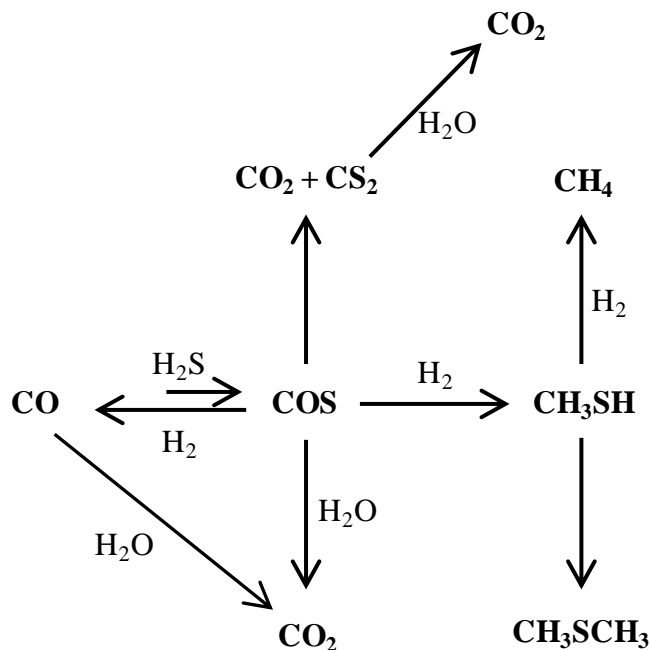
Figure 1.4: Reaction network for the synthesis of methyl mercaptan from CO and H_2S over vanadia-based catalysts as proposed by Mul et al [17].

In 2008 Chen et al. investigated the catalytic synthesis of methyl mercaptan from H_2S-rich synthesis gas ($H_2S/H_2/CO = 2/1/1$, v/v) over sulfided, SiO_2-supported Mo-based catalysts [18]. Their findings concerning the reaction network of the production of methanethiol from CO and H_2S in the presence of hydrogen closely resembles that set up by Barrault et al. as carbonyl sulfide is considered as primary product, which is hydrogenated to form methyl mercaptan (Fig. 1.5). However, Chen et al. observed the formation of methane, CS_2 and thioethers, which had not been reported by Barrault. CS_2 formation was attributed to the disproportionation of COS as already reported by Mul et al.

Since only very small amounts of CS_2 were detected, the disproportionation of carbonyl sulfide was ruled out as being the source of the considerable amount of CO_2 that was found. According to Le Chatelier's principle a high partial pressure of H_2S, as applied in this study, should suppress the hydrolysis of COS according to (XVII) and therefore it was concluded that carbon dioxide mostly originated from the water-gas shift reaction (XVI).

The formation of methane and thioethers was attributed to secondary reactions of methyl mercaptan, since their appearance went along with a decrease in the selectivity to methanethiol.
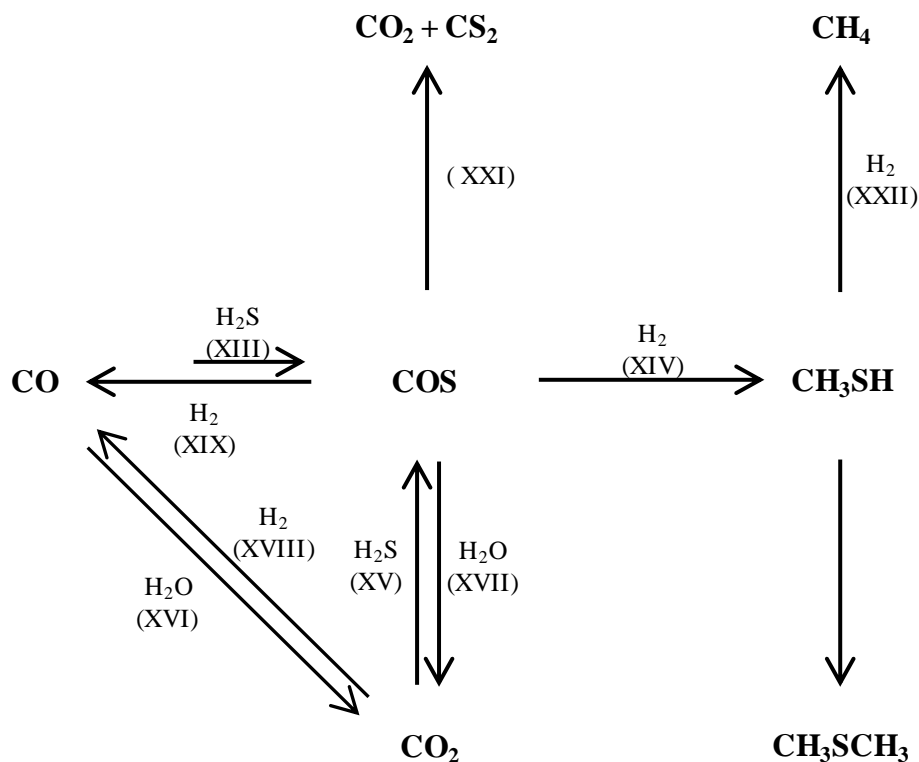
Figure 1.5: Extended reaction network for the synthesis of methyl mercaptan from carbon oxides and H_2S in presence of hydrogen according to the findings of Chen et al.

1.2.2. Other routes towards methyl mercaptan

Few more routes towards methyl mercaptan synthesis alternative to the thiolation of methanol have been proposed in patent and/or academic literature besides the approach to employ carbon oxides as C1-starting compounds in the synthesis of methanethiol, which is the focus of this thesis.

1.2.2.1. Methyl mercaptan from CS₂

The hydrogenation of carbon disulfide, which is predominantly produced by the reaction of methane with sulfur, which yields methyl mercaptan according to

$CS_2 + 3H_2 \rightarrow CH_3SH + H_2S$ (XXIII)

was first proposed by van Venrooy, who employed a commercial, NiMo-based sulfided hydrogenation catalyst. Substantial amounts of dimethyl sulfide were formed along with the desired methanethiol [19]. An increase in the selectivity to methyl mercaptan to about 65% at a CS_2 conversion of about 70% was achieved by employing alumina supported CoMo-based catalysts and adding H_2S to the reaction mixture [20]. Only recently, the quantitative conversion of carbon disulfide into methyl mercaptan has been reported over potassium promoted NiMo-based catalysts supported on alumina [21].

1.2.2.2. Methyl mercaptan from dimethyl sulfide and dimethyl disulfide

Dimethyl sulfide is the major byproduct in the thiolation of methanol. Dimethyl disulfide is also observed as a byproduct in the industrial synthesis of methyl mercaptan [22]. Processes for their conversion into methyl mercaptan have been developed to utilize these materials.

Dimethyl sulfide can be reacted with hydrogen sulfide to give methyl mercaptan according to

$$(CH_3)_2S + H_2S \rightarrow 2\ CH_3SH \qquad\qquad (XXIV)$$

which corresponds to the reverse reaction of its formation.

Beach et al. were the first ones to patent a process for catalytically converting dimethyl sulfide to methyl mercaptan by reacting it with hydrogen sulfide over a cadmium sulfide/ alumina catalyst. Molar conversions of dimethyl sulfide to methyl mercaptan of about 60% could be achieved [23]. Improvements of the efficiency of the process were achieved by employing various catalysts and optimizing process parameters. In 2008 Barth et al. reported almost 90% conversion of dimethyl sulfide to methyl mercaptan over cesium/alumina catalysts [22].

The synthesis of methyl mercaptan from dimethyl disulfide has been studied to a much lesser extent. The hydrogenolysis of dimethyl disulfide, which proceeds according to

$$(CH_3)_2S_2 + H_2 \rightarrow 2\ CH_3SH \qquad\qquad (XXV)$$

has attracted interest, since dimethyl disulfide is produced industrially on a large scale and, being a liquid at room temperature, can be handled much easier and safer than methyl mercaptan. Studies have been carried out over alumina-supported, nickel or cobalt promoted molybdenum or tungsten sulfide catalysts. At complete conversion of dimethyl disulfide the

product mixture consists solely of about equal amounts of the desired methyl mercaptan and dimethyl sulfide, which is believed to be produced from CH_3SH in a secondary reaction [24].

1.1.2.3. Diverse

The list of routes towards methyl mercaptan mentioned above is not exhaustive. For instance preparation of methanethiol by the hydrogenation of carbonyl sulfide [25], by conversion of formaldehyde with hydrogen sulfide and hydrogen [26], and more recently by reaction of methane and hydrogen sulfide in a non-thermal pulsed plasma corona reactor [27] has been reported.

1.3. Catalysts in the synthesis of methyl mercaptan from H$_2$S-containing synthesis gas

The catalysts applied in the synthesis of methyl mercaptan from synthesis gas comprising H_2S resemble those applied in hydroprocessing of crude oil (MoS_2 and WS_2 based catalysts), i.e. hydrodesulfurization, hydrodenitrogenation, hydrodeoxygenation, hydrodemetalation, hydrogenation, and hydrocracking [28], and have been extensively characterized for those applications. Alkali-promoted MoS_2-based catalysts have been the subject of numerous mechanistic and kinetic studies during the past two decades, owing to their ability to catalyze the formation of higher alcohols from synthesis gas [29]. These materials have exhibited the best results in methanethiol production from H_2S-containing synthesis gas and were therefore applied within this thesis. The application of unpromoted MoS_2 catalysts in the conversion of synthesis gas leads to the formation of hydrocarbons when the H_2S-content in the synthesis gas is relatively low and when alcohol synthesis conditions are applied [29].

The MoS_2 phase in its most common hexagonal 2H type is composed of two S-Mo-S layers stacked upon each other in z-direction within a hexagonal lattice system. Van der Waals forces between those layers are weak, leading to relatively large distances between the layers. Each layer is terminated by Mo and by S edges. Active sites are located on these edges, while the basal plane is considered to be catalytically inactive [30]. The molybdenum edge under sulfiding conditions is believed to be saturated with sulfur dimers, whereas in the case of sulfo-reductive conditions the molybdenum edge is concluded to be half covered by sulfur. The sulfur edge observed under sulfo-reductive conditions arises on adsorption of

hydrogen, forming stabilizing S-H groups [31]. This SH groups are the functional groups that provide hydrogen for hydrogenation and hydrogenolysis reactions [32].

Cobalt promotion drastically increases the activity of MoS_2 catalysts in hydrotreating reactions. The most accepted explanation for this promotional effect is given by the Co-Mo-S model in which molybdenum atoms at the edges of the MoS_2 slabs are substituted by cobalt atoms, as evidenced by numerous studies [33-37].

Table 1.2: Findings of Yang et al. concerning the synthesis of methyl mercaptan from a mixture of $CO:H_2:H_2S = 5:14:1$ at 0.2 MPa, 290 °C, GHSV = 3000 h^{-1} over various potassium promoted supported MoS_2 catalysts.

Catalyst	Selectivity		Yield of CH_3SH $(gh^{-1}g_{cat}^{-1})$	Mo^{6+}/Mo^{4+}	$S^{2-}/(S-S)^{2-}$	I_{Mo-S-K}/I_{MoS2}
	CH_4	CH_3SH				
MoS_2	80.1	-	-	0.00	0.00	0.00
K_2MoS_4/SiO_2 (0.15/1)	3.3	92.2	0.15	0.27	0.25	1.18
$K_2MoS_4/Fe_2O_3/SiO_2$ (0.15/0.03/1)	2.3	95.8	0.36	0.71	0.85	2.91
$K_2MoS_4/CoO/SiO_2$ (0.15/0.03/1)	1.7	95.8	0.37	0.80	0.90	3.08
$K_2MoS_4/NiO/SiO_2$ (0.15/0.03/1)	2.4	95.2	0.33	0.79	0.79	2.90
$K_2MoS_4/MnO_2/SiO_2$ (0.15/0.03/1)	5.7	90.6	0.26	0.43	0.15	1.88
$K_2MoS_4/CeO_2/SiO_2$ (0.15/0.03/1)	2.4	95.0	0.34	0.82	0.96	1.88
$K_2MoS_4/La_2O_3/SiO_2$ (0.15/0.03/1)	0.7	98.6	0.37	0.77	1.26	3.10

In a series of publications [38-41] Yang et al. investigated the catalytic properties of supported potassium promoted molybdenum sulfide catalysts with respect to the formation of methyl mercaptan from CO, H_2 and H_2S. Furthermore they explored the effect of the addition of transition metal oxides and rare-earth metal oxides to these catalysts on the catalytic conversion of H_2S-containing synthesis gas to methanethiol.

Their findings concerning the influence of the catalyst composition on the selectivities to methane and methanethiol are summarized in Table 1.2. The catalysts were characterized by means of X-ray diffraction and X-ray photoelectron spectroscopy after testing in the synthesis of methyl mercaptan. Reflections assignable to a Mo-S-K phase were observed in the XRD patterns of potassium promoted catalysts in addition to reflections characteristic for MoS_2. S(2p) XPS spectra revealed the presence of two species, i.e. $S^{2-}(2p)$ and $(S\text{-}S)^{2-}(2p)$, Mo(3d) XPS spectra exhibited peaks assignable to $Mo^{4+}(3d_{5/2})$ and $Mo^{6+}(3d_{5/2})$.

The authors suggested the Mo-S-K phase as active site for the formation of methyl mercaptan, whereas the MoS_2 phase was believed to be responsible for the formation of hydrocarbons. The S^{2-} surface species were concluded to increase the amount of available active hydrogen and thereby accelerate the hydrogenation of CO, leading to the formation of surface $-CH_3$ species. These allowed for the formation of methane on the MoS_2 phase according to Fig 1.6 or for the formation of methyl mercaptan on the Mo-S-K phase as depicted in Fig. 1.7.

Addition of transition metals to the catalyst increased the Mo^{6+}/Mo^{4+} ratio on the catalyst surface, indicating that the reduction of molybdenum species is hampered in the presence of transition metal oxides.
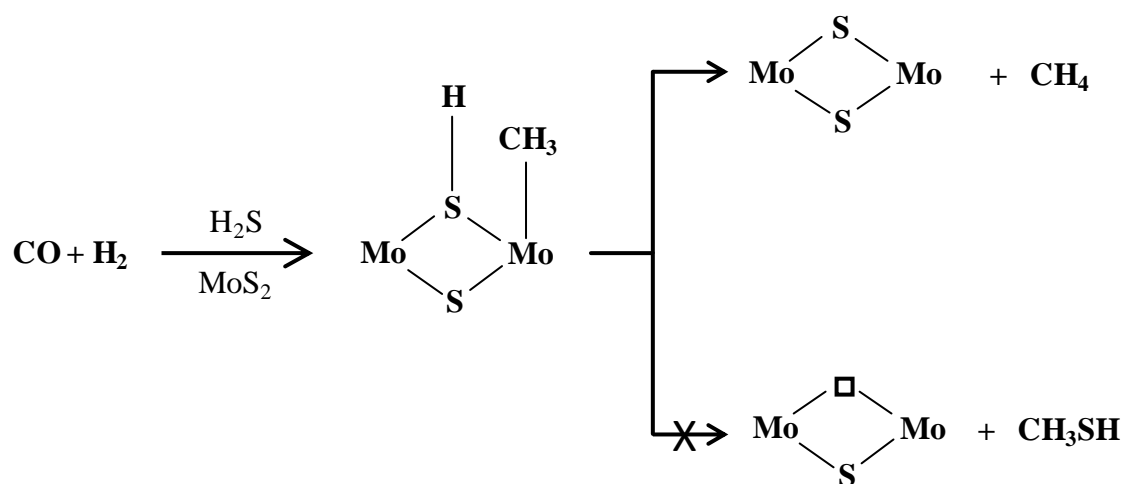
Figure 1.6: Formation of methane from H_2S-containing synthesis gas over the MoS_2-phase [33].
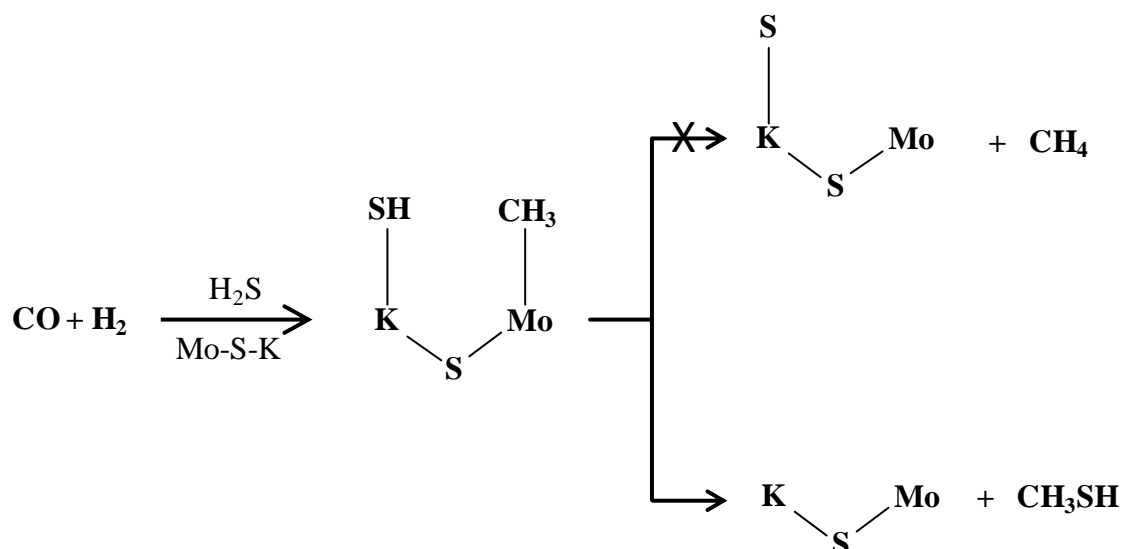
Figure 1.7: Formation of methyl mercaptan from H_2S-containing synthesis gas over the Mo-S-K phase [33].

Further studies on the synthesis of methyl mercaptan from H_2S-containing synthesis gas over promoted and unpromoted MoS_2 were conducted by Chen et al. [18, 42-44]. CO conversions and carbon selectivities achieved over the employed catalysts are summarized in Table 1.3.

Potassium was found to have the most beneficial effect on CO conversion and methyl mercaptan formation among the alkali metals. The more basic and nucleophilic cesium favored the formation of COS while reducing the selectivity to methyl mercaptan, whereas the less basic and nucleophilic lithium had the opposite effect.

The potassium promoted catalysts were thoroughly characterized and compared to the unpromoted ones and the cobalt promoted catalysts by conducting X-ray diffraction, CO-TPD, electron spin resonance and XPS measurements.

Temperature programmed desorption experiments showed that potassium promotes the non-dissociative adsorption of CO, which was explained by the basic character of the alkali metal. By transferring electrons to the metallic phase, the affinity towards electron-acceptor molecules like carbon monoxide increased, which results in the weakening of the C-O bond upon adsorption. On addition of cobalt, peaks characteristic for the dissociative adsorption of carbon monoxide could be detected, which is in good agreement with the increased selectivity to methane when the catalysts are promoted with cobalt, since the dissociative adsorption allows for the formation of hydrocarbons.

16

Table 1.3: CO conversions and carbon selectivities in the synthesis of methyl mercaptan from a mixture of $CO:H_2:H_2S = 1:1:2$ at 0.2 MPa, 300 °C, GHSV = 3000h^{-1} over various molybdenum based catalysts.

Catalyst	CO conversion (%)	Selectivity (%)				
		CH_4	COS	CO_2	CH_3SH	CS_2
SiO_2	1.7	3.8	94.7	Trace	1.5	-
Mo/SiO_2	4.6	1.5	96.2	Trace	2.3	-
$MoCo/SiO_2$	8.3	2.7	94.6	Trace	2.7	-
$LiMo/SiO_2$	19.5	1.0	17.5	29.9	51.6	Trace
KMo/SiO_2	42.7	0.3	19.1	31.7	48.5	0.1
$CsMo/SiO_2$	38.9	0.3	23.2	33.0	43.3	Trace
$KMoCo/SiO_2$	62.4	0.6	16.6	36.6	45.7	0.1
$KMoTe/SiO_2$[a]	62.1	0.2	20.6	30.1	49.1	-
$KMoNi/SiO_2$[a]	60.7	0.03	14.6	43.2	42.2	n.g.

[a] GHSV= 2000 h^{-1}

Two signals of Mo^{5+} species were found in the ESR spectra of the studied catalysts, one assignable to oxo-Mo^{5+} species, i.e. molybdenum coordinated only by oxygen atoms, the other assignable to oxysulfo-Mo^{5+} species, i.e. molybdenum coordinated by sulfur and oxygen. Potassium was shown to exert a stabilizing effect on oxysulfo-Mo^{5+} species. Double promotion with potassium and cobalt revealed that the cobalt improves the sulfidation of oxo-Mo^{5+} species to oxysulfo species.

XPS signals could be assigned to Mo^{6+}, Mo^{5+} and Mo^{4+} when recording Mo(3d) spectra and to a "low oxidation state sulfur" regime, termed S_L, as well as to a "high oxidation state sulfur" regime, termed S_H, when recording S(2p) spectra. The compositions and ratios determined for the molybdenum and sulfur species of the investigated catalysts are given in Table 1.4.

When correlating the results summarized in Table 1.4 with those shown in Table 1.3 it is evident, that a high ratio of Mo^{5+}/Mo^{4+} and an increase in the S_L/S_H ratio favor the formation of methyl mercaptan.

Table 1.4: Composition of promoted and unpromoted molybdenum catalysts in the synthesis of methyl mercaptan with respect to oxidation states of molybdenum and sulfur as determined by Chen et al.

Catalyst	Concentration (%)			Ratio	Concentration (%)		Ratio
	Mo^{4+}	Mo^{5+}	Mo^{6+}	Mo^{5+}/Mo^{4+}	S_L	S_H	S_L/S_H
Mo/SiO_2	69.1	10.5	20.4	0.2	44.0	56.0	0.8
$MoCo/SiO_2$	61.1	12.1	26.8	0.2	51.9	48.1	1.1
KMo/SiO_2	44.0	22.3	33.7	0.5	59.2	40.8	1.5
$KMoCo/SiO_2$	41.6	21.8	36.6	0.5	70.3	29.7	2.4
$KMoTe/SiO_2$	55.5	22.2	22.3	0.4	n.g.	n.g.	n.g.

Potassium promotion led to an increase in Mo^{5+} and a decrease in Mo^{4+}. This was attributed to a change in the coordination of molybdenum on the addition of potassium. Oxidic Mo(VI) which exists in octahedral as well as in tetrahedral coordination is more easily sulfided/reduced in its octahedral coordination state. Potassium promotion was therefore believed to transform some of the octahedrally coordinated Mo(VI) to tetrahedrally coordinated Mo(VI), which is less readily reduced. This explains the stabilization of Mo^{5+} species with respect to Mo^{4+} species. The abundance of "low oxidation state sulfur", comprising elemental sulfur, S^{2-}, S_2^{2-}, oxysulfides and polysulfides increased while the amount of "high oxidation state sulfur" – SO_4^{2-} decreased on addition of potassium and/or cobalt. The "low oxidation state sulfur" species S^{2-} and S_2^{2-} are known to activate hydrogen either by homolytic cleavage of H_2 according to

$$(S-S)^{2-} \;+\; H_2 \;\rightleftharpoons\; \overset{\displaystyle H \quad\quad H}{(S - S)^{2-}}$$
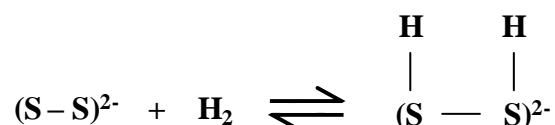
or by heterolytic cleavage according to

$$Mo^{4+}-S^{2-} \;+\; H_2 \;\rightleftharpoons\; \overset{\displaystyle H \quad\quad H}{Mo^{4+}- S^{2-}}$$
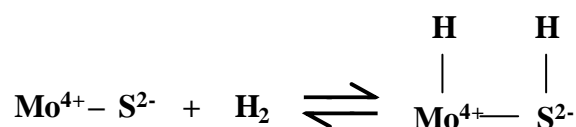
The fact that cobalt significantly increased the S_L/S_H ratio in the case of the doubly promoted catalyst is in good agreement with the higher selectivity to methane exhibited by the doubly promoted catalysts, i.e. increased hydrogenation capability on cobalt promotion.

In a very recent publication Cordova et al. [45] studied the formation of methyl mercaptan from H_2S-containing synthesis gas over alkali promoted MoS_2 based catalysts, focusing on the influence of the promoter and on gaining insight into the structure of the active phase. When conducting Mo 3d XPS they discovered a shift in the binding energy of the MoS_2 phase which was attributed to the formation of a K_xMoS_2 phase. More specifically they suggested that potassium is intercalated in between the layers of MoS_2 in the form of K^+ cations. This was further supported by high resolution TEM images which showed an increase in slab length and stacking degree of MoS_2 slabs in presence of potassium.

1.4. Scope of this thesis

Methyl mercaptan is a chemical feedstock employed in the synthesis of numerous products in the agricultural, plastics, rubber and chemical industries. It is predominantly produced by the reaction of methanol with hydrogen sulfide on an industrial scale. The idea to synthesize methyl mercaptan from synthesis gas directly, thereby omitting the methanol production step (where methanol is produced from synthesis gas), is intriguing and has received considerable interest.

It is commonly accepted in literature, that formation of methyl mercaptan from H_2S-containing synthesis gas proceeds via the formation of COS as a first step. However, the hydrogenation of COS has not been subject to detailed investigations prior to this thesis. Thus a two-step approach is adopted in order to study methanethiol formation within this thesis, i.e. the selective production of COS as a first process step conducted within a separate reactor, followed by the downstream synthesis of CH_3SH in a second, subsequent reactor.

Chapter 2 deals with the first step, i.e. the formation of COS from CO, CO_2 and liquid sulfur in presence and absence of H_2. A reaction network for the formation of COS is elucidated based on the results obtained from various experiments at different reaction temperatures, pressures, residence times and reactant ratios.

The method for the formation of COS presented in Chapter 2, allows the investigation of the second step of the production of methyl mercaptan from H_2S-containing synthesis gas, i.e. the conversion of COS to methyl mercaptan.

Chapter 3 of this thesis deals with the synthesis of methyl mercaptan from COS and H_2 in the presence of H_2S on K^+-promoted MoS_2 supported on silica. The reaction between COS, H_2 and H_2S over the employed catalyst is studied in the temperature range of 453-673 K by varying H_2/COS and H_2/H_2S ratios as well as by varying residence times. In order to get a better understanding of the reactions in which carbonyl sulfide is involved, experiments under exclusion of H_2 are also performed. Evaluation of these kinetic studies allows for setting up a reaction network for the synthesis of methyl mercaptan from COS and H_2 in the presence of H_2S. The catalyst is characterized in its oxide as well as in its sulfide state by atomic absorption spectroscopy, Raman spectroscopy and X-ray diffraction. NO adsorption experiments are performed on the sulfided catalyst and after treating the sulfided catalyst with COS. Analysis of these characterization results gives an indication towards the mechanisms by which the competing reactions in the synthesis of methanethiol take place on the catalyst surface.

The influence of potassium on the synthesis of methyl mercaptan from COS is investigated in more detail in Chapter 4. Pure MoS_2 and MoS_2 catalysts promoted with different concentrations of potassium (all of them supported on alumina) are tested in the synthesis of CH_3SH from COS to understand the key role of the alkali metal in the formation of methanethiol. Together with potassium-doped alumina, the MoS_2 catalysts are thoroughly characterized, in their oxide as well as in their sulfide state, by means of atomic absorption spectroscopy, N_2 physisorption, NO adsorption, X-ray diffraction, temperature-programmed sulfidation and Raman spectroscopy.

As cobalt is known to increase the hydrogenation performance of MoS_2 catalysts, it is added as a second promoter to the potassium-promoted MoS_2 catalysts in the catalytic conversion of COS, H_2, and H_2S to methyl mercaptan. This doubly promoted catalyst is also tested in the synthesis of methanethiol from CS_2, along with the unpromoted and the potassium-promoted MoS_2 catalysts. Chapter 5 presents the results of these reactions focusing on the influence of the catalyst composition.

A concise summary of the most important results and conclusions obtained within the scope of this thesis is given in Chapter 6.

1.5. References

[1] K.-M. Roy. Thiols and Organic Sulfides. Ullmann's Encyclopedia of Industrial Chemistry (2000).

[2] http://pubchem.ncbi.nlm.nih.gov/compound/methanethiol#section=Chemical-and-Physical-Properties, 18.07.2015.
http://pubchem.ncbi.nlm.nih.gov/compound/887#section=Chemical-and-Physical-Properties, 18.07.2015.

[3] J. Barrault, M. Boulinguiez, C. Forquy, R. Maurel, Appl. Catal. 33 (1987) 309.

[4] J. Sauer, W. Boeck, L. von Hippel, W. Burkhardt, S. Rautenberg, D. Arntz, W. Hofen, US patent 5 852 219, 1998.

[5] F. Müller, A. P. Applebyki. Weed Control, 2. Individual Herbicides. Ullmann's Encyclopedia of Industrial Chemistry (2010).

[6] C. Ratcliffe, P. Tromp, US patent 4 668 825, 1987.

[7] T. Willke, Applied Microbiology and Biotechnology 98 (2014) 9893.

[8] J. Gomes, D. Kumar, Enzyme and Microbial Technology 37 (2005) 3.

[9] W. Leuchtenberger, K. Huthmacher, K. Drauz, Appl. Microbiol. Biotechnol. 69 (2005) 1.

[10] K. Drauz, I. Grayson, A. Kleemann, H. P. Krimmer, W. Leuchtenberger, C. Weckbecker. Amino Acids. Ullmann's Encyclopedia of Industrial Chemistry (2007).

[11] H. Redlingshoefer, C. Weckbecker, A. Dörflein, M. Rückriegel, US patent 7 691 776, 2010.

[12] R. L. Kramer, E. E. Reid, JACS 43 (1921) 880.

[13] H. O. Folkins, E. L. Miller, I & EC Process Design and Development 1 (1962) 271.

[14] J. F. Olin, B. Buchholz, R. H. Goshorn, US patent 3 070 632, 1962.

[15] B. Buchholz, US patent 4 410 731, 1983.

[16] C. T. Ratcliffe, P. J. Tromp, I. E. Wachs, US patent 4 570 020, 1986.

[17] G. Mul, I. E. Wachs, A. S. Hirschon, Catal. Today 78 (2003) 327.

[18] A. P. Chen, Q. Wang, Y. J. Hao, W. P. Fang, Y. Q. Yang, Catal. Lett. 121 (2008) 260.

[19] J. J. van Venrooy, US patent 3 488 739, 1970.

[20] D. H. Kubicek, US patent 3 880 933, 1975.

[21] P. Barre, G. Fremy, A. Lozowsky, US patent 2011/0213184, 2011.

[22] J. Barth, H. Redlingshoefer, C. Weckbecker, K. Huthmacher, US patent 2008/0200730, 2008.

[23] L. K. Beach, A. E. Barnett, US patent 2 667 515, 1954.

[24] E. Cadot, M. Lacroix, M. Breysse, E. Arretz, J. Catal., 164 (1996), 490.

[25] D. H. Kubicek, US patent 4 120 944, 1978.

[26] D. H. Kubicek, US patent 3 994 980, 1976.

[27] P. K. Agarwal, R. Agarwal, T. M. Linjewile, A. S. Hull, Z. Chen, US patent 2004/0249217, 2004.

[28] O. Deutschmann, H. Knözinger, K. Kochloefl, T. Turek. Heterogeneous Catalysis and Solid Catalysts, 3. Industrial Applications. Ullmann's Encyclopedia of Industrial Chemistry. (2011).

[29] S. Zaman, K. J. Smith, Catal. Rev.-Sci. Eng., 54 (2012), 41.

[30] W. Bensch, Hydrotreating: Removal of Sulfur from Crude Oil Fractions with Sulfide Catalysts. Comprehensive Inorganic Chemistry II (2013).

[31] A. S. Walton, J. V. Lauritsen, H. Topsøe, F. Besenbacher, J. Catal. 308 (2013) 306.

[32] E. Schachtl, E. Kondratieva, O. Y. Gutiérrez, J. A. Lercher, J. Phys. Chem. Lett. 6 (2015) 2929.

[33] F. L. Deepak, R. Esparza, B. Borges, X. Lopez-Lozano, M. Jose-Yacaman, ACS Catal. 1 (2011) 537.

[34] T. G. Parham, R. P. Merrill, J. Catal. 85 (1984) 295.

[35] B. S. Clausen, H. Topsoe, R. Candia, J. Villadsen, B. Lengeler, J. Als-Nielsen, F. Christensen, J. Phys. Chem. 85 (1981) 3868.

[36] L. S. Byskov, J. K. Nørskov, B. S. Clausen, H. Topsøe, J. Catal. 187 (1999) 109.

[37] J. V. Lauritsen, J. Kibsgaard, G. H. Olesen, P. G. Moses, B. Hinnemann, S. Helveg, J. K. Nørskov, B. S. Clausen, H. Topsøe, E. Lægsgaard, F. Besenbacher, J. Catal. 249 (2007) 220.

[38] Y. Q. Yang, Y. Z. Yuan, S. J. Dai, B. Wang, H. B. Zhang, Catal. Lett. 54 (1998) 65.

[39] S. J. Dai, Y. Q. Yang, Y. Z. Yuan, D. L. Tang, R. C. Lin, H. B. Zhang, Catal. Lett (1999) 157.

[40] Y. Q. Yang, S. J. Dai, Y. Z. Yuan, R. C. Lin, D. L. Tang, H. B. Zhang, Appl. Catal. A 192 (2000) 175.

[41] Y. Q. Yang, H. Yang, Q. Wang, L. J. Yu, C. Wang, S. J. Dai, Y. Z. Yuan, Catal. Lett. 74 (2001) 221.

[42] A. Chen, Q. Wang, Y. Hao, W. Fang, Y. Yang, Catal. Lett. 118 (2007) 295.

[43] A. Chen, Q. Wang, Q. Li, Y. Hao, W. Fang, Y. Yang, J. Mol. Catal. A 283 (2008) 69.

[44] Y. Hao, Y. Zhang, A. Chen, W. Fang, Y. Yang, Catal. Lett. 129 (2009) 486.

[45] A. Cordova, P. Blanchard, C. Lancelot, G. Frémy, C. Lamonier, ACS Catalysis 5 (2015) 2966.

Chapter 2

Effect of H_2 in the synthesis of COS using
liquid sulfur and CO or CO_2 as reactants

The synthesis of COS from CO, CO_2 and liquid sulfur in the presence and absence of hydrogen was explored. The reaction of H_2 with liquid sulfur produced H_2S and polysulfanes, which increase the reactivity of liquid sulfur and provide alternative complementary reaction routes for the formation of COS. The reaction from CO_2 proceeds by forming CO as intermediate. Elevated pressure favors formation of COS from both carbon oxides due to the increasing residence time and the saturation of gases in the liquid. Above 350°C, the solubility of H_2S in sulfur and the hydrogenation of COS limit the conversion of CO. The approach provides a highly efficient method for the preparation of COS under mild reaction conditions, without using a catalyst or water adsorbents.

2.1. Introduction

COS is an important feedstock in chemical industry, mainly used for the synthesis of agricultural products such as pesticides and herbicides [1]. Applications also include the use as a catalyst or reactant in polymerization or in the synthesis of substituted ureas, urethanes and carbamates [2-5]. The detailed chemistry and physicochemical properties of COS are compiled in two reviews covering preparation, properties and chemical reactions related to COS as well as the industrial applications and environmental problems associated with COS [6,7].

In the laboratory, COS can be prepared using several methods starting with different carbon and sulfur sources [7]. CO or CO_2, however, are the most used carbon sources in large-scale processes. The method starting with CO can be dated back to Mittasch and Willfroth, who produced a gas mixture of COS, CO_2 and CS_2 by reacting CO with sulfur vapor at temperatures between 400 and 600°C [8]. A COS yield of about 60% was achieved at a CO conversion of 95%, when iron oxide supported on activated carbon or charcoal was used as catalysts. The COS yield could be further improved through reducing the reaction temperature (260-490°C) and using zeolite 5A and 13X as catalysts [6]. Using alkali metal sulfides as catalysts in the liquid sulfur phase and cobalt-, tungsten- and tin-sulfides as catalysts in the gas phase, Kanazawa et al. were able to obtain a COS yield as high as 97% [9]. In a noteworthy catalyst-free process, a COS yield of 94% was achieved by passing CO directly through liquid sulfur in a saturator at approximately 400°C [10]. All the aforementioned processes were conducted at atmospheric or slightly elevated pressures. A high pressure process (7-30 bar) was attempted in a patent using cobalt-, molybdenum- and cobalt-molybdenum-sulfides as catalysts. Unfortunately, the maximum yield to COS was only 30%. Such a low yield is probably due to the low reaction temperatures (120-200°C) they applied [7].

The processes based on CO_2 go back to Rühl and Otto who used Group II and Group IV oxides as catalysts to convert a 1:1 mixture of CO_2 and H_2S to COS [5]. Alkali salts of phosphoric and sulfuric acid were used as sorbents for water. The pressures applied were between 5 and 25 bar and temperatures were between 100 and 350°C. A yield to COS of 11% was obtained at 240°C and 10 bar. In another process, Ce-oxides were used as catalysts. The product stream was recirculated through the catalyst bed up to 15 times, while the water formed was externally removed [11]. A more recent process employed zeolites (NaX) as catalysts and sorbents [12]. In all processes using CO_2, water has to be separated from the reactant and product stream to avoid thermodynamic limitations.

Surprisingly, the production of COS in the presence of H_2 in the reaction system starting with CO or CO_2 as C source and liquid or gaseous elemental sulfur has not been explored. The aim of this work was to investigate this reaction route to COS. It has been of special interest how the presence of H_2S and H_2S_x species formed in situ influences the reaction network.

2.2. Experimental

2.2.1. Synthesis of catalysts

Two sulfide-based catalysts derived from oxide precursors, i.e., $CoO-K_2MoO_4/SiO_2$ and NiO/Al_2O_3, were tested for the synthesis of COS. All of them were prepared by the incipient wetness impregnation method. Typically, the desired amount of salt was dissolved in distilled water and added dropwise to the alumina (Aeroxide Alu C; Degussa) or silica (Aerosil 200; Degussa) support. The precursor salts were cobalt nitrate hexahydrate ($Co(NO_3)_2 \cdot 6H_2O$; Fluka), nickel nitrate hexahydrate ($Ni(NO_3)_2 \cdot 6H_2O$; Fluka) and potassium molybdate (K_2MoO_4; Aldrich). After impregnation, the oxidic forms of the catalysts were dried at 80°C over night and afterwards calcined at 500°C in synthetic air for 12 h.

2.2.2. Thermodynamic calculations

Thermodynamic calculations were performed using the HSC Chemistry 5.1 software.

2.2.3. Activity tests

The reactions were carried out in a semi-batch tank reactor, depicted in Fig. 2.1. As elemental liquid sulfur and sulfur vapor are extremely corrosive, the cylindrical reaction chamber (b) (30 mm diameter, 100 mm height) was made from V4-stainless steel which permits a reasonably long life of the reactor at the temperatures and pressures applied to the system (140–500°C, 10-40 bar). The reactant gases were mixed prior to entering the reaction chamber through an immersion tube (c) made of Hastelloy C, which introduced the gaseous educts into the liquid sulfur phase. The flow rates were controlled by Bronkhorst F201C mass flow controllers, the pressure of the system was controlled by a Bronkhorst P612C backpressure regulator. Above the reaction chamber, a sulfur condenser was applied to cool

the gas leaving the condensed phase to 140°C. A thermocouple sealed in a Hastelloy C tube (d) was inserted into the liquid phase to monitor its temperature. In the experiments, the loaded reactor was first heated to the desired temperature under a flow of 5 ml/min N_2. After 30 min at this temperature, the feed gas mixture was bubbled through the liquid sulfur. The outlet gases were analyzed by gas chromatography, using a Shimadzu GC 2014 equipped with a packed Haysep Q and a packed molecular sieve (13X) column. All the gases were supplied by Air Liquide. The measurements were taken after steady state of the system was achieved.
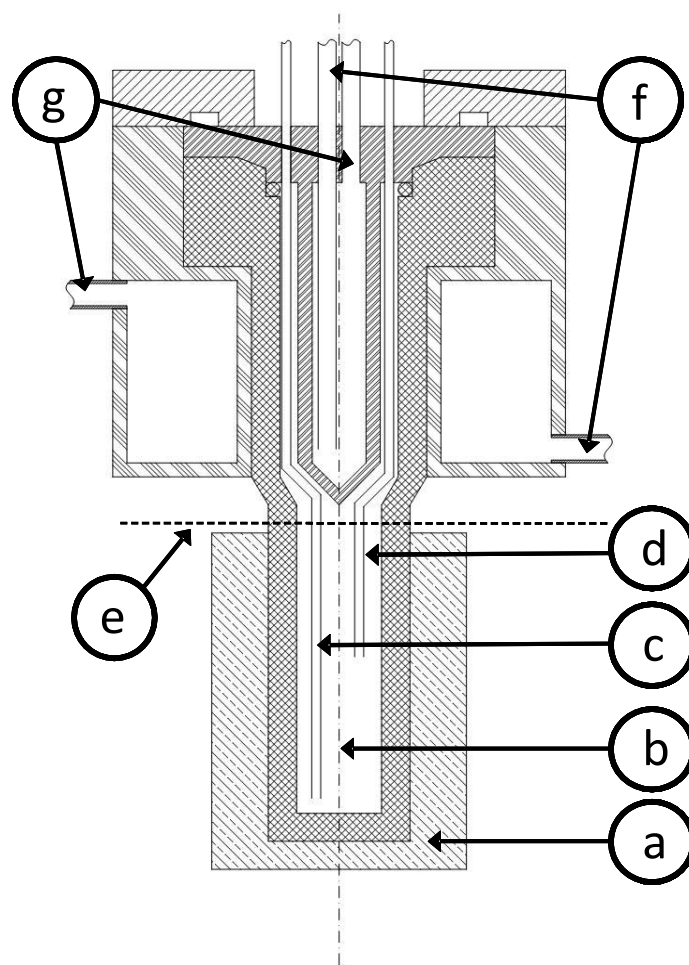
Figure 2.1: Scheme of the reactor. *a* oven, *b* reaction chamber, *c* immersion tube for educts inlet, *d* thermocouple, *e* sulfur level at beginning of each experiment, *f* coolant inlets, *g* coolant outlets.

Several catalysts forming slurry with liquid sulfur were tested for the reaction between liquid sulfur and a mixture of CO and H_2. These reactions were carried out in the temperature

range of 150-350°C at 30 bar with reactant flow rates of 3 and 18 mL/min for CO and H_2 respectively. To evaluate the effect of hydrogen, two series of experiments were conducted at 30 bar, while the temperature of the liquid sulfur phase varied between 250°C and 450°C. In the first set of experiments, CO and H_2 were passed through the liquid sulfur phase at a ratio of 1/6 (the flow rates were 3 and 18 mL/min for CO and H_2, respectively), whereas in the second set of experiments, H_2 was replaced by N_2. To explore the effect of pressure, the reactant flow rates were 3 and 18 mL/min for CO and H_2, respectively. When the flow rate and H_2/CO ratio were varied, the reaction conditions were kept constant at 350°C and 30 bar. Several experiments were conducted to evaluate the formation of COS from CO_2 and H_2 in liquid sulfur. In those experiments, 20% CO_2 in H_2 was used as reactant. The overall flow rate was 9.45 mL/min and the pressure was varied from 10 to 40 bar. The residence time was defined as V/ν where V is the volume inside the reactor below the cooling zone (75 mL) and ν is the volumetric flow rate, calculated for every set of experimental parameters under the assumption of ideal gas law.

2.3. Results

The formation of COS by reacting CO and CO_2 with molten sulfur has been investigated at temperatures between 250 and 500°C and pressures between 10 and 40 bar as well as in the presence and absence of H_2. The formation of SO_x type compounds or other species that are reported for the Claus process [13,14] was not observed. This is attributed to the fact that the present reaction conditions are significantly milder than those used in the Claus process (900-1200°C). In addition, in the more reducing environment in which the reactions take place, oxidation products of sulfur cannot form.

2.3.1. Formation of COS from CO, effect of catalyst

The activities of several catalysts in the synthesis of COS from CO and liquid sulfur in the presence of hydrogen were compared. The only products detected were H_2S, COS, CO_2 and CS_2. Conversion of CO and the yields to the products at 350°C are shown in Table 2.1. In all experiments, conversions of CO were nearly identical (88-92%) as well as the yields towards COS (84-86%). The yields to CO_2 and CS_2 were both approximately 2%. Obviously, no significant influence of the applied catalysts was observed. Therefore, all experiments discussed in the following, were conducted without using a catalyst.

Table 2.1: Product yields and conversion of CO for the reaction between CO, H_2 and liquid sulfur[a].

Catalyst	Amount (mg)	Yield (%)			Conversion of CO[b] (%)		
		COS	CO_2	CS_2	250	300	350
-	-	86.5	2.6	3.1	46.0	69.0	92.2
c	1500	84.7	2.3	2.0	44.5	66.0	89.0
d	500	84.3	1.6	1.8	43.0	65.6	87.7

[a] 30 bar, H_2/CO ratio: 6, residence time: 50 min
[b] At different temperatures (°C)
[c] CoO(2.9 wt%)/K_2MoO_4(28 wt%)/SiO_2
[d] NiO(19 wt%)/Al_2O_3

2.3.2. Formation of COS from CO, effect of H_2 and total pressure

The conversion of CO in the presence and absence of H_2 is compiled together with the conversion of hydrogen in Table 2.2, the respective yields to COS, CO_2 and CS_2 are depicted in Fig. 2.2. In the absence of hydrogen, below 250°C, the reaction proceeded very slowly leading to conversions of CO not exceeding 5%. Above 300°C, the conversion increased rapidly and COS yield reached the maximum of 88% at 400°C.

Table 2.2: Conversions of CO in liquid sulfur using N_2 + CO and H_2 + CO[a].

T (°C)	N_2 + CO	H_2 + CO	
	Conversion (%)	Conversion (%)	
	CO	CO	H_2
250	4.1	50.6	17.9
300	11.7	82.7	42.7
350	68.6	88.2	76.7
400	96.9	89.7	97.9
450	98.8	n.d.[b]	n.d.[b]

[a] 30 bar, H2/CO ratio: 6
[b] n.d. Not determined
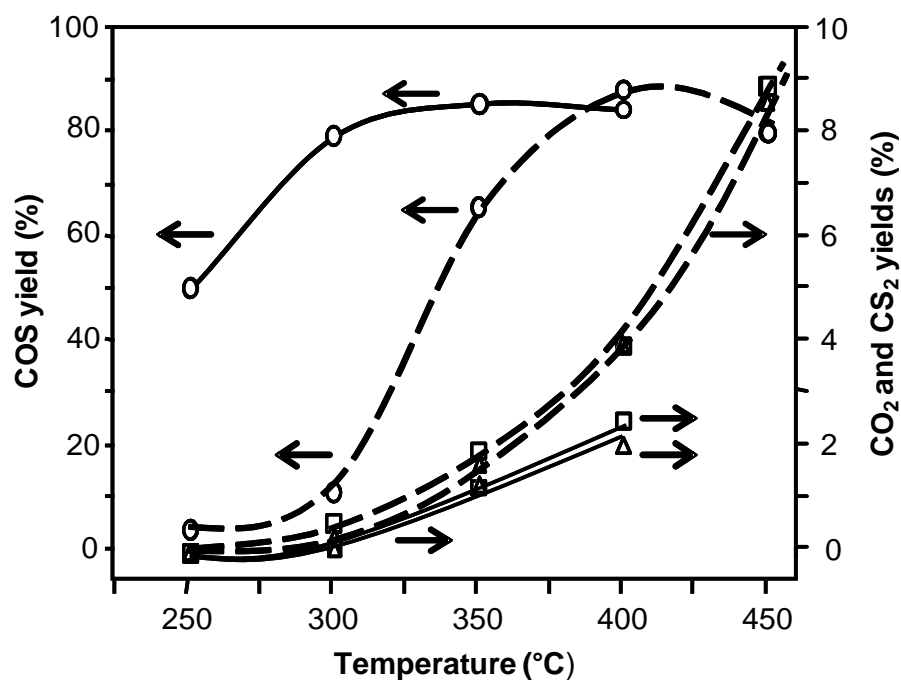
Figure 2.2: Yields to COS (circle), CO_2 (triangle) and CS_2 (square) at 30 bar in the absence of H_2 (dashed lines) and in the presence of H_2 (continuous lines).

In the presence of H_2, trace amounts of methyl mercaptan were also detected as additional byproduct. The conversion of CO below 350°C was drastically improved by the presence of H_2 (see Table 2.2), whereas the maximum yield to COS (about 85%) was obtained at 350°C. The yields to CS_2 and CO_2 were slightly lower than in the absence of H_2. Conversions of CO and product yields of the reaction between CO and liquid sulfur in the presence of hydrogen at several pressures (thus, residence times) are compiled in Table 2.3.

Increasing the pressure from 10 to 30 bar increased the residence time from 16.8 to 50.4 min and the conversion of CO from 51.4 to 92.2%. Further pressure increments led to higher residence times but only to minor changes in the conversion of CO and the yield to COS, which were already above 85 and 90%, respectively, at 30 bar.

Table 2.3: Conversion of CO and yields as function of pressure[a].

Pressure (bar)	Residence time (min)	Conversion (%)	Yield (%)		
		CO	COS	CO_2	CS_2
10	16.8	51.4	50.4	0.2	0.8
20	33.6	84.5	80.8	1.6	2.1
30	50.4	92.2	86.5	2.6	3.1

[a] 350°C, H_2/CO ratio: 6

2.3.3. Formation of COS from CO, effect of residence time and H_2/CO ratio

The impact of residence time and H_2/CO ratio was further tested with respect to the formation of COS; the results are presented in Table 2.4. It was observed that varying the residence time while keeping the H_2/CO ratio constant or vice versa hardly changed the conversion of CO and the product distribution. However, a trend could be noticed: as the H_2/CO ratio was lowered, the conversion of CO slightly increased. It varied from 84.6-86.5% to 94.9% by changing the H_2/CO ratio from 6 to 0.7.

Table 2.4: Conversion of CO and product yields at different residence times and H_2/CO ratios[a].

Residence time (min)	H_2/CO ratio	Reactant composition (mL/min)			Yield (%)			Conversion (%)
		N_2	H_2	CO	COS	CO_2	CS_2	CO
72.0	6.0	0	12.6	2.1	84.6	1.6	1.7	89.5
50.0	6.0	0	18.0	3.0	86.5	1.6	2.1	87.6
42.1	4.0	10.1	12.0	3.0	90.8	0.2	0.3	91.0
42.1	1.0	19.1	3.0	3.0	92.4	0.3	0.5	93.0
42.1	0.7	20.0	2.2	3.0	94.9	0.2	0.2	95.0

2.3.4. Formation of COS from CO_2, H_2 and liquid sulfur

The only carbon-containing products formed in the reaction originating from CO_2 were COS and CO. The corresponding concentrations of water were also detected. As shown in Fig. 2.3, the conversion of CO_2 increased with increasing temperature and pressure. The increase in the conversion of CO_2 with pressure was significant up to 30 bar and only of minor influence above. The selectivity to COS and CO is shown in Fig. 2.4. Interestingly, the selectivity to CO and COS were exact counterparts at all conditions applied, the higher the selectivity to CO, the lower the selectivity to COS and vice versa. The selectivity graphs are symmetric along an imaginary horizontal axis at 50%.
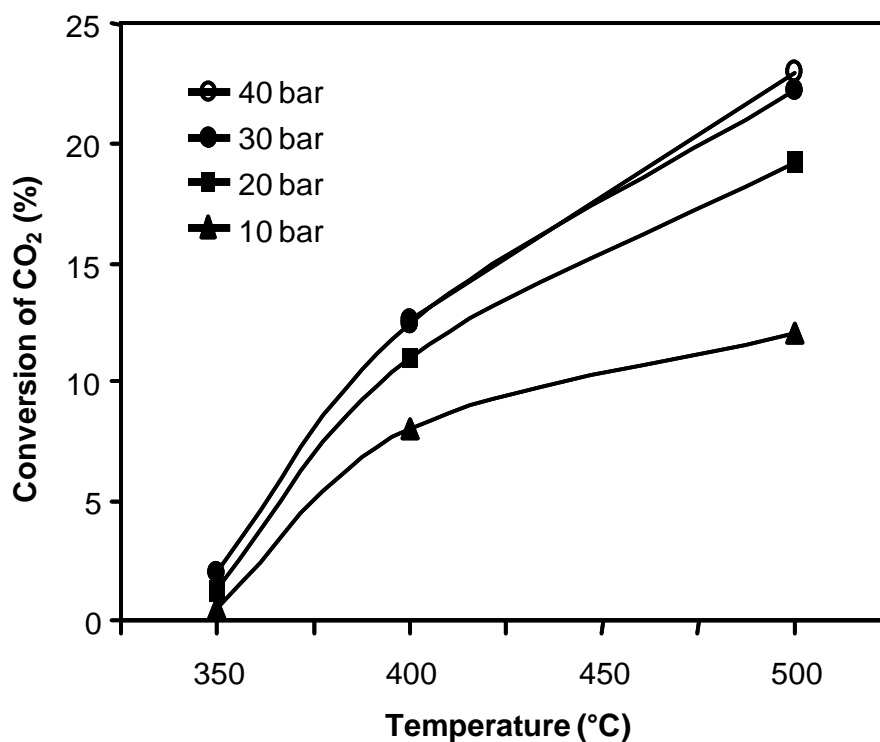
Figure 2.3: Conversion of CO_2 at different temperatures and pressures. Overall flow 9.45 mL/min and H_2/CO_2 ratio of 4.
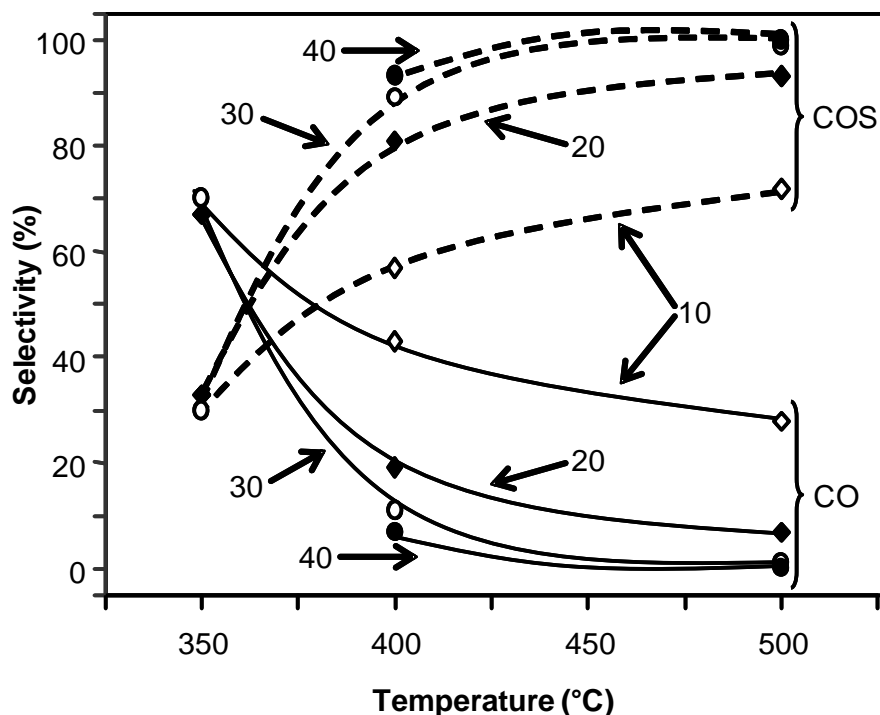
Figure 2.4: Selectivity to COS (dashed lines) and CO (continuous lines) as a function of temperature at pressures of 10, 20, 30 and 40 bar. Overall flow rate of 9.45 mL/min and H_2/CO_2 ratio of 4.

2.4. Discussion

2.4.1. Description of the reaction media

In order to explain the chemistry observed, the complex composition of gaseous and liquid sulfur [15,16] needs to be discussed briefly first. Figure 2.5 shows the composition of liquid and gaseous sulfur equilibrated at 1.13 bar. The data corresponding to the liquid phase were obtained by HPLC of quenched sulfur samples by Steudel et al. [17]. The sulfur gas composition was measured by Berkowitz and Marquart using mass spectrometry [18]. These experimental findings showed that in the gas phase the dominant species are sulfur rings with five to eight atoms; these species were concluded to be cyclic [19]. Below 320°C, gaseous sulfur is mainly composed of S_8 rings, whereas above that temperature, S_5, S_6 and S_7 rings become the most abundant species. The amount of small molecules (S_2, S_3 and S_4), which are sulfur chains, remains below 2 mol% in the whole temperature range shown in Fig. 2.5. Liquid sulfur is composed of homocyclic rings consisting of 6–35 atoms as well as diradical chains with a widely varying number of sulfur atoms. The properties of liquid sulfur are quite

different from those described for the gas phase, S_8 rings are the most abundant sulfur species, whereas the concentration of other rings is rather low, i.e., less than 7 mol% for S_6 and S_7 species together and about 2 mol% for bigger cycles (S_9–S_{23}).

The second main constituent of liquid sulfur is polymeric sulfur (denoted in Fig. 2.5 as $S\mu$) composed mainly of diradical chains with a number of S atoms ranging from 3 (thiozone, S_3) to thousands.
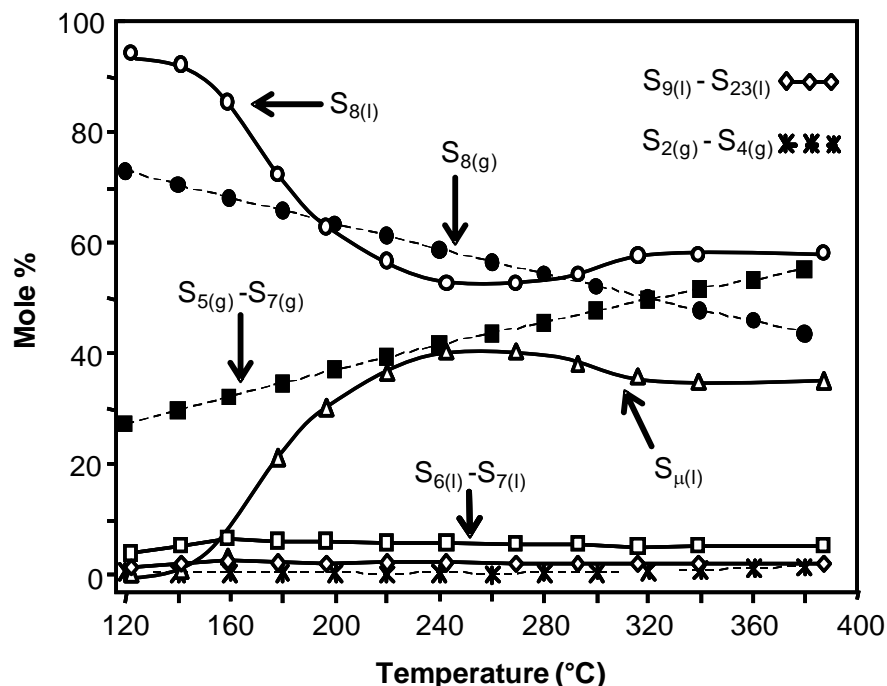
Figure 2.5: Mole composition (%) of equilibrated liquid (continuous lines) and gaseous (dashed lines) sulfur at 1.13 bar.

As observed in Fig. 2.5, the proportion of sulfur species in the gas phase changes steadily with temperature; however, sulfur rings are, by far, the most abundant species in the temperature range shown in the figure. In contrast, in liquid sulfur, the proportion of different sulfur species can significantly vary in a narrow temperature range [16]. Below ~159°C, the so-called ''transition temperature'', more than 90 mol% of liquid sulfur is composed of rings containing eight sulfur atoms [20,21]. Above the transition temperature, the concentration of polymeric sulfur chains increases at the expense of the rings with increasing temperature reaching a maximum at 250°C [22]. Furthermore, the average length of polymeric sulfur also changes to a great extent. Figure 2.6 shows a comparison between the $S\mu$ proportion experimentally found by Steudel et al. [17] and that theoretically determined by Touro and

Wiewiorowski [23]; both results are well in line. Touro and Wiewiorowski also determined the variation in the average sulfur chain length with temperature (denoted in Fig. 2.6 as number of sulfur atoms, *n*). The inset in Fig. 2.6 shows that the average sulfur chain length increases by four orders in magnitude around the transition temperature. Such variations in composition cause major changes in the physicochemical properties [16]. The most pronounced effect is that the viscosity increases rapidly by two orders of magnitude [15]. On the other hand, at temperatures above 250°C, liquid sulfur becomes highly reactive due to a significant presence of S_3, thiozone and other small agglomerates [24,25].
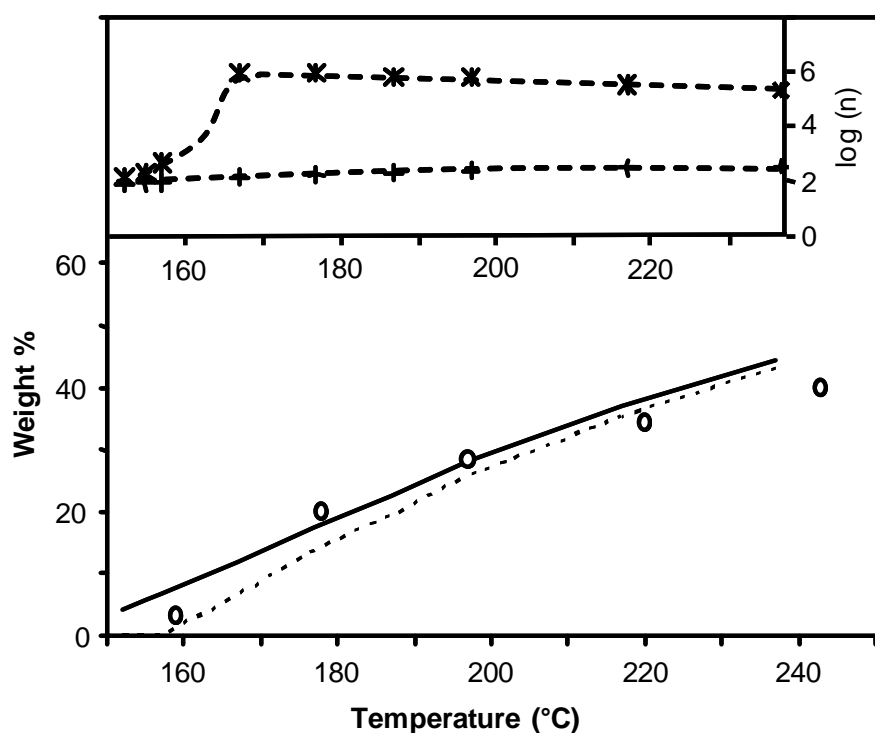
Figure 2.6: Weight % of polymeric sulfur experimentally reported in reference [17] for pure liquid sulfur (o) and calculated in reference [23] for pure liquid sulfur (dashed line) and polysulfanes in sulfur (continuous line). The inset shows the average number of sulfur atoms (*n*) in the sulfur chains of pure sulfur (*) and polysulfanes in sulfur (+).

The description of liquid sulfur becomes more complex in the presence of compounds like H_2S which can chemically interact with liquid sulfur, and thus change its physicochemical properties [16,26]. Figure 2.7 shows the solubility of H_2S in liquid sulfur as reported by Fanelli [15], starting from the melting point of sulfur (125°C at 1 bar). The solubility of H_2S in liquid sulfur increases with increasing temperature and passes through a broad maximum

between 200 and 385°C. Above 385°C, H_2S solubility declines to its lowest level near the boiling point of sulfur (445°C at 1 bar). The reason for this unusual behavior (solubility of gases in liquids decreases with temperature) is that H_2S reacts with sulfur - forming polysulfanes H_2S_x according to reaction (I) [27]. Hydrogen can also induce the formation of H_2S and polysulfanes via reaction (II).

$$H_2S + S_x \rightleftharpoons H_2S_{x+1} \qquad \text{(I)}$$

$$H_2 + S_x \rightleftharpoons H_2S_x \qquad \text{(II)}$$

Polysulfanes are chain-like H_2S_x molecules with x varying from 2 up to at least 35 [28]. The shorter the chain length, the more stable is the polysulfane molecule [29]. Touro and Wiewiorowski [23] determined the solubility of H_2S present in the form of monosulfide and found the behavior shown in Fig. 2.7 by the continuous line.
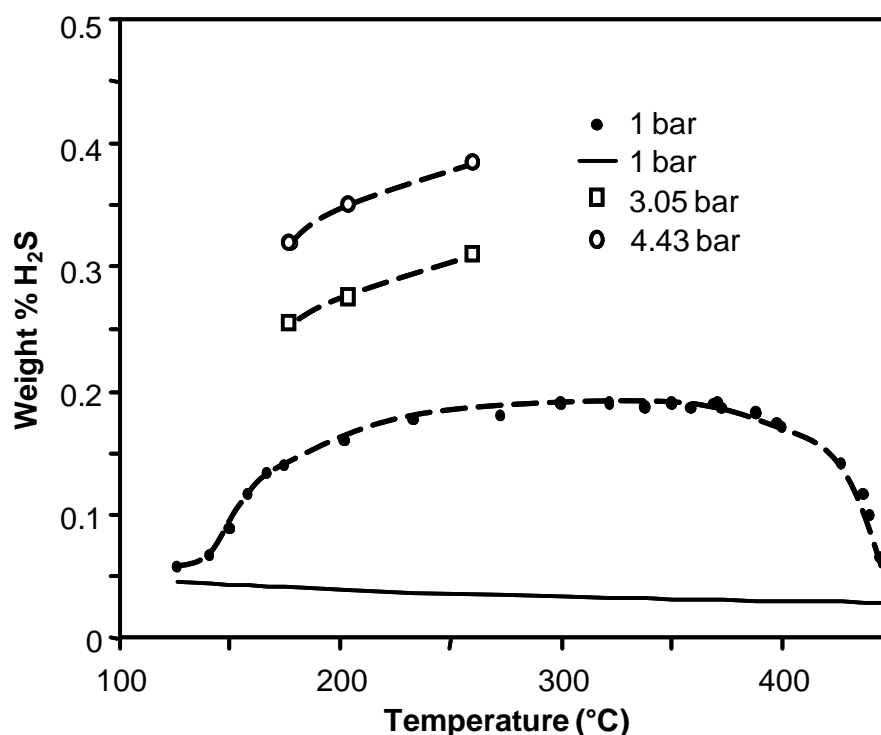
Figure 2.7: H_2S solubility (weight %) in liquid sulfur reported at 1 bar in reference [15] and at 3.05 and 4.43 bar reported in reference [30]. The continuous line corresponds to the amount of H_2S solubilized in liquid sulfur without forming polysulfanes [23].

Evidently, the concentration of H_2S present in the form of H_2S_x is higher than that of the monosulfide. Rubero [30] reported the H_2S solubility in liquid sulfur at pressures higher than atmospheric. These data are compared with Fanelli's results in Fig. 2.7. The weight percent of H_2S in sulfur increases about 72 and 117% by increasing the pressure from 1 to 3.05 and 4.43 bar, respectively. Unfortunately, solubility of H_2S at higher pressures cannot be found in the literature, but it can be assumed that the behavior at ambient pressures represents the lower boundary of the solubility and that the pressure used in this report (10-40 bar) should greatly increase the concentration of polysulfanes in liquid sulfur.

H_2S reduces the proportion and average length of sulfur chains as shown in Fig. 2.6 for which the data were taken from reference [27]. The difference between the polymeric sulfur proportion in the presence and absence of H_2S is low and decreases with temperature; however, the effect on the average length of the sulfur chains is very strong. In the inset of Fig. 2.6, it is obvious that in the sulfur-polysulfane system the average number of atoms in the sulfur chains hardly changes even around the transition temperature. Consequently, at a given temperature, the proportion of sulfur chains in the sulfur-polysulfane system is similar to that in liquid sulfur; however, in the polysulfane system, such chains are much shorter than in liquid sulfur.

Given that polysulfanes are unstable and tend to decompose quickly into sulfur and H_2S, there are no studies concerning the equilibrium characteristics of the sulfur-polysulfane system. The knowledge of polysulfane properties is limited to the shortest polysulfane compounds with 2–5 sulfur atoms [28].

Féher and Hitzemann determined the vapor pressure of polysulfanes from H_2S_2 to H_2S_5 at 20°C as well as the corresponding enthalpies of evaporation [31]. Using these data, the vapor pressure at several temperatures was determined using the Clausius-Clapeyron equation and compared with the values of equilibrium pressures of the analogous pure sulfur chains taken from the review of Meyer [24]. Both series of values are depicted in Fig. 2.8. Evidently, the vapor pressure of polysulfanes is several orders of magnitude higher than that of the corresponding sulfur chains. Additionally, the vapor pressure of polysulfanes is inversely proportional to the number of sulfur atoms in the chain. Information about the composition of gas equilibrated with the sulfur-polysulfane system is not available in the literature. Data concerning the concentration of sulfur species at high pressures in both systems, pure sulfur and sulfur-polysulfane, were not found. However, qualitatively, it can be stated that increasing pressure should lead to an enrichment of the gas phase with small chain sulfur molecules, whereas the proportion of large sulfur molecules (rings and chains) in the liquid

phase should increase as well. In the sulfur-polysulfane system, the liquid phase containing sulfur chains with a smaller average length and exhibiting a higher vapor pressure than the pure sulfur counterpart should increase the proportion of small chain sulfur molecules in the gas phase.
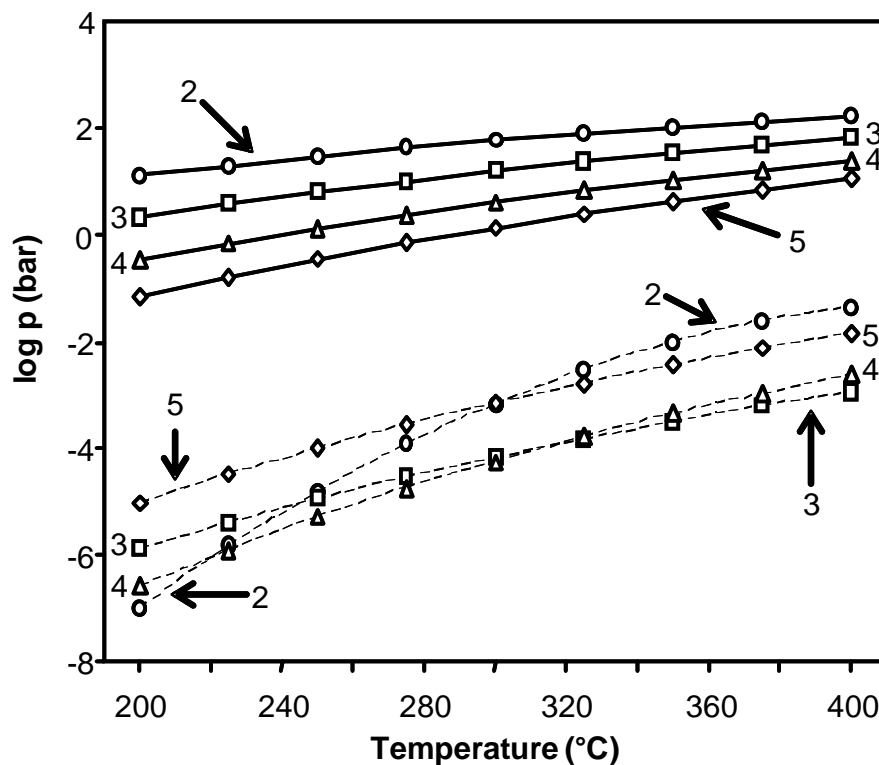
Figure 2.8: Vapor pressure of polysulfanes (continuous lines) and pure sulfur chains (dashed lines) containing from 2–5 sulfur atoms (the number of atoms is depicted in the figure).

2.4.2. Reaction network

In the absence of hydrogen, the reaction pathway is well known [2]. CO is directly oxidized by elemental sulfur leading to the formation of COS, as show in Eq. III. COS formed in Eq. III may undergo reverse thermal decomposition to form CO and elemental sulfur or disproportionate to produce secondary products as shown in reaction (IV). The products of reaction (IV), CS_2 and CO_2, were the only two carbon-containing byproducts observed in the experiments originating from CO. The yields of CS_2 and CO_2 are identical in absence of H_2, indicating that both are indeed produced via disproportionation of COS.

$$CO + S \rightleftharpoons COS \qquad \text{(III)}$$

$$2\,COS \rightleftharpoons CO_2 + CS_2 \qquad \text{(IV)}$$
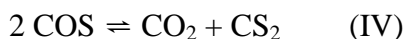
In the presence of hydrogen, apart from the route in Eq. (III), two alternative routes for the formation of COS exist. First, hydrogen is oxidized by elemental sulfur to form H_2S according to Eq. V. Then, H_2S reacts directly with CO to produce COS and H_2 as shown in Eq. VI. The second alternative is that polysulfanes formed via reaction (I) or (II) react with CO to form COS according to reaction (VII).

$$H_2 + S_x \rightleftharpoons H_2S + S_{x\text{-}1} \qquad \text{(V)}$$

$$CO + H_2S \rightleftharpoons COS + H_2 \qquad \text{(VI)}$$

$$CO + H_2S_x \rightleftharpoons COS + H_2S_{x\text{-}1} \qquad \text{(VII)}$$
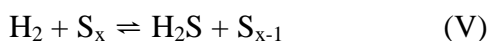
In Table 2.2, it was shown that hydrogen conversion increased with temperature reaching values higher than 70% at temperatures above 300°C. However, further increasing the H_2/CO ratio resulted in a decrease in the yield to COS and in the conversion of CO as shown in Table 2.4. From both observations, it can be deduced that sulfane synthesis (reactions II and V), which should be enhanced by H_2, is rather fast. Furthermore, data in Table 2.4 suggested that the rate of COS formation can be lower than that of the corresponding reverse reaction (VI) at H_2-rich conditions given that decreasing the H_2/CO ratio improved the yield to COS and the apparent CO conversion.

In the case of the experiments starting from CO_2, the direct reaction of CO_2 with H_2S is shown in Eq. VIII. The formation of CO from the reverse water gas shift reaction shown in Eq. IX is also possible. The following steps correspond to reactions (III) or (VI)-(VII), in which CO reacts with elemental sulfur, H_2S or polysulfanes to form COS. The data presented in Fig. 2.4 show that the amount of CO transformed by increasing pressure and temperature corresponds to the amount of COS produced. Thus, the rate of reaction (VIII) is concluded to be negligible compared to that of the reaction pathway induced by the reverse water gas shift.

$$CO_2 + H_2S \rightleftharpoons COS + H_2O \qquad \text{(VIII)}$$

$$CO_2 + H_2 \rightleftharpoons CO + H_2O \qquad \text{(IX)}$$
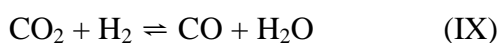
Figure 2.9 shows the conversion of CO_2 with increasing temperature at several pressures predicted by thermodynamics, when the reactant gas mixture has a H_2/CO_2 ratio of 4. For

comparative purposes, the experimental data are also shown. The predicted conversion of CO_2 decreases by increasing the total pressure, which is the opposite trend to what was experimentally observed. In fact, at high pressures, the conversion of CO_2 was higher than that thermodynamically expected for the isolated reactions. This apparent discrepancy can be explained by the formation of COS from CO, which shifts the equilibrium of (IX) to the product side. From the detection of CO, it can be concluded that the rate of (IX) is higher than the rate of COS formation from CO. By increasing temperature and pressure, the selectivity to CO went towards zero which indicates that the rate of COS formation increases faster than the rate of the reverse water gas shift reaction.
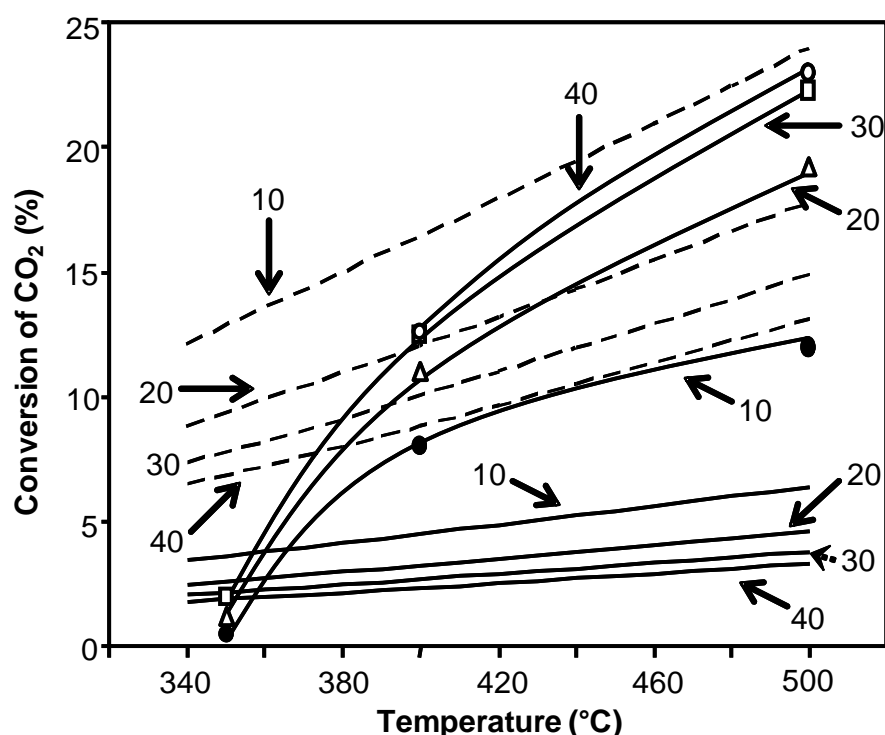
Figure 2.9: CO_2 conversions for (VIII) (continuous lines) and (IX) (dashed lines) thermodynamically allowed at several pressures. The experimental values are represented by the lines marked with symbols.

The reaction network for the formation of COS from CO and CO_2 in presence of hydrogen in liquid sulfur based on the present results is depicted in Fig. 2.10. CO reacts to COS directly with sulfur (III) or by reacting with sulfanes, including H_2S (VI)-(VII). Under certain conditions, COS production could be limited by the reverse reaction (VI), which forms CO and H_2S from COS and H_2. H_2S and polysulfanes are formed in the independent reaction

between H_2 and sulfur (I), (II) and (V). CO_2 either reacts with H_2S directly to form COS and water (VIII) or is converted to CO and water by means of the reverse water gas shift reaction (IX). COS can further form CS_2 and CO_2 via disproportionation (IV).
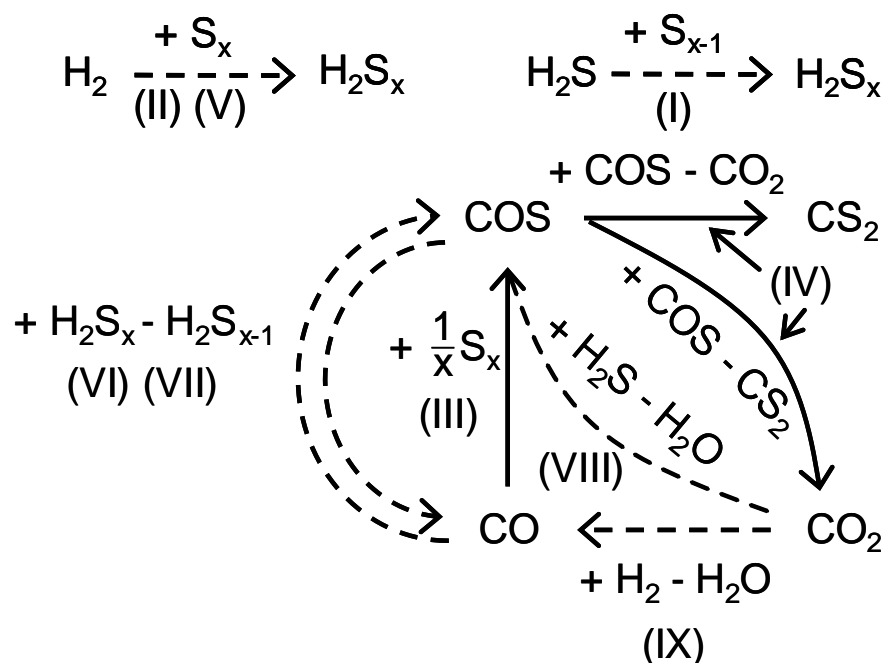
Figure 2.10: Reaction network of CO/CO_2 and sulfur in presence of H_2. Numbers in parentheses correspond to the reactions shown in the text. The dashed lines correspond to the pathways created by the introduction of H_2 into the reaction system.

2.4.3. Role of pressure and liquid sulfur

The beneficial pressure effect on the conversions of CO and CO_2 can be easily explained by the increase in residence time. In Table 2.3, it is shown that increasing pressure from 10 to 40 bar increases the residence time from 16.8 to 83.9 min. Pressure can also affect the properties of the liquid and the gas phase. The higher the pressure, the higher the concentrations of gases in the liquid phase sulfur. This is true especially for H_2S as shown in Fig. 2.7. On the other hand, it is likely that high pressures could also increase the concentration of the more reactive small chain sulfur molecules in the gas phase. Unfortunately, it is not possible to estimate the extent of both effects and, thus, to assert that the reaction system of Fig. 2.10 is taking place preferentially in a single phase.

However, qualitative evidence of a more important role of liquid sulfur than of the gas phase can be given. As described in 2.1., the reported processes for the COS production use CO or CO_2 as carbon sources together with vaporized sulfur. In the present experiments, the temperature of liquid sulfur was varied between 150 and 500°C, while the product gases were quenched to 140°C after leaving the liquid phase. Consequently, the possibility of reactions occurring in the gas phase above liquid sulfur is reduced.

The activity behavior presented in Fig. 2.2 can be better correlated with the changes in liquid sulfur than in the equilibrated gas phase. It was shown in Fig. 2.5 that the proportion of sulfur species with five to eight atoms in the gas phase scarcely changes by increasing temperature. The concentration of these kind of sulfur rings remains always around 98%, whereas the lowering of S_8 ring concentration favoring that of S_6 and S_7 rings occurs steadily. In contrast, the characteristics of liquid sulfur change markedly with temperature. Note in Table 2.2 that in absence of H_2, the conversion of CO suddenly increases above 300°C which corresponds to the temperature at which the presence of more reactive small chains in molten sulfur increases [16].

In the presence of H_2, the sulfur chains in liquid sulfur are shorter on average and are stabilized as shown in Fig. 2.6. Consequently, the CO conversion curve increases steadily. Table 2.2 shows that the conversion of CO increases appreciably in the range 250-300°C, from 50.6 to 82.7%, whereas at temperatures between 300 and 400°C, it increases only by 7%. This behavior is in line with the trend of H_2S solubility in molten sulfur (Fig. 2.7) which hardly increases from 250 to 350°C and then starts to decline. Hence, the conversion of CO by means of reactions (VI)-(VII) is concluded to be limited by the concentration of H_2S in the liquid phase. Another limiting factor for the CO conversion at hydrogen rich conditions or high temperatures could be the thermodynamic equilibrium of the reaction (VI) which consumes COS and H_2 to produce CO.

Two possibilities can be considered to explain the lack of catalytic effect, i.e., the reaction is thermodynamically and not kinetically controlled or the reactants do not interact with the catalyst. In order to differentiate between those two possibilities, a thermodynamic analysis was performed considering a sulfur-rich environment (S_8/CO molar ratios higher than 1). The result showed that CO conversion of 99% can be achieved in presence of H_2. Hence, the absence of catalytic effects cannot be attributed to thermodynamic control. At present, we speculate that the reactants do not interact with the catalyst suspended in liquid sulfur, because the active sites are blocked by strongly adsorbed sulfur species.

2.5. Conclusions

High yields to COS from CO or CO_2 and liquid sulfur can be achieved at 350-400°C in the presence of H_2 without addition of catalysts and water adsorbents. The experimental findings point to the fact that the reactions occur mainly in liquid sulfur. The introduction of hydrogen leads to the formation of polysulfanes, which increase the reactivity of liquid sulfur by shortening the length of linear sulfur species. Furthermore, the formation of COS in the presence of H_2 seems to be limited by the solubility of H_2S in liquid sulfur and at high temperatures, the reaction between COS and H_2 that produces CO. H_2, H_2S and polysulfanes formed in molten sulfur provide alternative reaction routes for the formation of COS from CO and CO_2. The rate of the reverse water gas shift reaction is faster than that of the formation of COS. The rate of the latter, however, increases faster with temperature and pressure. Higher pressures increase residence times and the concentration of the reactant gases in liquid sulfur. Starting from CO, stable and high yields to COS (>90%) are obtained at various reaction conditions. By using CO_2 as carbon source, the reaction proceeds via the reverse water gas shift reaction, with CO being a reaction intermediate.

2.6. References

[1]   M. Beck, G. Kauffman, Polyhedron 4, 775 (1985).

[2]   T. Carnelley, J. Chem. Soc. 28, 523 (1876).

[3]   G. Rühl, H. Schmitt, De. Pat. 953, 696 (1956).

[4]   G. Kerr, De. Pat., 1 136 316 (1960).

[5]   C. Parish, K. Urmy, US Pat., 3 416 893 (1968).

[6]   P. Svoronos, T. Bruno, Ind. Eng. Chem. Res. 41, 5321 (2002).

[7]   R. Ferm, Chem. Rev. 57, 621 (1957).

[8]   A. Mittasch, E. Willfroth, De. Pat., 398 322 (1924).

[9]   T. Kanazawa, S. Ogawa, S. Matsui, S. Masamichi, GB Pat., 1320 446 (1971).

[10] K. Büchler, K. Lienhard, De. Pat., 1 222 024 (1961).

[11] A. Böhm, K.-H. Schmidt, V. Schulze, De. Pat., 1 196 624 (1959).

[12] W. Lutz, P. Fellmuth, M. Bu¨low, F. Zobel, B. Kurzmann, Dd. Pat., 241 245 (1986).

[13] P. Clark, N. Dowling, M. Huang, W. Svrcek, W. Monnery,
    Ind. Eng. Chem. Res. 40, 497 (2001).

[14] I. Gargurevich, Ind. Eng. Chem. Res. 44, 7706 (2005).

[15] R. Fanelli, Ind. Eng. Chem. 41, 2031 (1949).

[16] R. Steudel, Top. Curr. Chem. 230, 81 (2003).

[17] R. Steudel, R. Strauss, Z. Fresenius', Anal. Chem. 326, 543 (1987).

[18] J. Berkowitz, J. Marquart, J. Chem. Phys. 39, 275 (1963).

[19] J. Berkowitz, C. Lifshitz, J. Chem. Phys. 48, 4346 (1968).

[20] H. Mäusle, R. Steudel, Z. Anorg. Allg. Chem. 478, 177 (1981).

[21] R. Steudel, R. Strauss, L. Koch, Angew. Chem. 97, 58 (1985).

[22] M. Thackray, J. Chem. Eng. Data 15, 495 (1970).

[23] F. Touro, T. Wiewiorowski, J. Phys. Chem. 70, 239 (1966).

[24] B. Meyer, Chem. Rev. 76, 367 (1976).

[25] B. Meyer, T. Hansen, T. Oommen, J. Mol. Spectrosc. 42, 335 (1972).

[26] H. Uchtmann, S. Kazitsyna, F. Hensel, V. Zdimal, B. Triska, J. Smolík,
    J. Phys. Chem. 105, 11754 (2001).

[27] F. Touro, T. Wiewiorowski, J. Phys. Chem. 70, 234 (1966).

[28] R. Steudel, Top. Curr. Chem. 231, 99 (2003).

[29] J. Hahn, Z. Naturforsch. B 40, 263 (1985).

[30] P. Rubero, J. Chem. Eng. Data 9, 481 (1964).

[31] F. Von Fehér, G. Hitzemann, Z. Anorg. Allg. Chem. 294, 50 (1957).

Chapter 3

Synthesis of methyl mercaptan from

carbonyl sulfide over sulfide K_2MoO_4/SiO_2

The synthesis of methyl mercaptan from COS and H_2 on K^+ promoted MoS_2 supported on silica is explored. The reaction proceeds via the disproportionation of COS to CO_2 and CS_2 and the consecutive hydrogenation of CS_2 to CH_3SH. In parallel to the disproportionation, COS also decomposes to CO and H_2S. The characterization of the catalyst by means of XRD, Raman spectroscopy, and adsorption of NO suggests that two active phases, i.e., relatively pure MoS_2 and K^+-decorated MoS_2, are present in the sulfide catalyst. The disproportionation of COS and the hydrogenation of CS_2 are favored on K^+-decorated MoS_2; the decomposition of COS to CO is the favored route on pure MoS_2. The reaction mechanisms for the decomposition of COS and the hydrogenation of CS_2 are discussed.

3.1. Introduction

Methyl mercaptan is an important chemical commodity widely used in the production of pesticides, pharmaceuticals, petrochemicals, and for material synthesis [1]. The main application of CH_3SH lies in the production of methionine, an amino acid used as an animal feed supplement [2]. With the rapid increase in the demand for methionine over the past 20 years, the demand for CH_3SH has been growing significantly [3]. Therefore, the synthesis of methyl mercaptan has been the subject of several studies and alternative routes for its production have been explored [4-6]. Industrially, methyl mercaptan is produced by thiolation of methanol. In this process, methanol and H_2S are reacted over alkali-promoted transition metal sulfides [1]. Considering that methanol is generated from synthesis gas, Olin et al. [7] proposed first to form CH_3SH directly from carbon oxides, hydrogen, and hydrogen sulfide. The catalysts for those reactions were based on alkali-promoted tungsten or molybdenum sulfides with transition metal oxides as additives [8]. The approach attracted significant interest, because it allowed avoiding the methanol synthesis step [9-14]. It is commonly accepted that the generation of CH_3SH from H_2S-containing syngas proceeds via the formation of carbonyl sulfide (COS) as the primary product and its subsequent hydrogenation to CH_3SH [15-17]. Preliminary experiments with COS as starting agent have indicated, however, that the direct hydrogenation of COS may not be a significant route. The objective of this study was, therefore, to explore the synthesis of methyl mercaptan using COS, H_2, and H_2S as reactants. A two-step approach was adopted to achieve this goal, i.e., the selective production of COS followed by the synthesis of CH_3SH in a separate reactor. The formation of COS by reacting CO and H_2 with elemental liquid sulfur was reported elsewhere [18]. In this first step, CO conversion of 100% with high yield of COS at various reaction conditions was achieved. In the present work, we analyzed the catalytic synthesis of CH_3SH in the presence of H_2S over sulfide K_2MoO_4/SiO_2 by combining physicochemical characterization of the catalyst with detailed kinetic measurements. The thermodynamic equilibria of reactants and products were calculated to explore potential operating conditions.

Thermodynamic considerations

Calculations addressing the formation of CH_3SH from CO, H_2S, and H_2 have been reported by Barrault et al. [15]. Conversion of CO to methyl mercaptan is assumed to proceed via reactions (I) and (II).

$$CO + H_2S \rightleftharpoons COS + H_2 \qquad (I)$$

$$COS + 3H_2 \rightleftharpoons CH_3SH + H_2O \qquad (II)$$

The overall formation of methyl mercaptan from CO is thermodynamically allowed between 448 and 698 K and it is favored at high pressures and excess of H_2S and H_2.
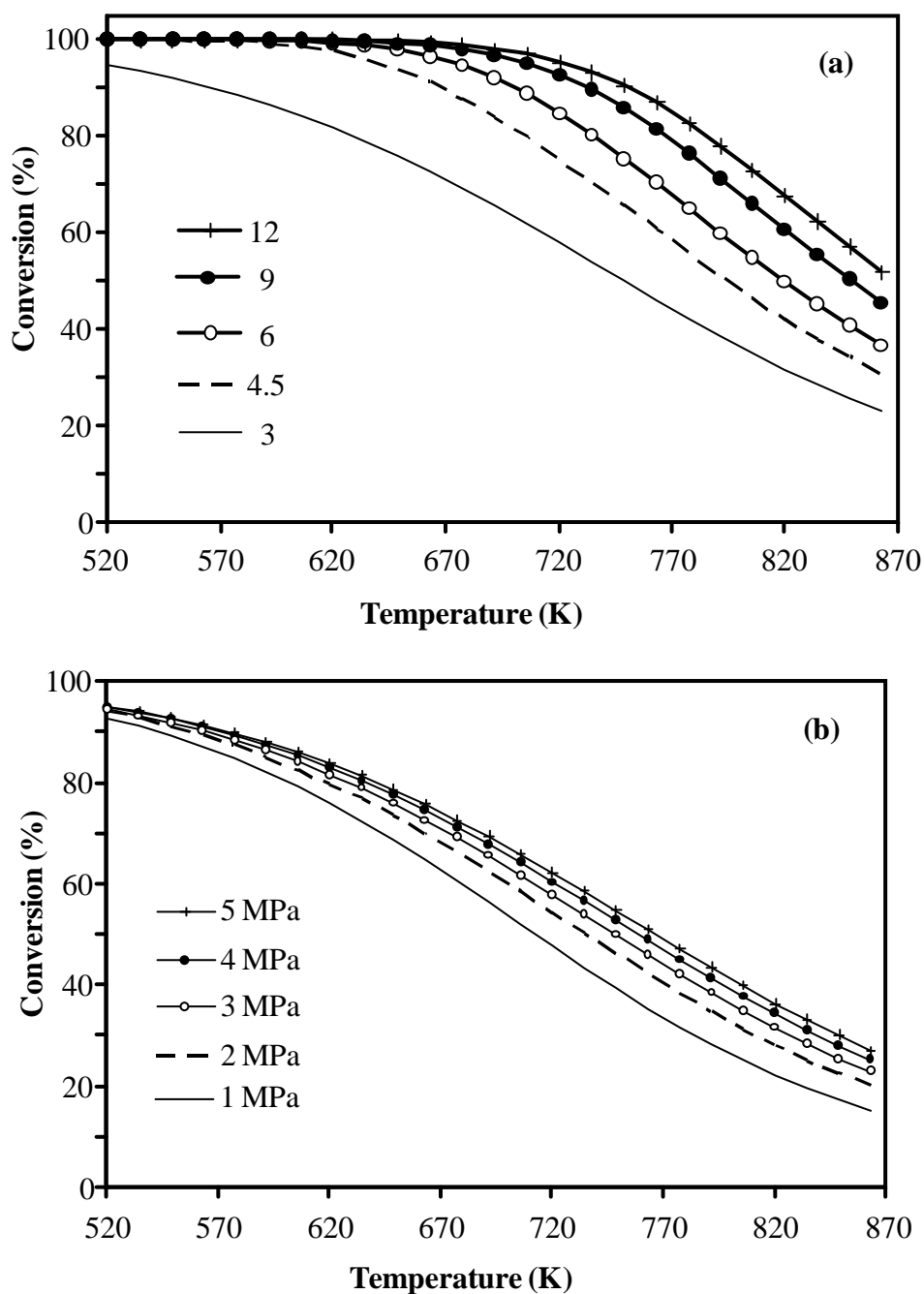
Figure 3.1: Thermodynamically allowed conversion of COS for reaction

$(COS+3H_2 \rightleftharpoons CH_3SH+H_2O)$ at 3 MPa and different H_2/COS ratios (values shown in the figure) (a) and different pressures ($H_2/COS = 3$) (b) over temperature.

Here, only the thermodynamic calculations focusing on step (II) are reported. The conversion of COS as a function of temperature at various H_2/COS ratios and different total pressures is calculated using the HSC Chemistry 5.1 software. The results are compiled in Fig. 3.1.

The lowest COS conversion is calculated for the stoichiometric ratio of H_2/COS = 3 (Fig. 3.1(a)). Higher H_2/COS ratios increase the thermodynamically possible COS conversion. For ratios higher than 4.5, a conversion of nearly 100% is possible up to 673 K. At higher temperatures, the maximum conversion of COS decreases, which is in line with the strongly exothermic nature of reaction (II), (ΔH^0 = -124 kJ/mol). Fig. 3.1(b) shows the dependence of the COS conversion on the temperature at pressures ranging from 1 to 5 MPa. As reaction (II) proceeds, the number of total molecules decreases, and thus high pressures are favorable to maximize conversion. Considering the results of Barrault et al. [15] and the thermodynamic calculations described here, the synthesis of CH_3SH is studied at 3 MPa in the temperature range of 453-673 K with H_2/COS ratios from 2 to 7.

3.2. Experimental

3.2.1. Catalyst preparation and activation

A SiO_2 (AEROSIL$^®$ 90, Degussa) supported molybdenum sulfide catalyst, promoted with a twofold molar potassium excess over molybdenum, was used. The oxide precursor was synthesized by the incipient-wetness impregnation method using an aqueous solution of K_2MoO_4 (Sigma Aldrich, 98%). After impregnation, the catalyst precursor was dried at 353 K overnight and treated at 773 K in synthetic air for 12 h. The loading of K_2MoO_4 on SiO_2 was 28 wt.%. Prior to each activity test, 0.5 g of the catalyst was activated by sulfidation in 10 vol.% H_2S in H_2 at 3 MPa and 673 K for 12 h.

3.2.2. Kinetic measurements

Kinetic measurements were carried out by using two reactors in a serial configuration with a GC connected to the outlet of each reactor to monitor both steps as shown in Fig. 3.2. The first reactor was a semi-batch tank reactor (pre-reactor) used to obtain mixtures of COS and H_2S from the reaction of CO and H_2 (continuous reactants) with liquid sulfur (batch reactant). The configuration of the pre-reactor and the reactions taking place in it were described in

detail elsewhere [18]. In this first step, the feed composition and reaction conditions were adjusted in order to achieve complete CO conversion and the H_2S/COS ratio required to perform the experiments in a subsequent plug-flow reactor with fixed catalyst bed (main reactor). The products from the pre-reactor were mixed with required concentrations of H_2 and N_2 prior to the second reaction step in the main reactor. Feed compositions reported in this work refer to the gas mixture introduced to the main reactor. The gas products were analyzed by gas chromatography using a Shimadzu GC 2014 equipped with a packed Haysep Q and a packed molecular sieve (13X) column.
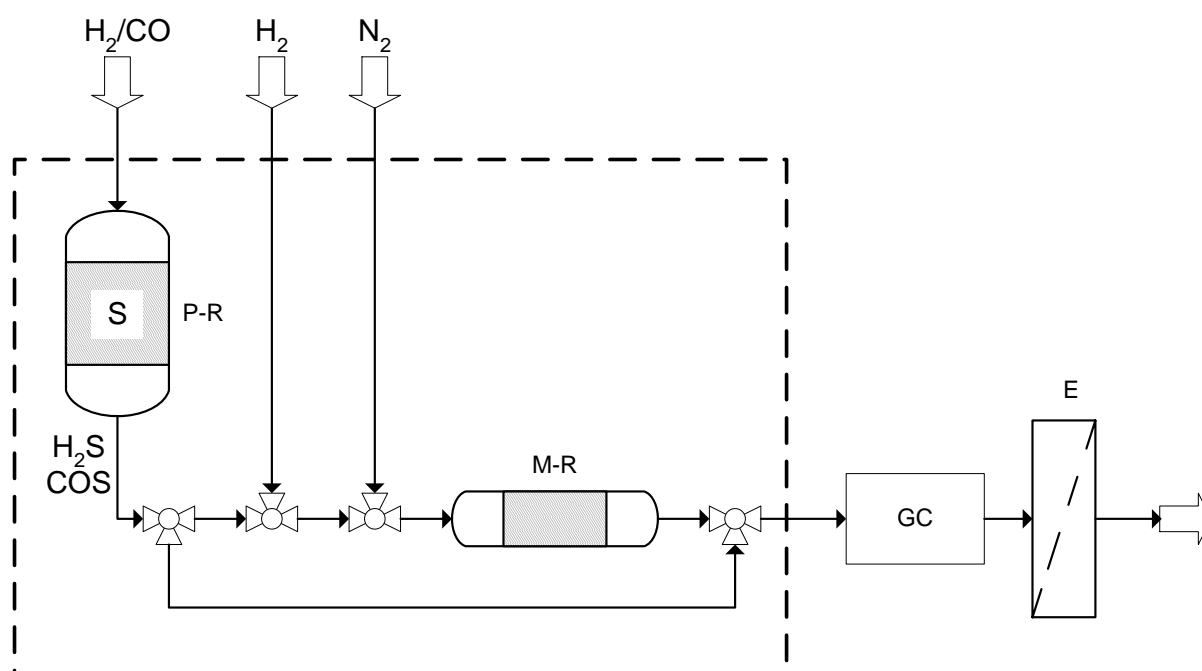
Figure 3.2: Simplified scheme of the reactor system; pre-reactor (P-R) loaded with elemental sulfur; main reactor (M-R); scrubber (E); heating box (dashed line); gas chromatograph (GC).

3.2.2.1. Activity tests at varying H_2/COS and H_2S ratios

In the experiments at varying reactant ratios, the content of COS in the gas mixture was 8.6 vol.%, with N_2 being added to keep an overall reactant flow rate of 37 cm^3/min (residence time of 0.68 s). The H_2/H_2S ratio was held constant at 4.5 to study the effect of the H_2/COS ratio, whereas a fixed H_2/COS ratio of 2.3 was chosen to study the effect of the H_2/H_2S ratio. GC measurements were taken in steps of 15 K from 453 to 673 K after steady state was achieved.

3.2.2.2. Activity tests at varying residence time

The effect of residence time on the reaction was studied at 523 and 598 K using constant ratios of $H_2/COS = 2.3$ and $H_2/H_2S = 2.8$. The mass of the catalyst was held constant (0.5 g), whereas the flow rates were varied in the range 6-60.5 cm^3/min at 598 K and 12-40 cm^3/min at 523 K. Residence time was defined as $\nu/V_{catalyst}$, where ν is the volumetric flow rate and $V_{catalyst}$ is the total volume of the catalyst bed.

3.2.2.3. Activity tests in the absence of H$_2$

Experiments in the absence of H_2 were conducted to obtain a better understanding of the reactions in which COS is involved. At the end of a typical activity test in the presence of H_2, the reactor was flushed thoroughly with N_2 at 673 K to remove all reactants and products. After decreasing the temperature to 437 K, a total flow of 40 cm^3/min of a gas mixture of 8.5 vol.% COS in N_2 was passed through the catalyst bed at 3 MPa. In the first experiment, the temperature was increased from 437 to 673 K in steps of 50 K, and the product was analyzed 5 min after reaching the desired temperature. In the second experiment, the temperature was increased from 437 to 523 K and kept constant for 5 h, and the products were analyzed every 50 min.

3.2.2.4. Catalytic test of bulk MoS$_2$ and sulfided K$_2$MoO$_4$

The sulfided form of bulk MoO_3 and K_2MoO_4 was tested in the reaction of COS with H_2. The reactor was loaded with 0.5 g of the oxide to perform the sulfidation in 10 vol.% H_2S in H_2 at 3 MPa and 673 K for 12 h. The overall reactant flow was 40 cm^3/min with a COS content of 8.6 vol.% and the ratios $H_2/COS = 3$ and $H_2/H_2S = 5.3$. The reaction temperature was increased from 448 to 598 K.

3.2.3. Elemental composition and textural properties

The elemental compositions of the oxide precursor and the used sulfide catalyst were determined by atomic absorption spectroscopy (AAS) using a UNICAM 939 spectrometer. The surface area and pore volume of the catalyst in the oxide and used sulfide forms were determined by nitrogen adsorption-desorption. The measurements were performed on a Porous Materials Incorporated automated BET sorptometer. Before adsorption, the samples were degassed in vacuum at 673 K for 2 h.

3.2.4. Raman spectroscopy

Raman spectra of the samples during the sulfidation-oxidation process were measured placing a sample of the catalyst in a suitable quartz tube reactor. The spectra of the oxide precursor were measured under N_2 at 290 K and under flow of 10 vol.% H_2S in H_2 at 290, 473, and 673 K. After sulfidation, the sample was cooled down to 290 K in N_2. New spectra were measured at 290 and 673 K after replacing N_2 by air. The Raman spectra were recorded on a Renishaw Raman Spectrometer Series 1000 Microscope with an Ar laser of 514 nm wavelength.

3.2.5. X-ray diffraction

The oxide precursor, the sulfide catalyst, and the catalyst used in the reaction were characterized by X-ray diffraction (XRD). Measurement of the sulfide catalyst was performed ex situ, after catalyst sulfidation for 12 h at 673 K and 3 MPa in 10 vol.% H_2S in H_2. A sample of the used catalyst was analyzed by XRD after cooling down the reactor to room temperature keeping the reactant mixture flow. The freshly sulfided catalyst and the sample of used catalyst were placed on a silicon single crystal with a (1 1 1) surface avoiding contact with air. Blank tests did not show any signals originating from the single crystal. A Philips X'Pert Pro System (Cu Kα1-radiation, 0.154056 nm) operating at 45 kV and 40 mA was used for recording XRD. Measurements were carried out using a step size of 0.017°(2θ) and 115 s as count time per step.

3.2.6. NO adsorption

Adsorption of NO on the catalyst was measured at room temperature by a pulse technique using a flow apparatus equipped with a mass spectrometer (QME 200, Pfeiffer Vacuum) as detector. For each experiment, a sample of 0.15 g was loaded in a quartz reactor and sulfided in situ (3 h at 673 K in 10 vol.% H_2S in H_2). In the first experiment, the sample was cooled down to room temperature in the H_2S/H_2 flow after sulfidation. NO pulses were periodically introduced after flushing the reactor with He. In the second experiment, the sample was cooled down to 523 K in the H_2S/H_2 flow after sulfidation and at constant temperature, the H_2S/H_2 flow was replaced by a COS/He mixture. After one hour, the sample was cooled down to room temperature in flowing COS/He. Subsequently, the sample was flushed with He and

the NO pulses were applied at regular intervals. In both experiments, the total amount of adsorbed NO was calculated as the sum of the NO uptakes per pulse.

3.3. Results

3.3.1. Catalyst characterization

3.3.1.1. Composition and textural characteristics

The elemental composition in the oxide precursor determined by AAS analysis were 11.4 and 8.8 wt.% for molybdenum and potassium (corresponding to 5.85 and 11.08 mol%). The concentrations in the precursor mixture during the synthesis step were 11.3 and 9.2 wt.% for molybdenum and potassium, respectively. The oxide precursor has a specific surface area of 50 m^2/g and pore volume of 0.06 cm^3/g.

The elemental composition of the used sulfide catalyst was 8.2, 6.2, and 9.5 wt.% for Mo, K, and S, respectively. Only traces of carbon were detected. The calculated S/Mo mol ratio was therefore 3.5, i.e., higher than the ratio expected for MoS_2 (S/Mo = 2), indicating that some sulfur was also associated with K^+ cations. The surface area and pore volume of the catalyst after reaction were 37 m^2/g and 0.05 cm^3/g, respectively.

3.3.1.2. Raman spectroscopy

Fig. 3.3 shows the Raman spectra of the K_2MoO_4/SiO_2 catalyst recorded at different temperatures during the sulfidation-oxidation process. Spectrum (a) corresponds to the oxide K_2MoO_4/SiO_2 precursor in N_2 at 290 K with all bands being characteristic for K_2MoO_4 [19]. The widths of the bands at 849 and 711 cm^{-1}, however, suggest the presence of $K_2Mo_2O_7$ [20] and this conclusion is in agreement with findings by XRD (see below). New bands at 463 and 485 cm^{-1} after exposure to H_2S/H_2 at 290 K (Spectrum (b)) indicate the formation of K_2MoOS_3 [21]. Maintaining the H_2S/H_2 flow, the temperature was increased to 473 K for Spectrum (c). Bands appeared at 913 and 457 cm^{-1}, which are attributed to K_2MoS_4 [22]. After keeping the H_2/H_2S atmosphere for 4 h at 673 K, MoS_2 is detected as the main phase (450, 408, 382 cm^{-1}) as shown in Fig. 3.3(d). After cooling the sample in N_2 flow to 290 K and applying synthetic air for 10 min, evidence of oxidation is not observed. Bands at 994, 816, 374, 336, 283, 237, and 219 cm^{-1} indicate the formation of MoO_3 after increasing the temperature to 673 K in synthetic air (Spectrum (e)) [23]. The bands at 964, 849 cm^{-1} and those in between correspond to the octamolybdate $K_4Mo_8O_{26}$ [19].
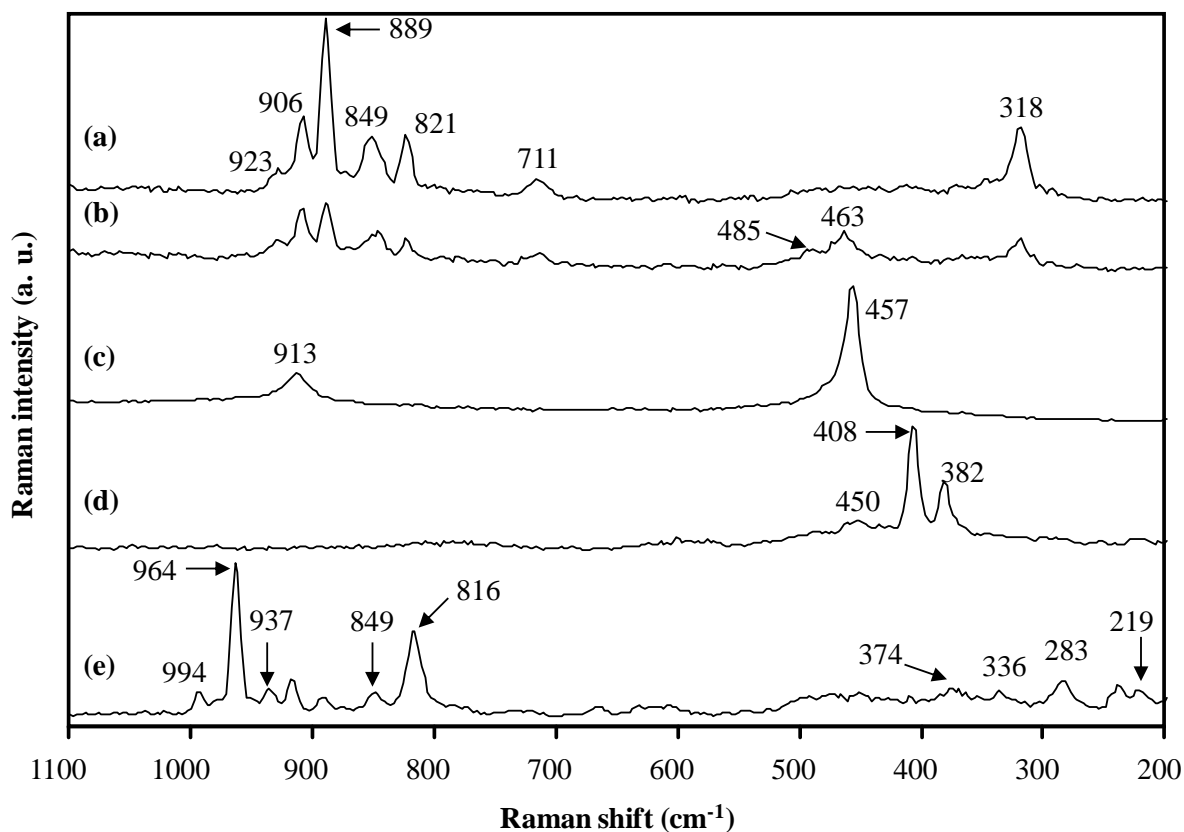
Figure 3.3: Raman spectra of oxide K_2MoO_4/SiO_2 precursor in N_2 at room temperature (a); and after exposure to H_2S/H_2 at room temperature (b); to H_2S/H_2 at 473 K (c); to H_2S/H_2 at 673 K (d); and to synthetic air at 673 K (e).

Detailed spectra of the sulfide catalyst are shown in Fig. 3.4. An example of the Raman spectra observed with the largest fraction of the sample is displayed in Spectrum (a). All bands are attributed to MoS_2 with those at 382, 408, and 450 cm^{-1} being the most intense [24]. The band at 382 cm^{-1} is assigned to the Mo-S stretching mode along the basal plane, while the one at 408 cm^{-1} corresponds to the S-Mo-S stretching mode along the C-axis. The band at 450 cm^{-1} is attributed to a second-order scattering [23]. At few spots of the sample (see Spectrum (b)), the bands at 1825, 1364, 911, 459, and ~200 cm^{-1} indicate the presence of a Resonance Raman Effect (RRE) typical for the MoS_4^{2-} ion [22,25]. Thus, we attribute these bands to K_2MoS_4 unevenly distributed in the solid.

The sequence of Raman spectra with the sulfidation in H_2S/H_2 atmosphere indicates that K_2MoS_4 is the first fully sulfided species formed, which is converted to MoS_2 in the next step. The Raman spectra do not allow deducing the location of all potassium cations. Some potassium cations remain in K_2MoS_4 that is not transformed to MoS_2 as indicated by the Raman spectra of the sulfide catalyst in Fig. 3.4(b). The observation of MoO_3 and

octamolybdates (K/Mo molar ratio of 0.5) after oxidation of the sulfide catalyst, however, suggests partial segregation of potassium from Mo-containing phases.
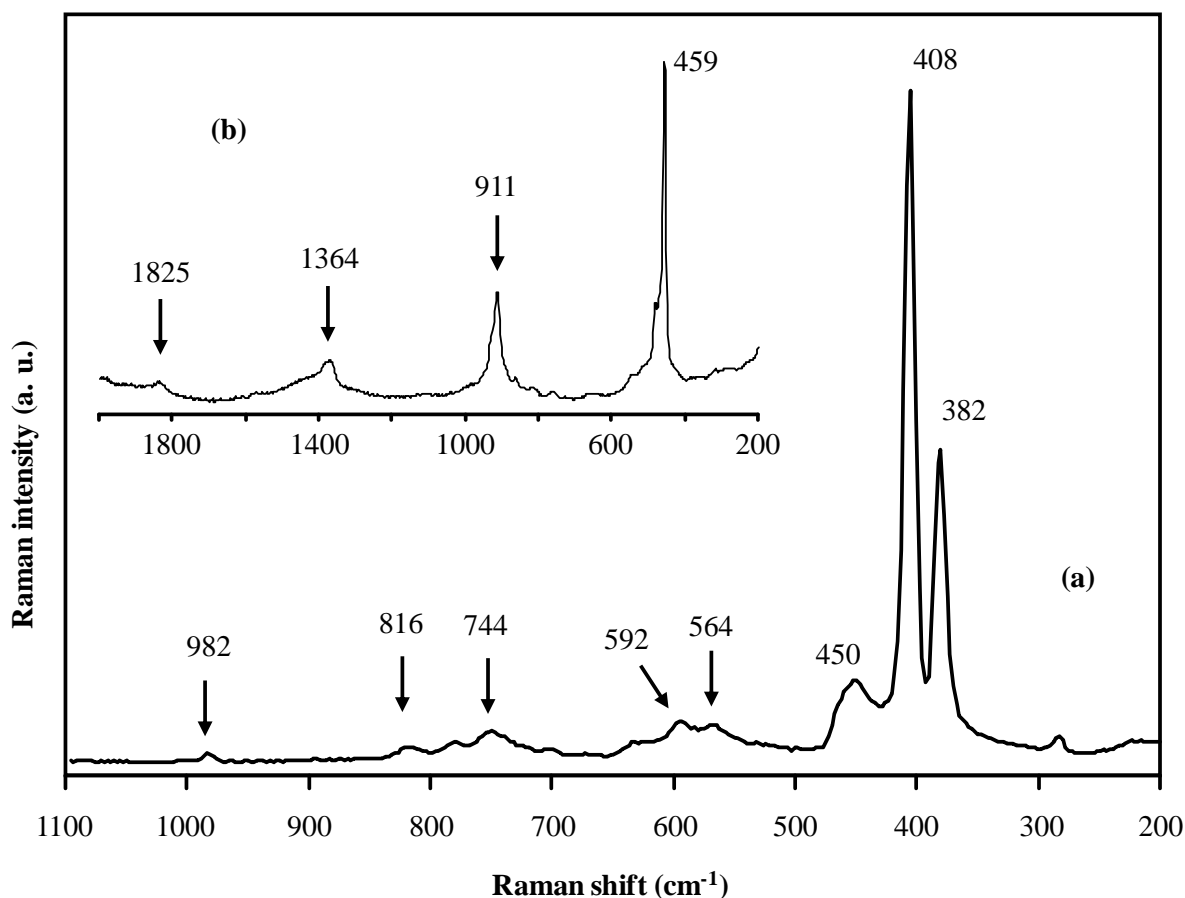
Figure 3.4: Raman spectra of sulfide K_2MoO_4/SiO_2 catalyst observed typically (a) and in few spots of the sample (b).

3.3.1.3. X-ray diffraction measurements

The X-ray diffractograms of the catalyst in the oxide and the sulfide form are shown in Fig. 3.5. The oxide precursor consists of a mixture of K_2MoO_4 (PDF number: 00-024-0880) and $K_2Mo_2O_7$ (PDF number: 00-036-0347), the latter phase is formed during thermal treatment in synthetic air. After sulfidation, most of the signals are characteristic of MoS_2 (PDF number: 00-024-0513). The peak at $10.3°(2\theta)$ cannot be assigned to a defined crystalline structure. We speculate that it corresponds to a K-intercalated MoS_2 (K_xMoS_2, $x < 1$). The position of that peak and the relative intensity of weak signals at 32.5 and $57.5°(2\theta)$ are in accordance with the powder diffraction data reported for intercalated

MoS$_2$ [26]. The formation of K$_x$MoS$_2$ (cationic potassium) takes place by the consecutive reactions (III) and (IV) [27].

$$K_2MoO_4 + 4H_2S \rightarrow K_2MoS_4 + 4H_2O \qquad \text{(III)}$$
$$2K_2MoS_4 + 3H_2 \rightarrow 2K_xMoS_2 + (2 - 2x)K^0 + K_2S + 3H_2S \qquad \text{(IV)}$$
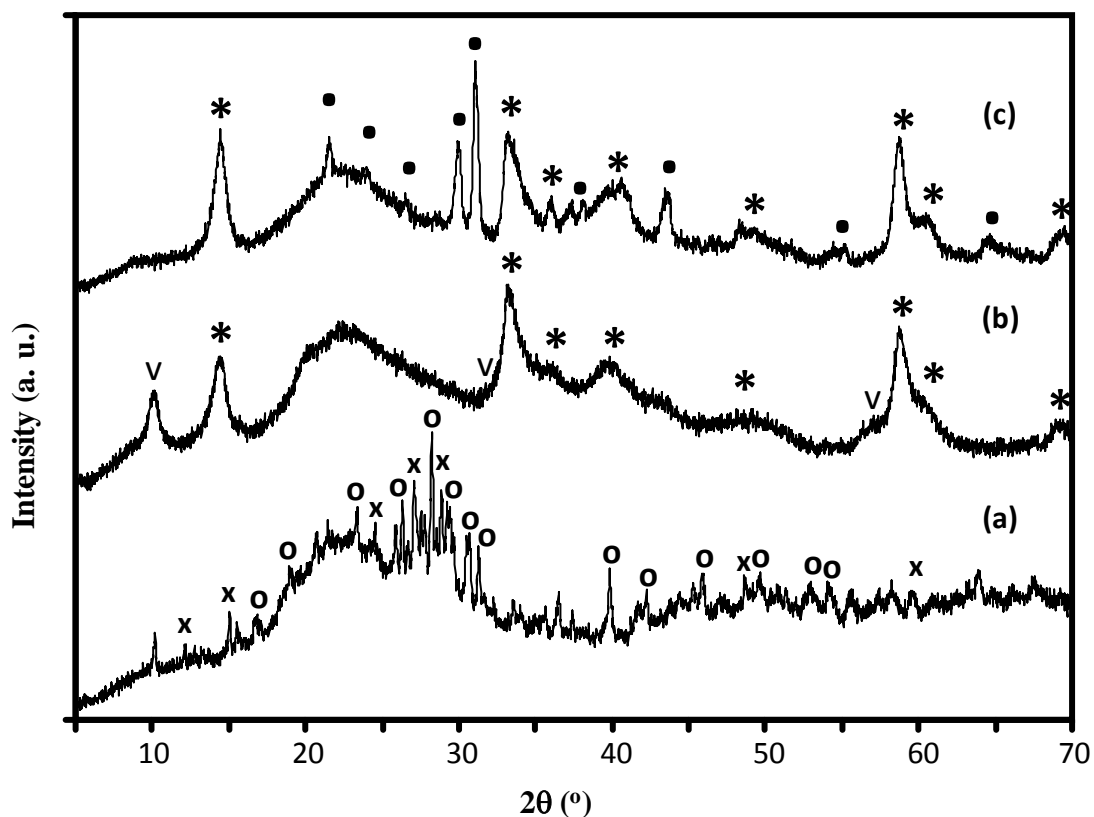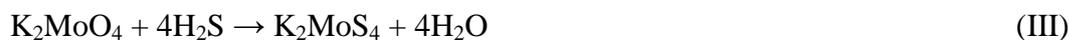
Figure 3.5: XRD diffractograms of the oxide precursor (a), the sulfide K$_2$MoO$_4$/SiO$_2$ catalyst (b) and the catalyst after the reaction of COS and H$_2$ to CH$_3$SH. K$_2$MoO$_4$ (o), K$_2$Mo$_2$O$_7$ (x), MoS$_2$ (*), K$_x$MoS$_2$ (V) and K$_2$SO$_4$ (●).

The diffractogram of the used catalyst in Fig. 3.5 (c) shows that the initial structure of the catalyst was not preserved under reaction conditions. The diffraction peaks attributed to K$_x$MoS$_2$ disappear, and new diffraction peaks corresponding to K$_2$SO$_4$ (PDF number: 00-003-0608) appear at 21.8, 23.9, 29.9, 31.1, and 43.6°(2θ). The formation of K$_2$SO$_4$ is consistent with the excess of sulfur found by elemental analysis in the used catalyst (S/Mo molar ratio of 3.5). The crystalline K$_2$SO$_4$ increases the density of the catalyst and blocks some pores leading to the decrease in surface area and pore volume per gram of material detected in the catalyst after activity tests.

56

According to reactions (III) and (IV), K_2MoS_4 was an intermediate in the sulfidation process, which was also indicated by the Raman spectra described above. A separate K_2S phase was not detected by XRD or Raman spectroscopy implying that it had to be highly dispersed and well-distributed in the catalyst. Under reaction conditions, however, it reacted readily and irreversibly with water leading finally to the agglomerated K_2SO_4 phase.

3.3.1.4. NO adsorption measurements

The concentration of NO adsorbed on coordinatively unsaturated metal cations at room temperature for the sulfided catalyst and the sulfided sample exposed to COS/He flow at 523 K are shown in Fig. 3.6. The corresponding peaks of the NO pulses are presented in Fig. 3.7. In both cases, the NO uptake is initially high, but decreases to zero as the maximum uptake capacity of the sample is reached. The NO uptake of the sample exposed to COS reaches steady state faster than the sample after sulfidation, i.e., the concentration of the accessible coordinatively unsaturated metal cations is much lower in the latter sample. The total NO concentration taken up for the as-sulfided sample is 229 μmol per gram of catalyst (molar ratio NO/Mo = 0.195), while the concentration of NO adsorbed on the COS pretreated sample is 113 μmol per gram of catalyst (molar ratio NO/ Mo = 0.09).
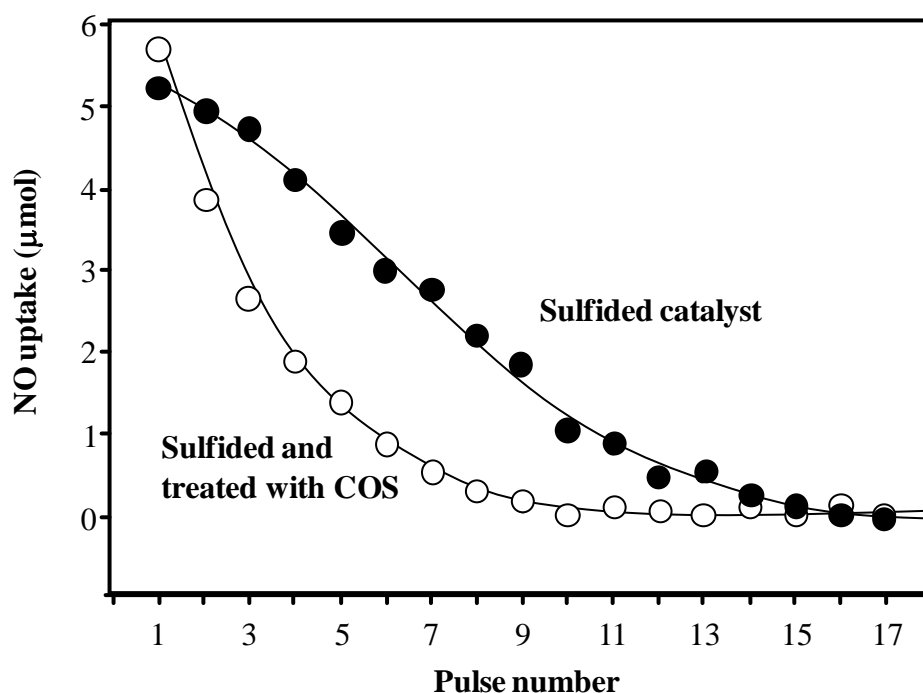
Figure 3.6: NO uptake at room temperature over the freshly sulfided catalyst (●) and the sulfide catalyst exposed to COS/He flow at 523 K for 1 h (○).
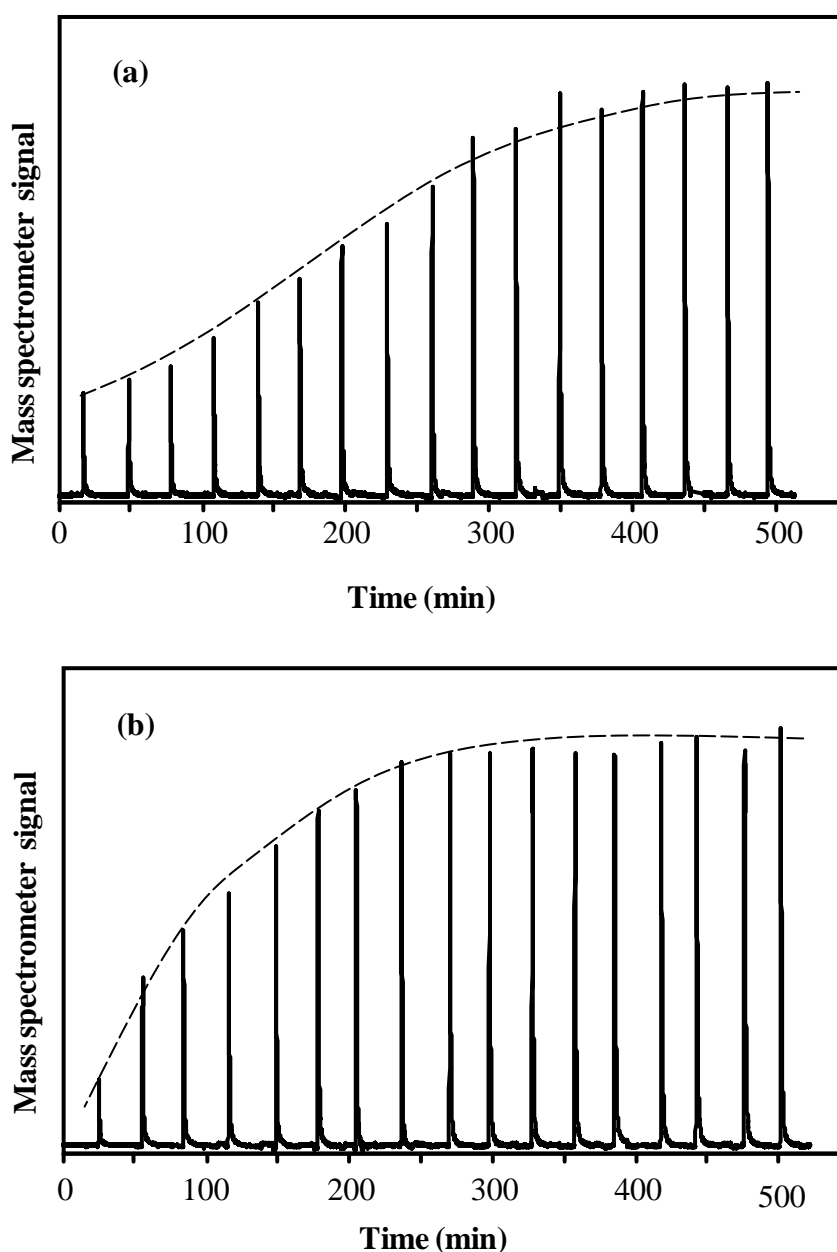
Figure 3.7: NO peaks obtained in the pulse flow experiments on K_2MoO_4/SiO_2 sulfided at 673 K for 3 h. As-sulfided sample (a); sample sulfided and exposed to COS/He at 523 K for 1 h (b).

3.3.2. Conversion of COS with varying H_2/COS ratio

Three different conditions were studied to evaluate the influence of the H_2/COS ratio, i.e., excess of hydrogen (H_2/COS = 7), near the stoichiometric ratio (H_2/COS = 4), and hydrogen deficient (H_2/COS = 2). The conversion of COS is presented in Table 3.1. The H_2/COS ratio had a strong effect on the conversion of COS. At 558 K, for example, the conversion of COS was 63% with H_2/COS = 2; it increased to 91% for H_2/COS = 4 and to 95% for H_2/COS = 7.

The main products detected were CO_2, CO, and CH_3SH. CS_2 was also observed at low temperatures under H_2 deficient conditions. H_2O and traces of CH_4 were detected in the product stream above 560 K. Unfortunately, it was not possible to quantitatively determine the concentration of water. The yield of carbon oxides, CH_3SH, and CS_2 are shown in Fig. 3.8.
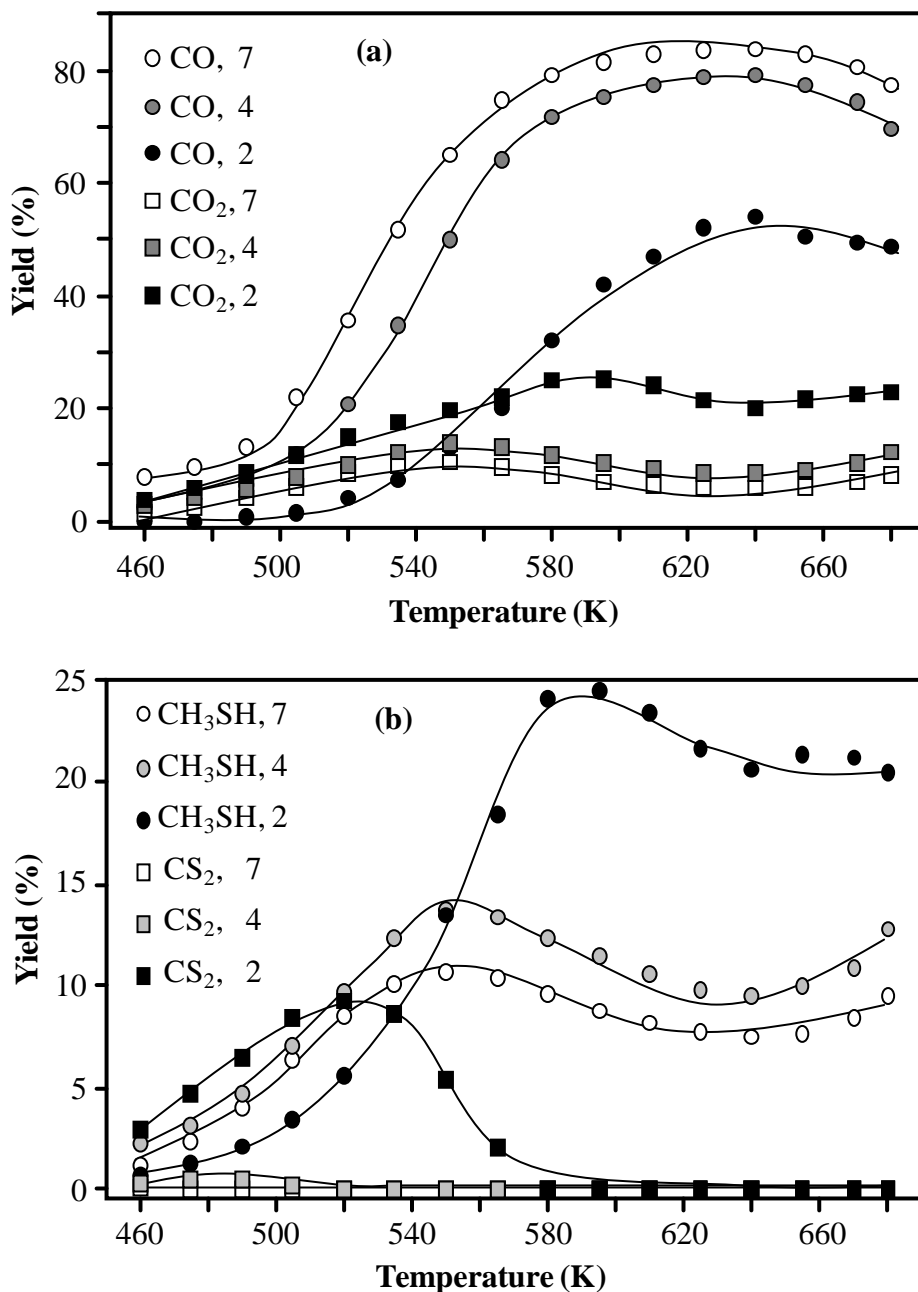
Figure 3.8: Product yield on sulfide K_2MoO_4/SiO_2 at different H_2/COS ratios (white symbols 7, gray symbols 4, black symbols 2). CO (circles) and CO_2 (squares) (a); CH_3SH (circles) and CS_2 (squares) (b). 3 MPa, 37 cm^3/min overall flow rate (residence time 0.68 s) and constant H_2/H_2S ratio of 4.5.

CO was the main product at all temperatures with H_2/COS ratios of 7 and 4 and temperatures above 560 K at $H_2/COS = 2$. Fig. 3.8(a) shows that at a given temperature, the yield of CO_2 decreased with increasing H_2/COS ratio. At 560 K, for example, the yield of CO_2 decreased from 22% to 13% and 9.6%, when the H_2/COS ratio varied from 2 to 4 and 7, respectively. In contrast, the yield of CO increased with increasing H_2/COS ratio, for instance at 560 K, from 22 to 64 and 75% by increasing the H_2/COS ratio from 2 to 4 and finally to 7. Fig. 3.8(b) shows that CS_2 was observed only below 570 K at $H_2/COS = 2$ and below 510 K at $H_2/COS = 4$. CS_2 was not detected at higher H_2/COS ratios. The yield of CH_3SH reached its maximum at a H_2/COS ratio of 4 below 550 K. At higher temperatures, the yield of CH_3SH is favored by low H_2/COS ratio.

Table 3.1: Conversion of COS on sulfide K_2MoO_4/SiO_2 at different H_2/COS ratios (constant H_2/H_2S ratio of 4.5) at 3 MPa and 37 cm^3/min overall flow rate (residence time 0.68 s).

Temperature (K)	H_2/COS ratio		
	7	4	2
453	11	8	8
468	15	12	12
483	22	17	18
498	35	27	25
513	52	41	34
528	72	60	42
543	86	77	52
558	95	91	63
573	97	96	81
588	98	97	92
603	98	98	95
618	98	98	96
633	98	98	96
648	98	98	96
663	98	98	96
673	98	98	96

3.3.3. Conversion of COS with varying H_2/H_2S ratio

Three series of experiments were carried out at H_2/H_2S ratios of 3.1, 1.4, and 0.6, at a fixed H_2/COS ratio of 2.3. The conversion of COS was almost complete above 573 K and was not influenced by the H_2/H_2S ratio (see Table 3.2).

Table 3.2: Conversion of COS on sulfide K_2MoO_4/SiO_2 at different H_2/H_2S ratios (constant H_2/COS ratio of 2.3) at 3 MPa and 37 cm^3/min overall flow rate (residence time 0.68 s).

Temperature (K)	H_2/H_2S ratio		
	3.1	1.4	0.6
453	18	17	13
468	26	24	22
483	33	32	30
498	38	38	37
513	43	44	45
528	54	55	57
543	69	71	76
558	88	89	88
573	96	95	93
588	98	97	95
603	98	97	96
618	98	97	96
633	98	97	96
648	98	97	96
663	98	97	96
673	98	97	96

The product yield is compiled in Fig. 3.9. The variation of the H_2/H_2S ratio did not affect the yield of carbon oxides significantly from 450 to 560 K. At higher temperatures, the increasing H_2/H_2S ratio led to a decrease in the yield of CO_2 and an increase in the yield of CO. Decreasing H_2/H_2S ratio decreased the yield of CS_2, but favored the yield of CH_3SH in the studied temperature range.
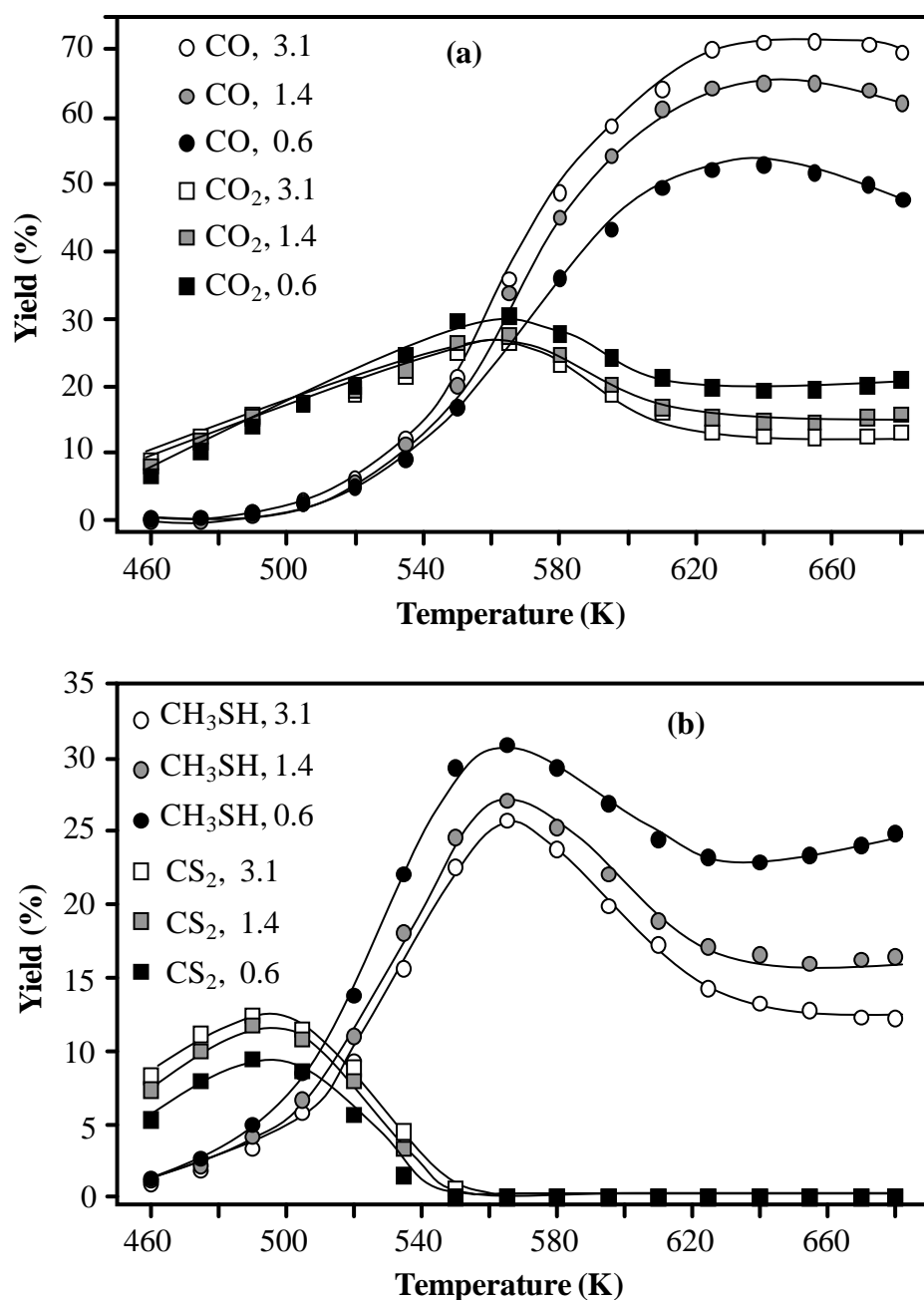
Figure 3.9: Product yield on sulfide K_2MoO_4/SiO_2 at different H_2/H_2S ratios (white symbols 3.1, gray symbols 1.4, black symbols 0.6). CO (circles) and CO_2 (squares) (a); CH_3SH (circles) and CS_2 (squares) (b). 3 MPa, 37 cm^3/min overall flow rate (residence time 0.68 s) and constant H_2/H_2S ratio of 2.3.

3.3.4. Conversion of COS with varying residence time

The effect of residence time was studied at 523 K and 598 K as shown in Fig. 3.10 in terms of selectivity (the corresponding yield at 523 K is shown in Fig. 3.13). At 523 K, the conversion of COS increased from 41% to 60% with increasing residence time, CS_2, CO, CO_2, and CH_3SH being the main products. The selectivity to carbon oxides was not affected

to a significant extent by increasing the residence time; selectivity to CS_2, however, clearly decreased, whereas the selectivity to CH_3SH increased.
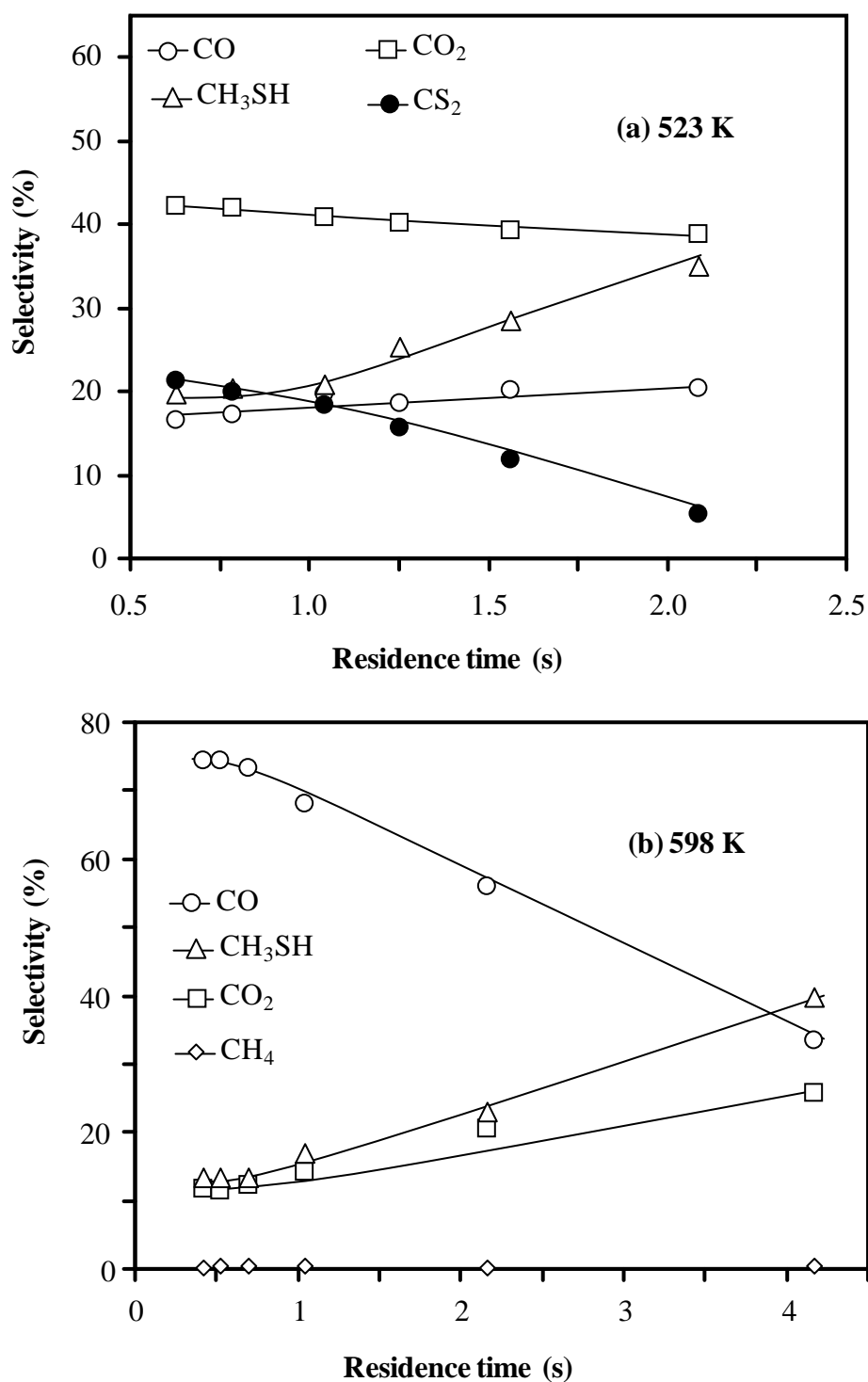
Figure 3.10: Product selectivity as a function of residence time for the hydrogenation of COS over sulfide K_2MoO_4/SiO_2 at 3 MPa, 523 K (a) and 598 K (b). CO (○), CO_2 (□), CH_3SH (Δ), CS_2 (●) and CH4 (◇).

At 598 K, the conversion of COS was above 96.5% in all experiments. Carbon oxides, methyl mercaptan, and a negligible amount of CH_4 were formed; CS_2 was not detected. At low residence time, CO was the main product; however, the selectivity to CO declined sharply at residence times higher than 0.72 s, while the selectivity to methyl mercaptan increased.
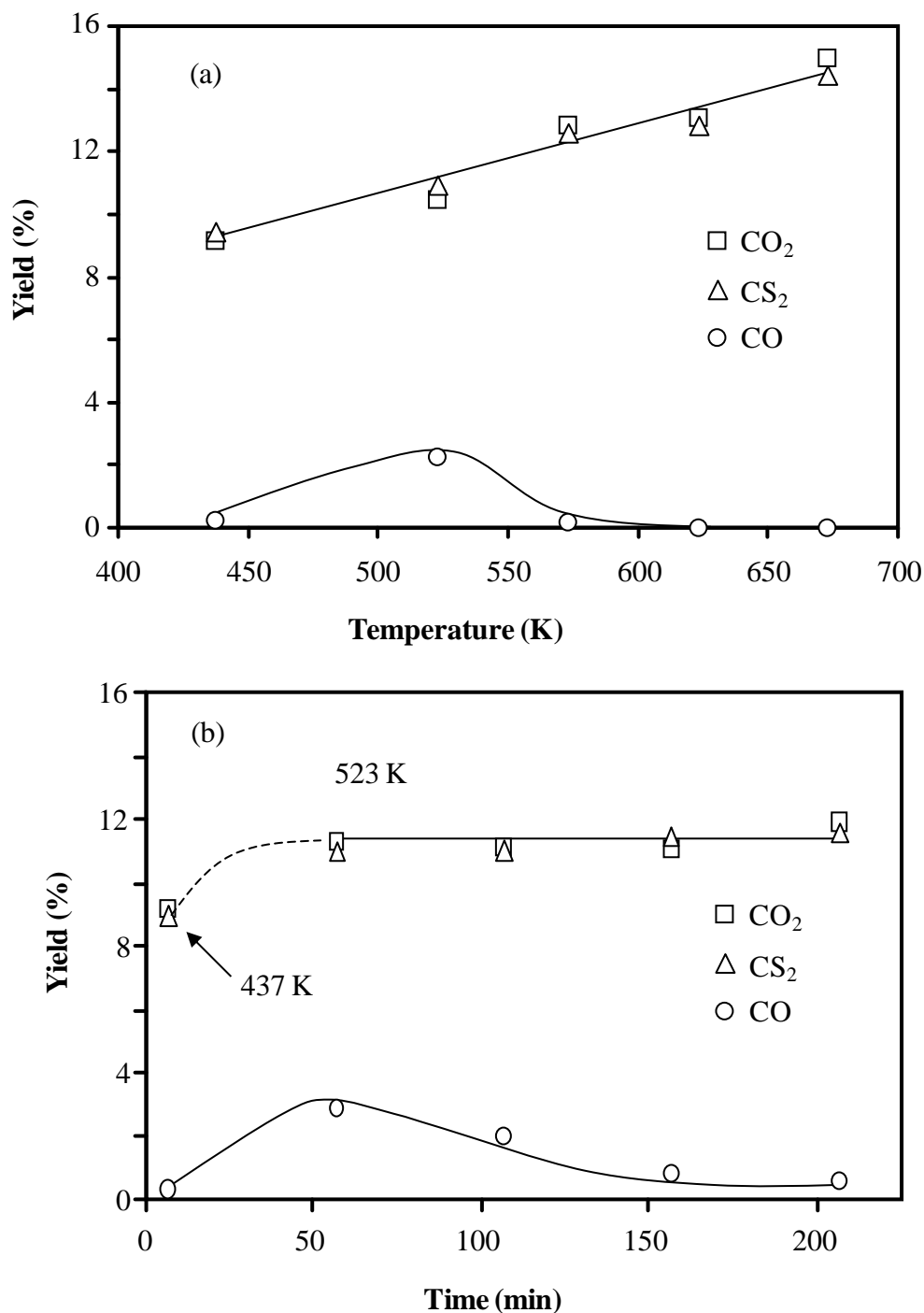
Figure 3.11: Yield of CO ($\circ$), CO_2 ($\square$) and CS_2 ($\triangle$) obtained by passing a gas mixture of 8.5 vol. % COS in N_2 through the catalyst bed at 3 MPa and residence time 0.68 s. Yields as a function of increasing temperature (a) and time (isothermally at 523 K) (b). The first measurement in (b) was taken at 437 K.

3.3.5. Catalytic tests in the absence of H_2

The product yields observed in the experiments performed in the absence of H_2 are shown in Fig. 3.11. In the first experiment (437-673 K), the conversion of COS increased from 23% to 29% (not shown here). At 437 K, CO_2 and CS_2 were the only products. CO was formed at 523 K, but declined afterward and only CO_2 and CS_2 were observed again. In the second experiment, the temperature was raised from 437 K to 523 K and then kept constant. At 437 K, only CO_2 and CS_2 were produced. At 523 K, CO was also observed, but declined afterward. This indicates that the formation of CO did not occur below 523 K and was residence time dependent at higher temperatures. In both experiments, H_2S was not detected, whereas CO_2 and CS_2 were observed in equimolar amounts pointing to disproportionation of COS.

3.3.6. Catalytic test of bulk MoS_2 and sulfided K_2MoO_4

The selectivity obtained on bulk MoS_2 and sulfided K_2MoO_4 along with the conversion of COS is presented in Fig. 3.12. The corresponding yields are compiled in Tables 3.3 and 3.4.

With MoS_2, the preferred product was CO, whereas the selectivity to CO_2 and CH_3SH was very low. Only traces of CH_4 were observed. With sulfide K_2MoO_4, CO was the main product in most of the conversion range. Significant concentrations of the other products, however, were detected. The selectivity to CO_2 and CH_3SH was initially higher than that to CO, but decreased with COS conversion. CS_2 was detected at COS conversions below 20%.

Table 3.3: Conversion of COS and product yield on MoS_2 at different temperatures (H_2/H_2S=5.3, H_2/COS=3) at 3 MPa and 40 cm^3/min overall flow rate.

Temperature (K)	Conversion (%)	Yield (%)			
		CO	CO_2	CH_3SH	CH_4
448	8.3	7.3	0.50	0.46	0.00
498	62.9	61.7	0.54	0.59	0.00
548	91.9	90.7	0.61	0.39	0.22
598	93.6	92.1	0.76	0.08	0.68
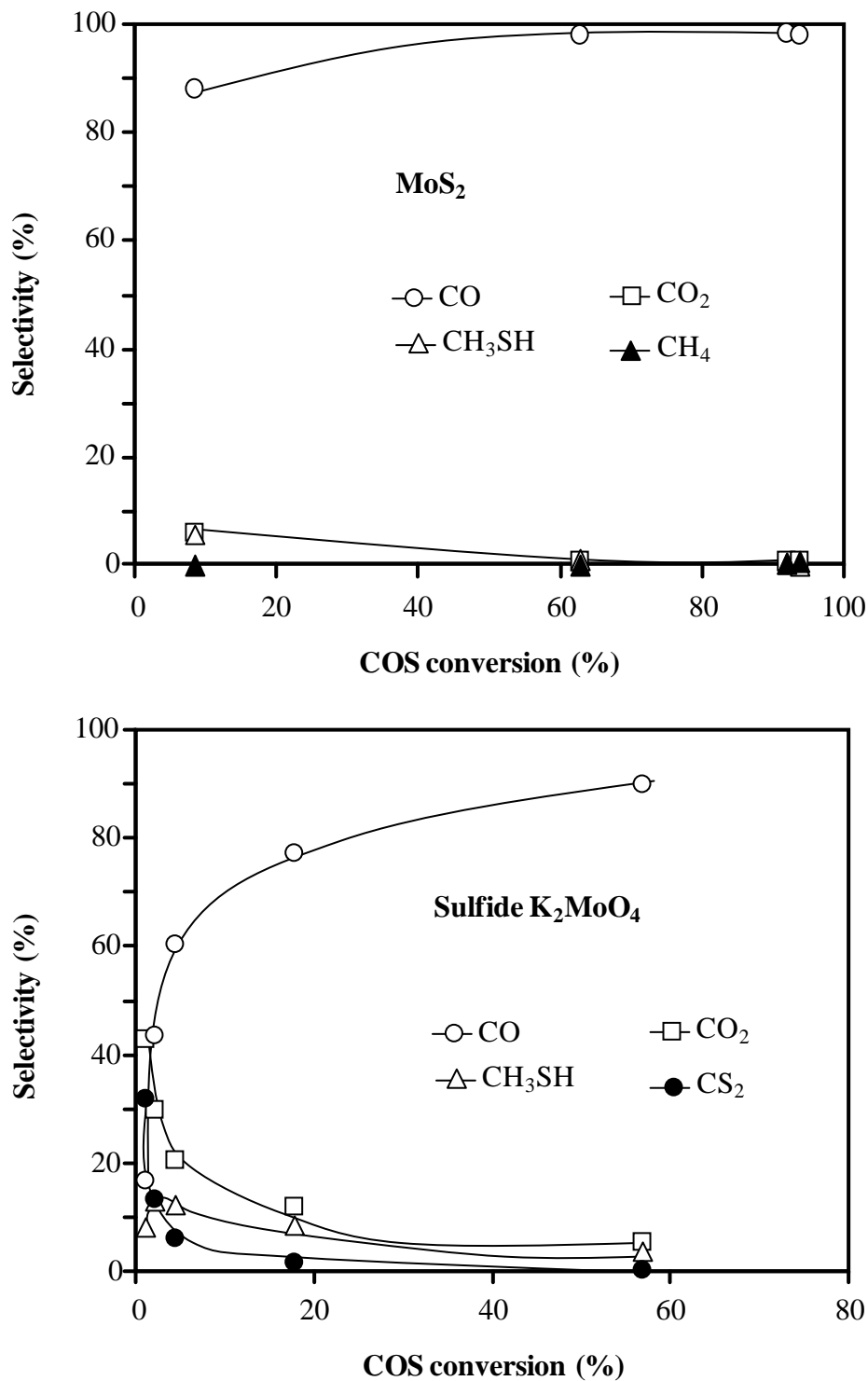
Figure 3.12: Product selectivity as a function of COS conversion in the reaction of COS with H_2 on bulk MoS_2 and sulfided K_2MoO_4.

Table 3.4: Conversion of COS and product yield on sulfided K_2MoO_4 at different temperatures ($H_2/H_2S=5.3$, $H_2/COS=3$) at 3 MPa and 40 cm^3/min overall flow rate.

Temperature (K)	Conversion (%)	Yield (%)			
		CO	CO_2	CS_2	CH_3SH
448	1.0	0.17	0.43	0.32	0.08
498	4.4	2.67	0.92	0.28	0.54
548	17.8	13.80	2.17	0.34	1.52
598	56.8	51.21	3.21	0.24	2.13

3.4. Discussion

3.4.1. Evaluation of the reaction pathway

The conversion of COS as well as the CO yield increased rapidly at the temperatures from 498 to 538 K (see e.g., Table 3.1 and Fig. 3.8) pointing to the direct hydrodecomposition of COS (V) in line with the thermodynamic equilibrium favoring CO in the reversible reaction $CO + H_2S \rightarrow COS + H_2$ [28]. Thus, COS is concluded to rapidly decompose to CO and H_2S in accordance with the fact that the formation of COS by (I) is much faster than the subsequent reactions in the synthesis of CH_3SH from H_2S-containing syngas [15-17].

$$COS + H_2 \rightarrow CO + H_2S \qquad \text{(V)}$$

CO_2 and CS_2 are formed by disproportionation of COS according to reaction (VI), as it was demonstrated by the experiments in the absence of H_2 (Fig. 3.11) in agreement with Ref. [16]. However, in the presence of H_2, the yield of CO_2 is always higher than the observed yield of CS_2 (see Fig. 3.9). This low CS_2/CO_2 ratio observed in the product stream is related to the reaction of CS_2 with hydrogen to form CH_3SH according to Eq. (VII). This is deduced from the fact that CS_2 is only detected at low temperatures and under H_2 deficient conditions and that the increase in the yield of CH_3SH occurs in parallel to the decrease in the CS_2 formation rate (see Figs. 3.5 and 3.6).

$$2\,COS \rightarrow CO_2 + CS_2 \qquad \text{(VI)}$$
$$CS_2 + 3\,H_2 \rightarrow CH_3SH + H_2S \qquad \text{(VII)}$$
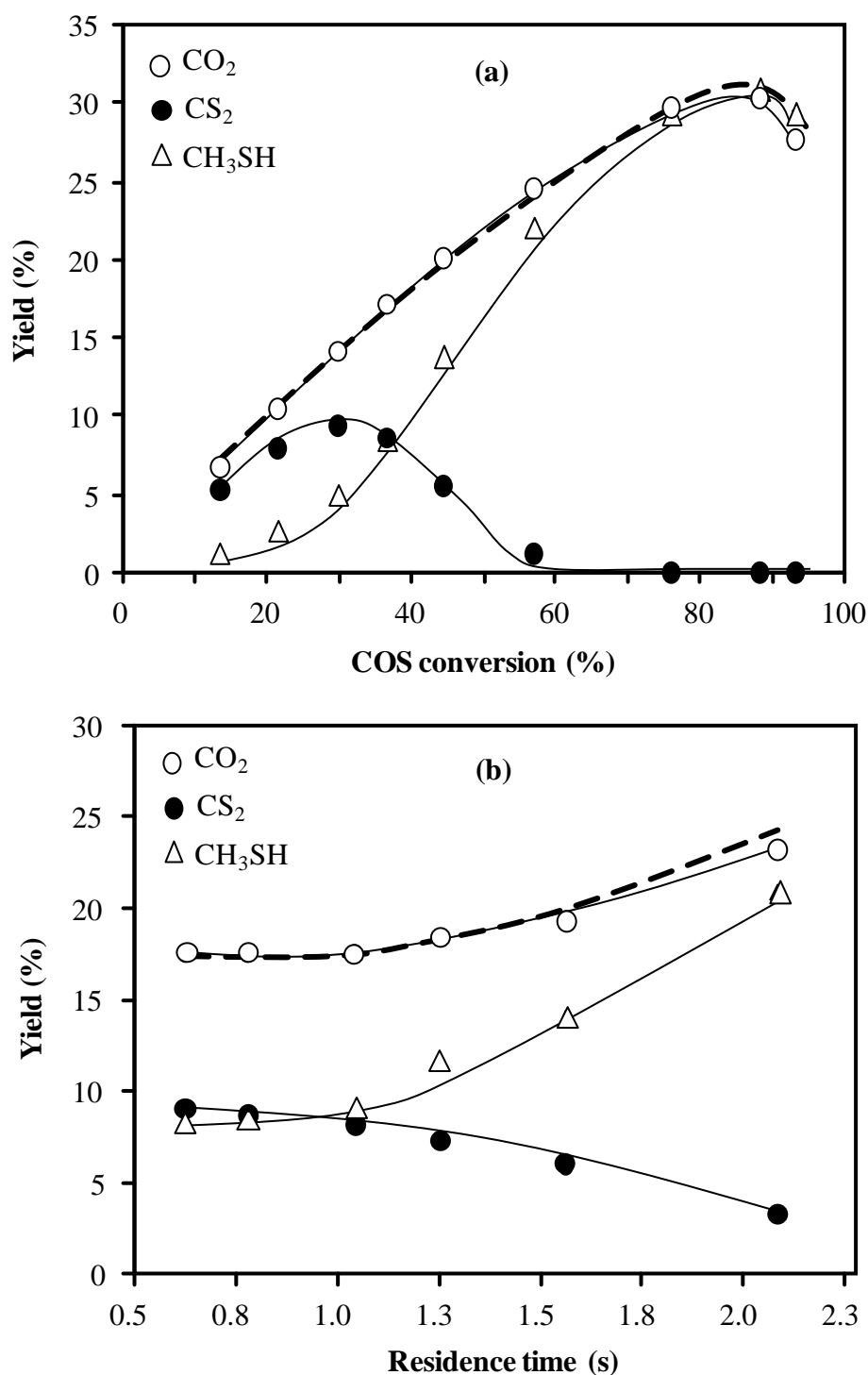
Figure 3.13: Yield of CO_2 (○), CS_2 (●) and CH_3SH (Δ) over sulfide K_2MoO_4/SiO_2 as a function of COS conversion (a) and residence times at 523 K (b). The dashed lines give the sum of the yield of CH_3SH and CS_2 ($H_2/COS=2.3$, $H_2/H_2S=2.8$).

Let us now discuss in depth the role of CS_2 in the reaction sequence. Fig. 3.13a shows the yield of CO_2, CS_2, and CH_3SH as well as the sum of the CS_2 and CH_3SH yield (dashed line)

as a function of the conversion of COS ($H_2/H_2S = 0.6$). CO_2 and CS_2 are primary products. In contrast to CO_2, CS_2 is converted to CH_3SH at increasing COS conversion. The nearly equal concentration of CO_2 and of the sum of the concentrations of CS_2 and CH_3SH indicates that CS_2 is quantitatively converted to CH_3SH. While it should be noted that the points in Fig. 3.13a are constructed of data measured at different temperatures, the identical behavior is also observed, when the residence time is varied at 523 K (see Fig. 3.13b). This allows us to conclude that CH_3SH is solely produced by the hydrogenation of CS_2.

Methyl mercaptan is not formed by the direct hydrogenation of COS according to reaction (II), because it would imply that a parallel reaction would have to exist that forms CO_2 with a rate identical to the sum of the rates to CS_2 and CH_3SH and that all these reactions would have the same apparent energy of activation. These potential reactions to form CO_2 would be the hydrolysis of COS ($COS + H_2O \rightarrow CO_2 + H_2S$) and the water gas shift reaction ($CO + H_2O \rightarrow CO_2 + H_2$).

Fig. 3.13a also indicates that below conversion of 40% (500 K), the reaction (VII) is the rate determining step, because the CS_2 yield is higher than the yield of CH_3SH. At increasing temperature, the CH_3SH yield is higher than the CS_2 yield and at conversion of 60% (540 K) or above CS_2 is not detected. This implies that the rate of CS_2 hydrogenation exceeds that of the disproportionation of COS under these conditions, i.e., reaction (VI) becomes the rate determining step.

As it is shown that the disproportionation of COS to CO_2 and CS_2 is the first step of the overall reaction, CO_2 has to be formed at the same rate as CS_2 and CH_3SH together. This is the case below 573 K. Above 573 K, however, the rate of CO_2 formation is lower than the sum of the other two. Thus, CO_2 must be transformed at these temperatures. The possibilities for the decrease in the CO_2 yield are reactions (VIII) and (IX).

$$CO_2 + H_2 \rightleftharpoons CO + H_2O \qquad \text{(VIII)}$$

$$CO_2 + H_2S \rightleftharpoons COS + H_2O \qquad \text{(IX)}$$

To evaluate the relative rate of reactions (VIII) and (IX), the difference of the CH_3SH and the CO_2 yield in dependence of the H_2/H_2S ratio and the reaction temperature is presented in Fig. 3.14. It is noticed that the difference (CH_3SH yield and CO_2 yield) increased as the H_2/H_2S ratio decreased, i.e., the higher the concentration of H_2S the more CO_2 was consumed. Therefore, it is inferred that reaction (IX), in which CO_2 reacts with H_2S, dominates under the

experimental conditions. Finally, the presence of traces of CH_4 at complete COS conversion (Fig. 3.10b) indicates the hydrogenation of methyl mercaptan to methane (reaction (X)).

$$CH_3SH + H_2 \rightarrow CH_4 + H_2S \qquad (X)$$
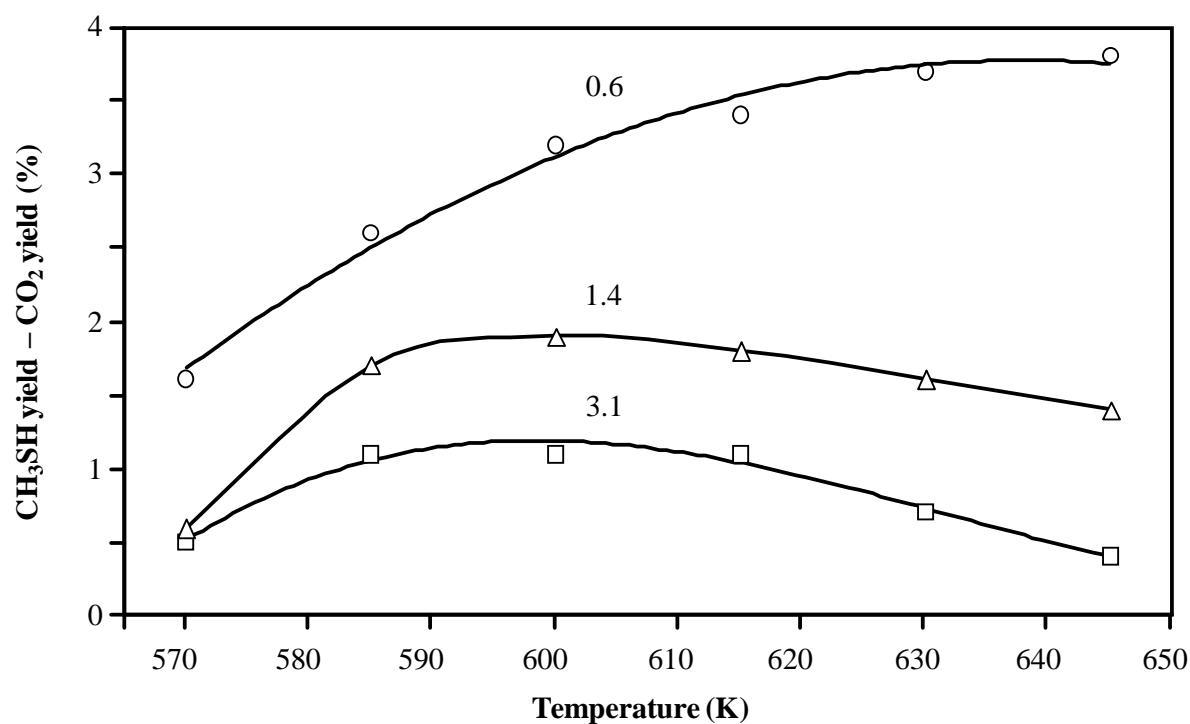
Figure 3.14: Difference of the yield of CH_3SH and CO_2 (the CO_2 yield was subtracted from the CH_3SH yield) at $H_2/COS = 2.3$ and different H_2/H_2S ratios: 0.6 (o), 1.4 (Δ), and 3.1 (□).

Thus, we conclude that the reaction pathway follows the routes depicted in Fig. 3.15. COS rapidly decomposes to CO and H_2S and in parallel disproportionates to CO_2 and CS_2. CS_2 is the species being hydrogenated to CH_3SH. At higher temperatures, CO_2 reacts with H_2S to form COS and H_2O, whereas the reaction to CO by the water gas shift reaction appears to be less significant. Methane is formed by hydrogenation of CH_3SH.
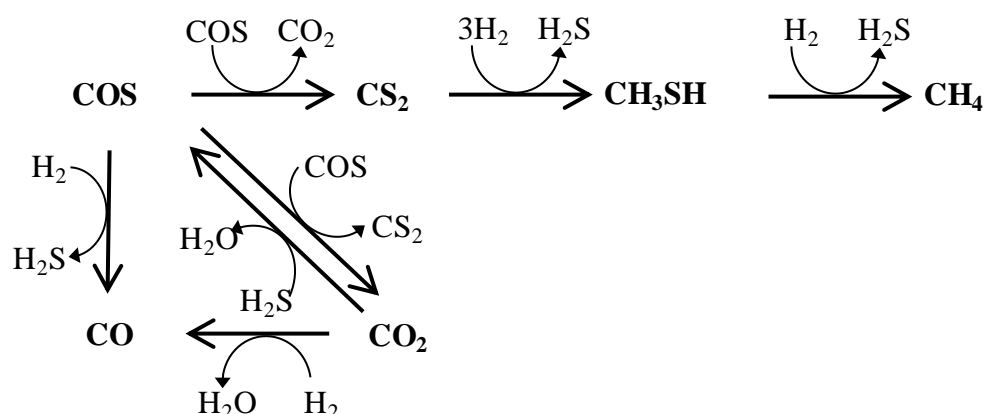
Figure 3.15: Reaction pathway for the hydrogenation of COS over sulfide K_2MoO_4/SiO_2.

3.4.2. On the optimum conditions for the synthesis of CH₃SH from COS

The synthesis of methyl mercaptan proceeds through the COS disproportionation followed by the hydrogenation of CS_2. Clearly, the strategy to optimize the formation of methyl mercaptan either from H_2S-containing syngas or COS is to promote the COS disproportionation, CS_2 hydrogenation sequence, and to suppress the decomposition of COS. Increasing temperature and partial pressure of H_2 accelerate the production of CH_3SH. The rate of COS decomposition, however, increases faster than the rate of other reactions. Thus, the yield of methyl mercaptan is improved by increasing the H_2/COS ratio only from 2 to 4 below 550 K, and the CH_3SH yield reaches its maximum values at 540-580 K decreasing at higher temperatures. The concentration of H_2S is beneficial for the CH_3SH yield by increasing the concentration of COS available for disproportionation via reaction (IX).

Thus, to optimize the yield of methyl mercaptan, it is necessary to apply concentrations of H_2 not higher than the stoichiometric concentration needed in the presence of H_2S and to limit the reaction temperature in a narrow range. For the system studied in this work, for instance, the optimum conditions are 580 K, H_2/COS = 2 and H_2/H_2S = 0.6. At this temperature, CS_2 is fully hydrogenated, whereas the yield of CO and CH_3SH is 36% and 31%, respectively.

The selectivity to CH_3SH can be further improved by modifying the catalyst formulation, e.g., using high surface area supports or adding a second promoter to the catalyst as shown in Ref. [29].

3.4.3. Active phases in the sulfide K_2MoO_4/SiO_2 catalyst

The catalytic activity observed is attributed to MoS_2, which is the main phase in the catalyst after sulfidation (XRD and Raman characterization) and is known to catalyze reactions involving heteroatoms [30-32]. The initial mixture of K_2MoO_4 and $K_2Mo_2O_7$ in the oxide precursor is transformed to MoS_2 by sulfiding as deduced from the in situ Raman spectra. In this process, the K^+ cations tend to segregate from Mo-containing species and only a minor fraction remains as K_2MoS_4 or is incorporated in the K_xMoS_2 phase (XRD of the sulfide catalyst). Because the K_xMoS_2 phase is not preserved during the reaction, we conclude that K^+ cations are not structurally associated with Mo-containing crystalline solids in the active material. However, K^+ cations decorate the MoS_2 surface as concluded from X-ray photoelectron spectroscopy (XPS) analysis of sulfide K_2MoO_4/SiO_2 catalyst (metal salt loadings close to 28 wt.%) [17]. For the studied catalyst, a fraction of K^+ adsorbs on MoS_2, while potassium species not associated with MoS_2 are speculated to form K_2SO_4 by reacting with oxidizing compounds (H_2O, CO_2) and H_2S under reaction conditions.

The segregation of the phases observed in the sulfidation-oxidation cycle (Fig. 3.3) suggests that not all the MoS_2 phase is decorated by K^+ probably due to the random distribution of K^+ on the surface. The MoO_3 observed in the reoxidized catalyst is speculated to be formed from K^+-free MoS_2, whereas $K_4Mo_8O_{26}$ forms from MoS_2 interacting with K^+ cations.

Thus, we conclude that two active phases, MoS_2 and K^+-decorated MoS_2, coexist in the sulfide K_2MoO_4/SiO_2 catalyst [33,34]. It is worth clarifying the difference between the K_xMoS_2 detected after sulfidation and the K^+-decorated MoS_2 phase. In the former structure, K^+ cations occupy defined positions, i.e., they intercalate between the MoS_2 slabs leading to additional reflections in the XRD pattern. In the K^+-decorated phase, the cations are distributed randomly on the MoS_2 surface, thus they do not modify the crystalline structure of the MoS_2 cluster. It is not possible to differentiate the pure MoS_2 phase and that decorated by K^+ by means of XRD.

The MoS_2 phase has coordinatively unsaturated sites (CUS) at the perimeter of the (1 0 1 0) plane, which act as active sites in hydrogenolysis and hydrogenation reactions [30-32]. The structure of the K^+-decorated MoS_2, i.e., the specific position of the K^+ cations with respect to the CUS remains unspecified. It has been proposed, however, that the presence of K^+ stabilizes oxygenated intermediates preventing C-O bond cleavage in the synthesis of alcohols and affects the electronic properties of the MoS_2 phase [35-37]. In the synthesis of CH_3SH from H_2S-containing syngas, the promoter effect of potassium on the

selectivity has been related to the increasing concentration and the chemical environment of the Mo^{5+} that can be expected at the not completely coordinated Mo-edges interacting with oxidizing agents [17]. Thus, we conclude that the active sites in K^+-decorated MoS_2 are CUS. The presence of K^+ in the active phase, however, modifies the chemical and electronic environment of the active sites, i.e., the relative rate of hydrogenation and C-S bond cleavage.

Bulk MoS_2 and sulfide K_2MoO_4 were used in the reaction of COS with H_2 to clarify the role of MoS_2 and K^+-decorated MoS_2, which obviously has to form from the sulfided K_2MoO_4. Fig. 3.12 shows that the presence of K^+ increases drastically the selectivity to CO_2, CS_2, and CH_3SH and reduces the selectivity to CO. This is in line with the low conversion and poor CH_3SH yield obtained in the synthesis of methyl mercaptan from H_2S-containing syngas using unpromoted MoS_2 [14]. Thus, we conclude that the hydrodecomposition of COS takes place preferentially at MoS_2, whereas the disproportionation of COS and the consecutive hydrogenation of CS_2 is catalyzed faster on the K^+-decorated MoS_2 phase.

Note that the bulk sulfide K_2MoO_4 catalyst leads to very low conversion compared with the SiO_2-supported counterpart. This low activity is related to the low dispersion of the sulfides in that case. Also note in Fig. 3.12 that the difference in product selectivity between both bulk catalysts diminishes with increasing COS conversion. This is related to the fact that the points for high conversions have been measured above 540 K. At this high temperature, the decomposition to CO is favored over the other reactions and in consequence the promoter effect of potassium becomes less evident.

3.4.4. Active sites for the decomposition of COS

From the experiments performed in the absence of H_2, we deduce that the decomposition of COS to CO takes place at the CUS in MoS_2 as depicted in Fig. 3.16. COS first coordinates to the CUS in the MoS_2 structure. Then, the C-S cleavage results in CO desorption leaving the sulfur anion at the CUS. This is supported by the fact that the formation of CO stops in the absence of hydrogen (see Fig. 3.11) after some time on stream, implying that the reaction only occurs as long as accessible cations are available. Under the used reaction conditions, the CUS are regenerated by the reaction of hydrogen with the sulfur bridged Mo-edge of the active MoS_2 phase [38]. In contrast to the dissociation of COS, the disproportionation does not cease in the absence of H_2 indicating that it depends less or not at all on the presence of CUS in the MoS_2 phase.
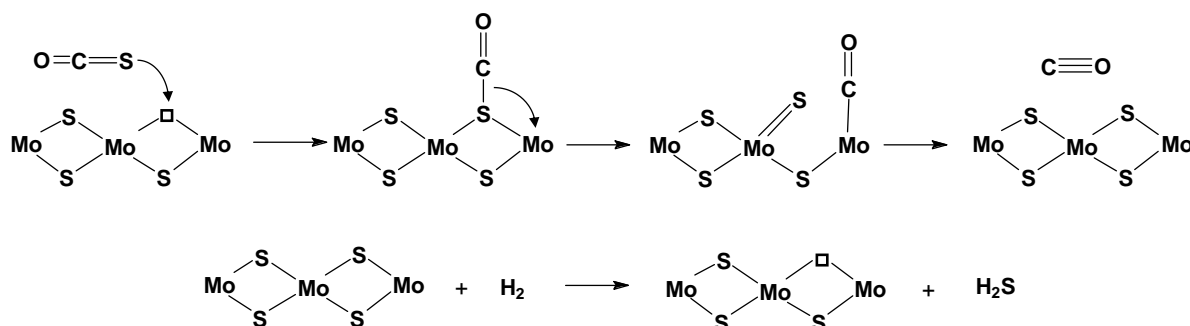
Figure 3.16: Mechanism for the formation of CO from COS at the coordinatively unsaturated sites (CUS).

Further evidence of the role of CUS in MoS$_2$ and K-promoted MoS$_2$ is obtained by NO adsorption. NO adsorbs on the CUS of promoted or unpromoted MoS$_2$, thus the concentration of NO adsorbed is correlated with the concentration of CUS in the catalyst [39,40]. In the pulse experiments, the NO uptake of the sample exposed to COS at 523 K was nearly 60% lower than the uptake of the fresh sulfided sample. This is in line with the mechanism in Fig. 3.16, because the concentration of CUS in the catalyst is drastically diminished after flowing COS in the absence of hydrogen. Furthermore, the disproportionation of COS occurs faster than the decomposition in the K$^+$-decorated MoS$_2$. Thus, the CUS in this phase are less susceptible to deactivation and remain able to adsorb NO.

3.4.5. Active sites for the hydrogenation of CS$_2$

Two surface intermediates have been proposed for the direct hydrogenation of COS to methyl mercaptan, i.e., adsorbed thioformic acid (HSCHO) and adsorbed methanethiol (CH$_3$S) [16]. The former species has been postulated, but not observed, whereas the methanethiol fragment has been observed by vibrational spectroscopy on TiO$_2$, Al$_2$O$_3$, and MoS$_2$ [41-43]. Because the experiments reported here indicate that CS$_2$ is the species being hydrogenated, the intermediate formed cannot be related to thioformic acid, but rather to a dithioformic acid-based molecule. The postulated overall surface process that leads to the formation of methyl mercaptan is illustrated in Fig. 3.17. CS$_2$ coordinates to a CUS in the first step. Then, a nearby hydrogen atom reacts with the adsorbed CS$_2$ to form a HSCS species. It has been confirmed by spectroscopic techniques and ab initio calculations that the reaction between hydrogen atoms and CS$_2$ to form the HSCS species is spontaneous and has low activation energy [44]. The rearrangement and interaction of the HSCS fragment with

hydrogen leads to the release of a H_2S molecule and one adsorbed methanethiol. Then, the combination of the adsorbed methanethiol with hydrogen in the surface releases the methanethiol, whereas the hydrogen atoms adjacent to the CUS are generated by dissociative adsorption of H_2.
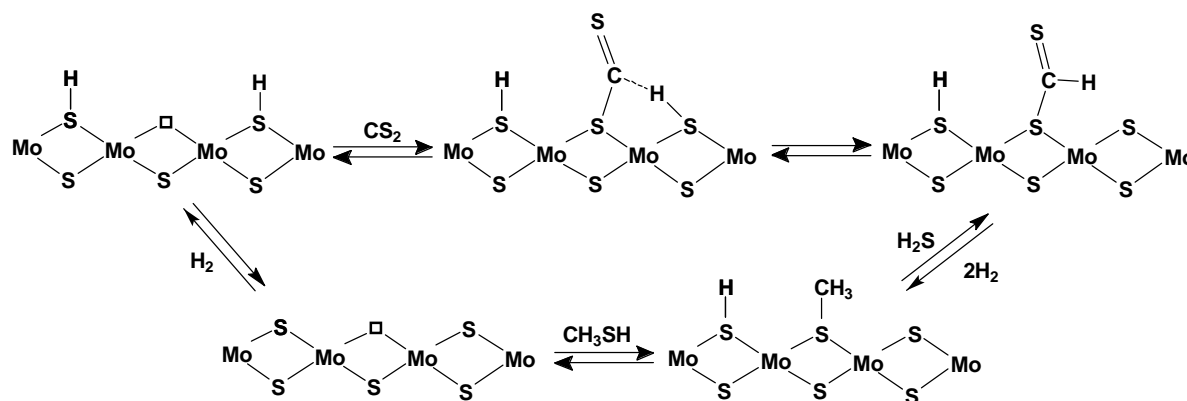
Figure 3.17: Catalytic cycle for the hydrogenation of CS_2 to CH_3SH at the coordinatively unsaturated sites.

At present, the exact mechanism of the rearrangement of the HSCS species to adsorbed methanethiol can only be derived from ab initio DFT calculations. The combination of a second hydrogen atom with the HSCS species leads to the formation of a dithioformic acid fragment (HCSSH) [45,46]. The decomposition of dithioformic acid can take place by dehydrogensulfidation yielding H_2S and C=S or by dehydrogenation to CS_2 and H_2 [46,45]. The former mechanism is favored over the dehydrogenation which is well in line with the necessary H_2S release from the adsorbed dithioformic acid to form the methanethiol fragment (see Fig. 3.17). Interestingly, the two pathways for the HCSSH decomposition can be assisted by H_2 or H_2S and can comprise the formation of a dithiohydroxy carbene (HSCSH). This species, adsorbed at a CUS, could form the methanethiol fragment after H_2S release and hydrogenation.

Although the adsorbed species could interact directly with molecular hydrogen from the gas phase, the hydrogen provided by the surface SH groups seems to play a key role in the hydrogen addition steps in the mechanism of Fig. 3.17. Chen et al. [17,29] have reported the XPS characterization of sulfided K_2MoO_4/SiO_2 catalysts and the synthesis of methyl mercaptan from syngas. In that report the yield of CH_3SH was related to the concentration of low valence Mo and S species, i.e., $(S–S)^{2-}$ and $Mo^{4+}-S^{2-}$. These species form SH groups by heterolytic or homolytic dissociation of hydrogen [47,48]. Furthermore, the SH groups

formed by the interaction of the sulfide surface with H_2 or H_2S under reaction conditions are claimed to provide the hydrogen in hydrotreatment applications [49-51]. As the active sites in MoS_2 and K^+-MoS_2 are fundamentally the same (CUS), the hydrogenation of CS_2 can take place on both phases. The presence of K^+, however, could promote the hydrogenation of CS_2, because it could increase the concentration of SH groups in the surface via adsorption of H_2S ($K^+ + H_2S + S^{2-} \rightleftharpoons K–SH + SH$).

3.5. Conclusions

The synthesis of CH_3SH over sulfide K_2MoO_4/SiO_2 is explored using COS, H_2, and H_2S as educts. COS decomposes rapidly to CO and H_2S. In parallel, COS disproportionates to CO_2 and CS_2. CS_2 is the reaction intermediate that is hydrogenated to CH_3SH. CO_2 and CH_3SH are consumed at high temperatures. CO_2 reacts with H_2S to COS and H_2O, while the reverse water gas shift reaction can take place to a lower extent. CH_3SH is further hydrogenated to CH_4.

During the sulfidation reaction, the main phases present in the catalyst are MoS_2, K^+-promoted MoS_2, and K_2SO_4. The MoS_2 phase catalyzes the decomposition of COS to CO, whereas the disproportionation of COS and subsequent hydrogenation of CS_2 is faster on the K^+-decorated MoS_2 phase. The active sites in both phases for the decomposition of COS and hydrogenation of CS_2 are CUS. The role of the K^+ cations in the K^+-decorated MoS_2 phase is to accelerate the rates of the disproportionation of COS and of the hydrogenation of CS_2.

3.6. References

[1]   J. Sauer, W. Boeck, L. von Hippel, W. Burkhardt, S. Rautenberg, D. Arntz, W. Hofen, US patent 5 852 219, 1998.

[2]   Y. Yang, S. Dai, Y. Yuan, R. Lin, D. Tang, H. Zhang, Appl. Catal. A 192 (2000) 175.

[3]   W. Leuchtenberger, K. Huthmacher, K. Drauz, Appl. Microbiol. Biotechnol. 69 (2005) 1.

[4]   B. Buchholz, US patent 4 410 731, 1983.

[5]   M. Boulinguiez, C. Forquy, J. Barrault, US patent 4 665 242, 1987.

[6]   Y. Yang, Q. Wang, R. Lin, H. Zhang, Y. Yuan, W. Fang, Z. Quanxing, D. Shenjun, X. Yan, A. Chen; J-O. Barth, C. Weckbecker, K. Huthmacher, H. Redlingshoefer; S. Ackermann, US patent 7 569 731, 2009.

[7]   J. Olin, B. Buchholz, B. Loev, R. Goshorn, US patent 3 070 632, 1962.

[8]   P. Haines, US patent 4 449 006, 1984.

[9]   D. Kubicek, US patent 4 120 944, 1978.

[10] I. Wachs, GB patent 2 344 343, 1998.

[11] C. Ratcliffe, P. Tromp, US patent 4 668 825, 1987.

[12] B. Zhang, S. Taylor, G. Hutchings, New J. Chem. 28 (2004) 471.

[13] Y. Yang, Y. Yuan, S. Dai, B. Wang, H. Zhang, Catal. Lett. 54 (1998) 65.

[14] Y. Yang, H. Yang, Q. Wang, L. Yu, C. Wang, S. Dai, Y. Yuan, Catal. Lett. 74 (2001) 221.

[15] J. Barrault, M. Boulinguiez, C. Forquy, R. Maurel, Appl. Catal. 33 (1987) 309.

[16] G. Mul, I. Wachs, A. Hirschon, Catal. Today 78 (2003) 327.

[17] A. Chen, Q. Wang, Q. Li, Y. Hao, W. Fang, J. Mol. Catal. A 283 (2008) 69.

[18] C. Kaufmann, O. Gutiérrez, Y. Zhu, J. Lercher, Res. Chem. Int. 36 (2010) 211.

[19] N. Verbruggen, G. Mest, L. von Hippel, B. Lengeler, H. Knözinger, Langmuir 10 (1994) 3063.

[20] V. Kettmann, P. Balgavy, L. Sokol, J. Catal. 112 (1988) 93.

[21] A. von Müller, H. Schulze, W. Sievert, N. Weinstock, Z. Anorg. Allg. Chem. 403 (1974) 310.

[22] A. Ranade, M. Stockburger, Chem. Phys. Lett. 22 (1973) 257.

[23] G. Schrader, C. Cheng, J. Catal. 80 (1983) 369.

[24] A. Stacy, D. Hodul, J. Phys. Chem. Solids 46 (1985) 405.

[25] W. Kiefer, H. Bernstein, Chem. Phys. Lett. 8 (1971) 381.

[26] R. Somoano, V. Hadek, A. Rembaum, J. Chem. Phys. 58 (1973) 697.

[27] F. Wypych, C. Solenthaler, R. Prins, Th. Weber,
   J. Solid State Chem. 144 (1999) 430.

[28] F. Farhad, I. Safarik, O. Strausz, M. Torres, E. Yildirim,
   Ind. Eng. Chem. Res. 35 (1996) 3854.

[29] A. Chen, Q. Wang, Y. Hao, W. Fang, Y. Yang, Catal. Lett. 118 (2007) 295.

[30] A. Startsev, Catal. Rev. – Sci. Eng. 37 (1995) 353.

[31] R. Chianelli, M. Siadati, M. De la Rosa, G. Berhault, J. Wilcoxon, R. Bearden Jr.,
   B. Abrams, Catal. Rev. 48 (2006) 1.

[32] M. Breysse, E. Furimsky, S. Kasztelan, M. Lacroix, G. Perot,
   Catal. Rev. – Sci. Eng. 44 (2002) 651.

[33] M. Jiang, G. Bian, Y. Fu, J. Catal. 146 (1994) 144.

[34] J. Lee, S. Kim, K. Lee, I. Nam, J. Chung, Y. Kim, H. Woo,
   Appl. Catal. A 110 (1994) 11.

[35] A. Anderson, J. Yu, J. Catal. 119 (1989) 135.

[36] Y. Li, R. Wang, L. Chang, Catal. Today 51 (1999) 25.

[37] K. Park, J. Kong, Top. Catal. 18 (2002) 175.

[38] F. Dumeignil, J. Paul, E. Veilly, E. Qian, A. Ishihara, E. Payen, T. Kabe,
   App. Catal. A 289 (2005).

[39] Y. Okamoto, M. Kawano, T. Kubota, Chem. Commun. 9 (2003) 1086.

[40] N. Topsøe, H. Topsøe, J. Catal. 84 (1986) 386.

[41] D. Beck, J. White, C. Ratcliffe, J. Phys. Chem. 90 (1986) 3132.

[42] O. Saur, T. Chevreau, J. Lamotte, J. Travert, J. Lavalley,
   J. Chem. Soc. Faraday Trans. 1 77 (1981) 427.

[43] A. Tsyganenko, F. Can, A. Travert, F. Maugé, Appl. Catal. A 268 (2004) 189.

[44] R. Bohn, G. Brabson, A. Lester, J. Phys. Chem. 96 (1992) 1582.

[45] X. Xie, Y. Tao, H. Cao, W. Duang, Chem. Phys. 213 (1996) 133.

[46] M. Nguyen, T. Nguyen, H. Le, J. Phys. Chem. A 103 (1999) 5758.

[47] J. Spirko, M. Neiman, A. Oelker, K. Klier, Surf. Sci. 572 (2004) 191.

[48] A. Startsev, I. Zakharov, V. Parmon, J. Mol. Catal. A 192 (2003) 113.

[49] J. Lipsch, G. Shuit, J. Catal. 15 (1969) 179.

[50] H. Kwart, G. Shuit, B. Gates, J. Catal. 61 (1980) 128.

[51] F. Bataille, J. Lemberton, P. Michaud, G. Pérot, M. Vrinat, M. Lemaire, E. Schultz,
   M. Breysse, S. Kasztelan, J. Catal. 191 (2000) 409.

Chapter 4

Influence of Potassium on the Synthesis of Methanethiol from Carbonyl Sulfide on Sulfided Mo/Al$_2$O$_3$ Catalyst

Potassium-doped MoS$_2$ catalysts supported on Al$_2$O$_3$ were synthesized, characterized by using atomic absorption spectroscopy, N$_2$ physisorption, NO adsorption, X-ray diffraction, temperature-programmed sulfidation, and Raman spectroscopy, and tested in the synthesis of methanethiol from carbonyl sulfide (COS) and H$_2$. The results revealed that two phases, pure MoS$_2$ and potassium-decorated MoS$_2$ (formed at high potassium loadings), were present in the active catalysts. The main effect of potassium during sulfidation and during the catalytic reaction was to increase the mobility of surface oxygen or sulfur atoms. Thus, potassium promoted the disproportionation of COS to CO$_2$ and CS$_2$ and the production of CO from CO$_2$. Additionally, potassium cations hindered the reductive decomposition of COS to CO and H$_2$S and the hydrogenolysis of methanethiol to methane. Mars-van Krevelen-type mechanisms were proposed to explain the disproportionation of COS on alumina and on the MoS$_2$ phases. The catalytic site in the potassium-decorated MoS$_2$ phase was proposed to include a potassium cation as adsorption site.

4.1. Introduction

Methyl mercaptan, or methanethiol, (CH_3SH) is a raw material of large industrial relevance and is used in the synthesis of valuable organosulfur compounds, such as pesticides, pharmaceuticals, and solvents. The main application of methanethiol is in the production of methionine, which is used as a feed supplement [1]. A state-of-the-art reaction route for the formation of methanethiol is the thiolation of methanol on sulfide tungsten catalysts [2, 3]. However, as early as 1962, Olin et al.[4] demonstrated that methanethiol can be obtained from H_2S containing synthesis gas. Such a direct route from syngas to methanethiol would have a significant economic advantage over the currently practiced routes [5–17].

Alkali-doped MoS_2 catalysts are among the most studied systems for the synthesis of methanethiol from H_2S containing syngas because of their high selectivity to methanethiol. For example, Chen et al.[17] report that sulfided molybdenum catalysts show low CO conversions and carbonyl sulfide (COS) as the most abundant product. The conversion of CO increases from less than 10% to 20, 43, and 39% after incorporating Li, K, or Cs, respectively, into the catalyst. The selectivity to CH_3SH was higher than 40% after the addition of alkali metals. The most common alkali metal used to increase the selectivity to methanethiol is potassium; the promoter effect of potassium on sulfided catalysts was observed in molybdenum- and tungsten- based catalysts using any carbon oxide as starting material [8,12,13]. Thus, the presence of potassium in sulfided catalysts plays a fundamental role in the H_2S syngas route by improving the main reaction steps to CH_3SH or suppressing undesired side reactions.

COS is the first intermediate observed in the synthesis of methanethiol starting from H_2S containing syngas [8,9,15]. However, the synthesis of CH_3SH using COS as a starting material has received only limited attention. We explored this approach, performing the synthesis of CH_3SH from a syngas mixture in two consecutive reactors. In the first reactor, the synthesis of COS and H_2S was achieved by reacting mixtures of carbon oxides and hydrogen with liquid sulfur [18]. In the second stage, the synthesis of methanethiol from COS and H_2 in the presence of H_2S was completed by using a flow reactor loaded with a catalyst bed [19]. The synthesis of methanethiol from COS does not proceed in a single hydrogenation step, but through disproportionation of COS to CO_2 and CS_2 followed by consecutive hydrogenation of CS_2 to methanethiol.

Considering the key role of alkali metals in the synthesis of methanethiol, the aim of this work is to explore the effect of potassium on the main steps of the reaction pathway for the synthesis of CH_3SH from COS. A detailed description of this effect can be provided by

performing kinetic experiments on alumina, potassium-doped alumina, and sulfided Mo/Al_2O_3 catalysts doped with increasing amounts of potassium. The effect of potassium in several reactions, that is, the sulfidation of the catalysts and disproportionation and decomposition of COS, is elucidated by combining detailed kinetic measurements and physicochemical characterization of the materials.

4.2. Experimental

4.2.1. Catalyst preparation and activation

The catalysts were prepared by using the incipient wetness impregnation technique using Al_2O_3 (Aeroxide Alu C, Degussa) as support and K_2MoO_4 (Sigma Aldrich, 98%) or $(NH_4)_6Mo_7O_{24} \cdot 4H_2O$ (Sigma Aldrich, 99.98%) as molybdenum precursor. Two potassium-containing catalysts were prepared by applying a second impregnation step to the MoO_3/Al_2O_3 oxide precursor using aqueous solutions of KOH (Sigma Aldrich, 99.99 %). Potassium-doped Al_2O_3 ($K-Al_2O_3$) was obtained by impregnation of pure alumina with an aqueous solution of KOH (2 mmol KOH per gram of alumina). The materials were dried at 353 K for 12 h and treated in dry air at 773 K for 12 h after each impregnation. The molybdenum loading was kept constant at 1.17 mmol/g in all the molybdenum-containing precursors, whereas in the doped materials the loading of potassium was varied to achieve cationic ratios K/Mo of 0.16, 0.6 and 2. The catalysts were denoted as MoK_x/Al_2O_3, in which x is the K/Mo molar ratio (Mo/Al_2O_3 was the undoped catalyst). Prior to activity measurements, the catalysts (0.5 g) were sulfided in situ in a gas stream with 10 vol % H_2S in H_2 at 3 MPa and 673 K for 12 h.

4.2.2. Elemental composition and textural properties

Atomic absorption spectroscopy (AAS) was used to determine the molybdenum and potassium contents of the oxide precursors by using a UNICAM 939 spectrometer. The nitrogen adsorption-desorption technique was used to determine the surface area and pore volume of the oxide precursors by using a PMI automated BET sorptometer. The samples were degassed in vacuum at 673 K for 2 h before N_2 adsorption.

4.2.3. X-ray diffraction

The oxide precursors and the sulfide catalysts used in the reactions were characterized by using X-ray diffraction (XRD). The samples of the used catalysts were analyzed using XRD after cooling down the reactor to room temperature while maintaining a reactant mixture stream. A Philips X'Pert Pro System (Cu Kα1-radiation, λ= 0.154056 nm) operating at 45 kV and 40 mA was used for recording the diffractograms. Measurements were performed by using a step size of 2θ = 0.0178 and 115 s as counting time per step.

4.2.4. Temperature-programmed sulfidation

The materials were characterized by performing temperature-programmed sulfidation (TPS) in a flow apparatus equipped with a mass spectrometer (QME 200, Pfeiffer Vacuum) as detector. A sample of the oxide precursor (0.1 g) was loaded in a quartz reactor and dried in situ (2 h at 673 K in a helium gas stream) before each TPS experiment. After drying and cooling down to room temperature, the materials were heated to 673 K in a mixture of H_2S/H_2 (10 vol % H_2S/H_2), at a flow rate of 2 cm^3/min, and diluted with helium at a flow rate of 8 cm^3/min. Finally, the sample was kept at 673 K under the same $H_2S/H_2/He$ mixture for 2 h.

4.2.5. NO adsorption

The volume of adsorbed NO was measured in a flow apparatus equipped with a mass spectrometer (QME 200, Pfeiffer Vacuum) by means of a pulse technique. A sample of each catalyst (0.1 g) was loaded in a quartz reactor and sulfided in 10 vol % H_2S/H_2 at 673 K for 3 h. After flushing the reactor with helium at 300 K for 5 h, pulses of 10 vol % of NO in helium were introduced periodically. The total concentration of adsorbed NO was determined from the sum of the NO adsorption per pulse.

4.2.6. Raman spectroscopy

Raman characterization of the catalysts was applied to determine the effect of COS on the catalytic surface. A sample of each catalyst was sulfided in situ under a flow of 10 vol % H_2S in H_2 at 673 K and atmospheric pressure for 2 h. The samples were cooled down to 290 K in N_2 to record the corresponding spectra. Then, the as-sulfided sample was exposed to a stream of pure COS (Aldrich, >97.5%) at 673 K for 30 min. New spectra were acquired after cooling

down to 290 K in N_2. Raman spectra were recorded on a Renishaw Raman Spectrometer Series 1000 Microscope equipped with an argon laser with a wavelength of λ=514 nm.

4.2.7. Kinetic measurements

The H_2S and COS mixtures were synthesized in a semi-batch reactor (pre-reactor) by reacting flowing CO and H_2 with liquid sulfur. The reaction conditions in this step were adapted to achieve complete conversions of CO to COS and the desired concentration of H_2S. The product of the pre-reactor was mixed with H_2 and N_2 to adjust the desired H_2/COS ratio and the total gas flow rate before entering the second reactor (main reactor), in which the catalyst bed was located. All starting reactant compositions given in this work refer to the gas mixture entering the main reactor. Details of the experimental setup can be found in previous reports [18,19].

The catalytic properties of Al_2O_3, K-Al_2O_3 and molybdenum-containing catalysts were determined at 3 MPa using a feed of 10 vol % COS, 20 vol % H_2S, and 70 vol % H_2 with a total flow rate of 21 cm^3/min, which corresponds to a gas hourly space velocity (GHSV) of 3024 h^{-1}. GHSV was defined as ν/$V_{catalyst}$ (ν is the volumetric flow rate and $V_{catalyst}$ is the total volume of the catalyst bed). The effect of the H_2/COS ratio was investigated at 3 MPa and an overall flow rate of 37 cm^3/min (GHSV=5328 h^{-1}) using a fixed concentration of COS (8 vol %) and a H_2/H_2S ratio of 5.3. The products were analyzed by performing gas chromatography using a Shimadzu GC 2014 equipped with a packed Haysep Q and a packed molecular sieve (13X) column.

4.3. Results

4.3.1. Elemental composition and textural properties

The concentrations of potassium and molybdenum in the precursor mixture and the elemental contents of the catalysts, as determined by using atomic absorption spectroscopy (AAS) analysis, are compiled in Table 4.1. Good agreement was found between the concentrations used in the preparation step and those found in the final oxide materials. The catalysts are denoted as MoK_x/Al_2O_3, where x is the K/Mo molar ratio (Mo/Al_2O_3 is the undoped catalyst). An overview of the textural characteristics of the oxide catalysts is also given in Table 4.1. The Brunauer-Emmett-Teller (BET) surface area, as well as the pore

volume of the oxide materials, increased as potassium was added to the Mo/Al_2O_3 catalyst. For example, the BET surface area increased from 55 m^2/g for the Mo/Al_2O_3 catalyst to74, 68, and 65 m^2/g as the K/Mo ratio increased to 0.16, 0.6, and 2, respectively.

Table 4.1: Potassium and molybdenum concentrations determined by using AAS. BET surface area and pore volume determined by performing N_2 physisorption. Concentration of NO adsorbed on the sulfide catalysts.

Material	K (wt. %)[a]	Mo (wt. %)[a]	BET surface area (m^2/g)	Pore volume (cm^3/g)	Adsorbed NO ($\mu mol\ g^{-1}$)
Mo/Al_2O_3	-	(13.3) 13.0	55	0.09	55
$MoK_{0.16}/Al_2O_3$	(0.65) 0.6	(13.3) 12.8	74	0.16	75
$MoK_{0.6}/Al_2O_3$	(1.3) 1.1	(13.3) 12.5	68	0.13	90
MoK_2/Al_2O_3	(10.8) 9.0	(13.3) 12.6	65	0.12	270

[a] As determined in the precursor mixture (in parentheses) and in the oxide materials

4.3.2. X-ray diffraction measurements

The X-ray diffraction (XRD) patterns of the catalysts in their oxide form are shown in Figure 4.1. Signals corresponding to the supporting Al_2O_3 are neither marked nor discussed here. The species formed in the oxide precursors after thermal treatment depended to a large extent on the potassium-loading and the precursor. Regarding Mo/Al_2O_3, two molybdenum-containing crystalline phases were detected, MoO_3 (PDF number 00-005-0508) and $Al_2(MoO_4)_3$ (PDF number 01-085-2286). On doping the molybdenum catalysts with an increasing amount of potassium, the concentration of these phases decreased rapidly, and $KAl(MoO_4)_2$ (PDF number 01-074-2008) became the most abundant phase. In the MoK_2/Al_2O_3 catalyst, the only observed molybdenum-containing crystalline phase was the precursor, K_2MoO_4 (PDF number 00-024-0880). The XRD patterns suggested the presence of relatively large crystals of molybdenum-containing species. Comparing the potassium-free catalyst to the $MoK_{0.16}/Al_2O_3$ sample, the amount of the crystalline species increased after loading with potassium. Thus, we speculated that the space between the crystals of the molybdenum species, formed on addition of potassium, contributed to the textural properties

and resulted in an increase of the BET surface area and the pore volume observed by performing physisorption of N_2 (Table 4.1). Increasing the loading of potassium did not further increase the textural properties, probably because of an increase in the density of the material.

After the activity tests, the catalysts were collected and the corresponding XRD patterns were also measured. Regardless of the crystalline species present in the oxide precursor, only crystalline signals corresponding to the support and MoS_2 (PDF number 00-024-0513) were observed in the sulfide and used catalyst. As an example, the XRD patterns of the sulfided and used MoK_2/Al_2O_3 catalyst are shown in Figure 4.1.
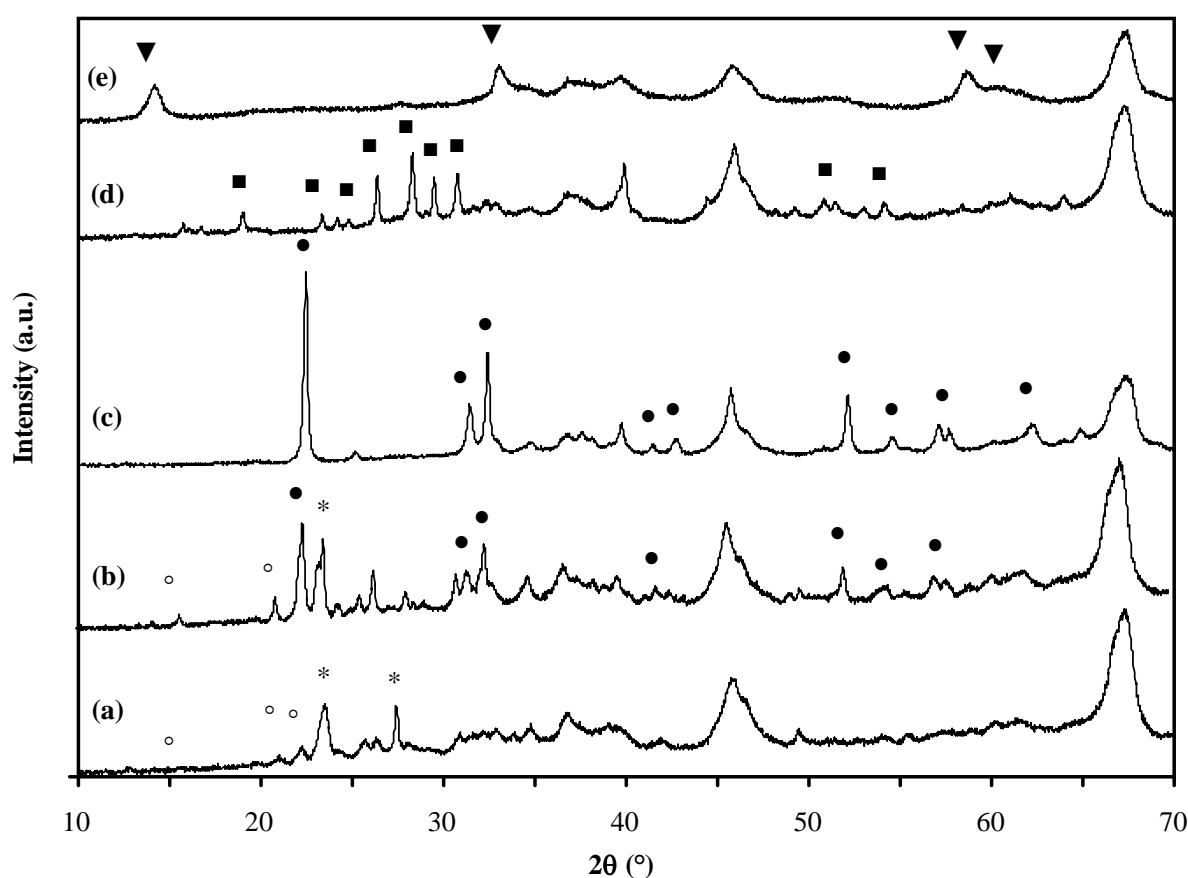
Figure 4.1: XRD patterns of the oxide precursors (a) Mo/Al_2O_3 ; (b) $MoK_{0.16}/Al_2O_3$;
(c) $MoK_{0.6}/Al_2O_3$; (d) MoK_2/Al_2O_3 ; and (e) the sulfided MoK_2/Al_2O_3 catalyst after the reaction of COS and H_2 to CH_3SH. * MoO_3, o $Al_2(MoO_4)_3$, ● $KAl(MoO_4)_2$, ■ K_2MoO_4, and ▼ MoS_2.

4.3.3. Temperature-programmed sulfidation

H_2S consumption profiles recorded during temperature-programmed sulfidation (TPS) experiments of selected materials are shown in Figure 4.2. The potassium-doped Al_2O_3 sample exhibits continuous H_2S consumption from 400 to 673 K. In contrast, pure alumina does not consume H_2S during the experiment (not shown). The H_2S consumption profiles of the molybdenum-containing materials having a K/Mo ratio of 0.6 or lower can be divided into three main regions. The first one is characterized by a small and continuous H_2S consumption in the temperature range from 350 to 540 K. The second stage is best represented by a "shoulder" and a rapid H_2S adsorption at approximately 550 K. Finally, as the temperature is kept constant at 673 K, a quasi-constant H_2S adsorption is observed before the profile returns to the baseline.
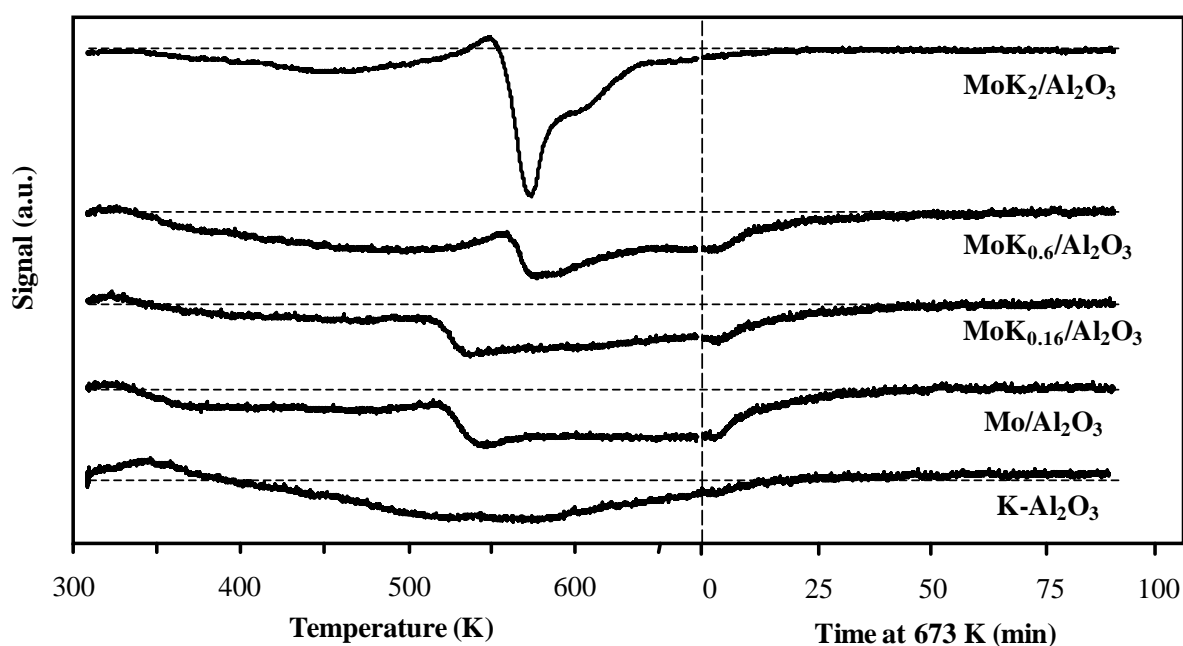
Figure 4.2: H_2S-consumption profiles of the TPS experiments performed on the oxide precursors of the molybdenum catalysts and K-Al_2O_3.

The H_2S adsorption profile of the MoK_2/Al_2O_3 sample differs from the profiles of the other catalysts. This is attributable to the different oxide precursor (see the XRD patterns in Figure 4.1). For this sample, the H_2S adsorption between 300 and 500 K is followed by a small H_2S release peak. Then, H_2S is consumed rapidly, reaching a minimum in the consumption profile at 560 K. Finally, the H_2S consumption line returns to zero, displaying a small, almost constant region at 590 K. Notably, it takes less time for the H_2S signal in this

experiment to return to the baseline than for the other materials. The relative H_2S consumption is determined as the area of the corresponding H_2S adsorption curve from Figure 4.2. If the H_2S consumption of the Mo/Al_2O_3 catalyst is set as 100 %, the H_2S adsorption of the other molybdenum catalysts is 87, 98, and 137% for $MoK_{0.16}/Al_2O_3$, $MoK_{0.6}/Al_2O_3$, and MoK_2/Al_2O_3, respectively.

4.3.4. NO adsorption

The adsorption of NO per pulse on the samples sulfided in situ is presented in Table 4.1. NO adsorption on the Mo/Al_2O_3 sample is 55 mmol/g and increases to 75, 90, and 270 mmol/g on the $MoK_{0.16}/Al_2O_3$, $MoK_{0.6}/Al_2O_3$, and MoK_2/Al_2O_3 samples, respectively. Therefore, we conclude that the adsorption of NO increases linearly with the concentration of potassium.

4.3.5. In situ Raman spectroscopy

The Raman spectra of the sulfide catalysts before and after COS exposure are compiled in Figure 4.3. In all the spectra of the as-sulfided catalysts the following bands corresponding to MoS_2 are observed: $\tilde{\nu}$ =380 (Mo-S stretching mode along the basal plane), 405 (S-Mo-S stretching mode along the c-axis), and 450 cm^{-1} (second-order scattering) as well as the discernible signals between $\tilde{\nu}$ =500 and 900 cm^{-1} [20]. Bands corresponding to oxide species or potassium-containing species are not present after in situ sulfidation.

In the spectra recorded after exposure to COS at 673 K, no significant changes are observed for the catalysts with low potassium content, Mo/Al_2O_3 and $MoK_{0.16}/Al_2O_3$. At high potassium concentrations, that is, the $MoK_{0.6}/Al_2O_3$ and MoK_2/Al_2O_3 catalysts, the spectra recorded after COS treatment exhibit two additional bands at approximately $\tilde{\nu}$ =440 and 490 cm^{-1}. According to Schrader and Cheng [20], both bands are assigned to metal-sulfur vibrations for the oxysulfide species.
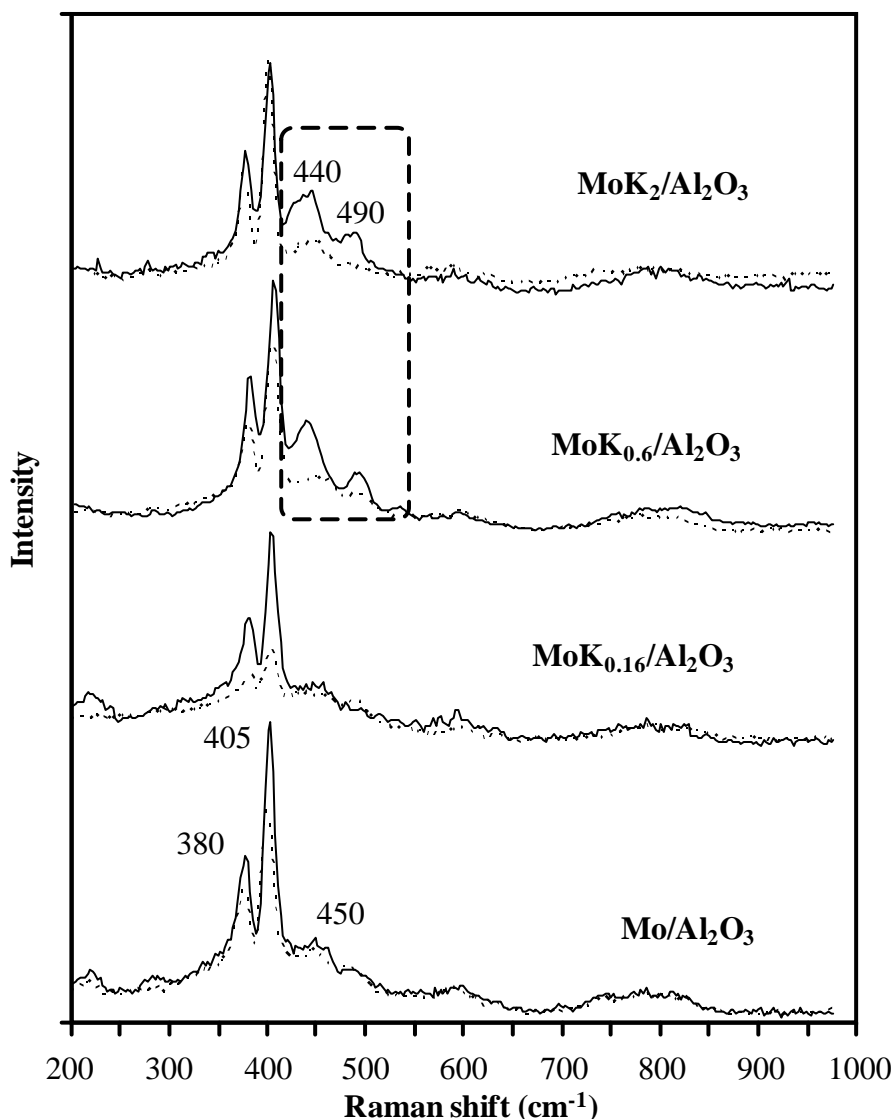
Figure 4.3: Raman spectra of sulfided molybdenum catalysts before (——) and after (·······) flowing COS for 30 min at 673 K.

4.3.6. Effect of potassium on the catalytic activity

The molybdenum catalysts, alumina (Al_2O_3), and potassium-doped alumina ($K-Al_2O_3$) are tested in the synthesis of CH_3SH from H_2 and COS. The conversion and product yield obtained on Al_2O_3 and $K-Al_2O_3$ are shown in Figure 4.4. On pure alumina, the conversion of COS increases linearly from 6% at 423 K to 50% at 573 K and then rapidly rises to approximately 90% above 573 K. At temperatures below 573 K, CO_2 and CS_2 are the main products and are produced at identical concentrations. CO is the most abundant product above 573 K, whereas the yield of CS_2 decreases faster than that of CO_2. This decrease in the CS_2

yield is accompanied by an increase in the yield of CH_3SH. On potassium-doped alumina, the conversion of COS is lower than on pure alumina in the evaluated temperature range. Interestingly, the yields of CO_2, CS_2, and CH_3SH are very similar on Al_2O_3 and $K-Al_2O_3$. The yield of CO, however, is significantly lower on potassium-doped alumina; hence, the lower conversion of COS on $K-Al_2O_3$ is attributed to the inhibition of the conversion of COS to CO.
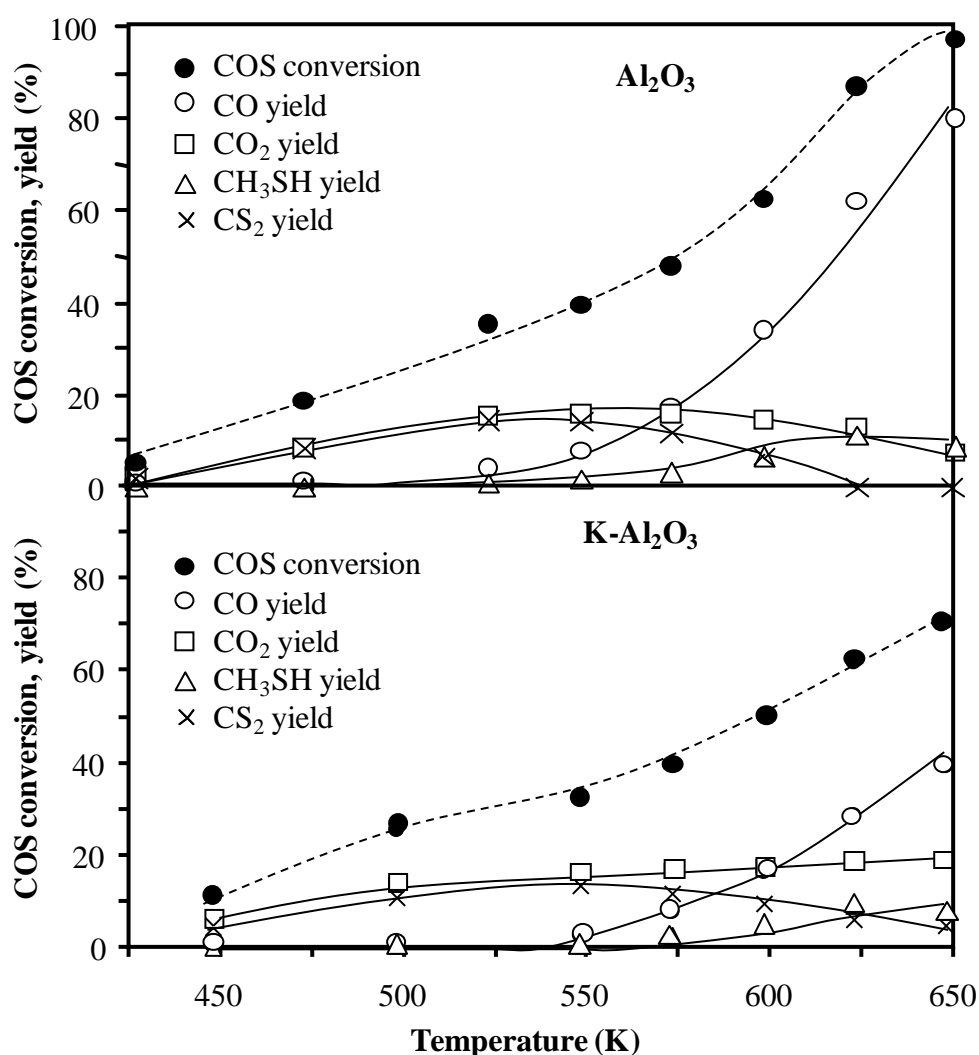
Figure 4.4: COS conversion (●) and product yields (o CO, □ CO_2, Δ CH_3SH, and x CS_2) on pure Al_2O_3 and $K-Al_2O_3$. 30 MPa, 10 vol% COS, 20 vol% H_2S, 70 vol% H_2, 21 cm^3/min overall flow rate or GHSV=3024 h^{-1}.

Using an H_2/COS ratio of 7 on MoS_2-containing catalysts, the conversion of COS is higher than 94% in the temperature range of 523-673 K, regardless of the concentration of potassium. The product yield is illustrated in Figures 4.5 and 4.6 (CS_2 was not detected in this series of experiments). For clarity, the results for the $MoK_{0.16}/Al_2O_3$ catalyst are not shown,

because the low potassium content (1 wt %) does not influence the catalytic performance significantly.

The dependence of the yield of carbon oxides on temperature and potassium loading is presented in Figure 4.5. The yield of CO_2 increases as potassium is added to the catalyst up to 598 K. Above that temperature, increasing the potassium loading results in a lower yield of CO_2. The yield of CO displays an opposite trend: below 598 K, the yield of CO decreases, but it increases at higher temperatures and with increasing potassium concentration.
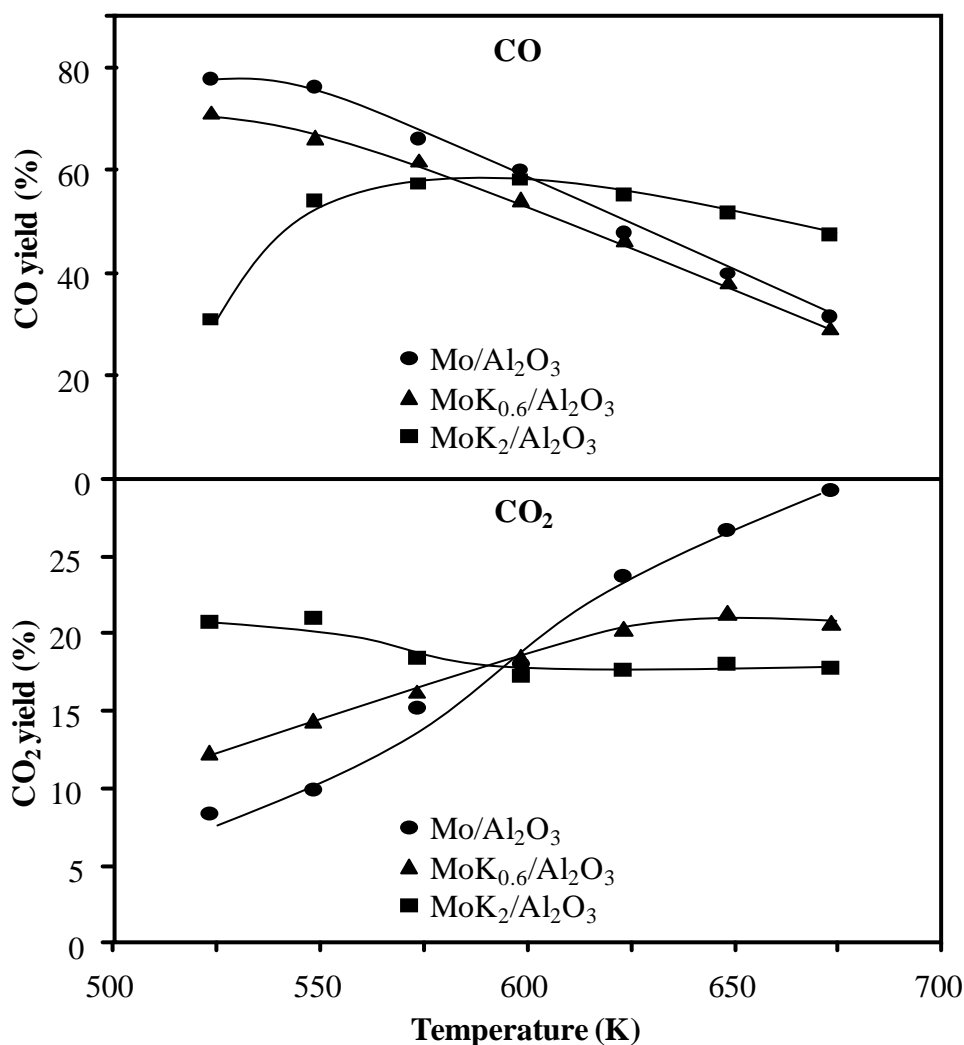
Figure 4.5: Yield of CO and CO_2 on Mo/Al_2O_3 (●), MoK$_{0.6}$/Al_2O_3 (▲) and MoK$_2$/Al_2O_3 (■). 30 MPa, 10 vol% COS, 20 vol% H_2S, 70 vol% H_2, 21 cm^3/min overall flow rate or GHSV=3024 h^{-1}.

The increase in the potassium concentration results in an increase in the yield of CH_3SH (Figure 4.6). The maximum yield of CH_3SH is 6.8% at 523 K on the potassium-free catalyst and decreased with higher temperatures, whereas the MoK$_{0.6}$/Al_2O_3 catalyst has a maximum

of 18.3% at 598 K. The yield of CH_3SH is stable between 17 and 23% over the MoK_2/Al_2O_3 catalyst in the evaluated temperature range. The formation of methane (CH_4) is favored on increasing the temperature, but is suppressed by increasing the potassium content (Figure 4.6). On MoK_2/Al_2O_3, for instance, the CH_4 yield remains below 10% even at 673 K.

It is evident from these results that the main differences were observed between the Mo/Al_2O_3 and MoK_2/Al_2O_3 catalysts. Consequently, the influence of the reaction conditions on the synthesis of methanethiol was studied by focusing on these two catalysts.
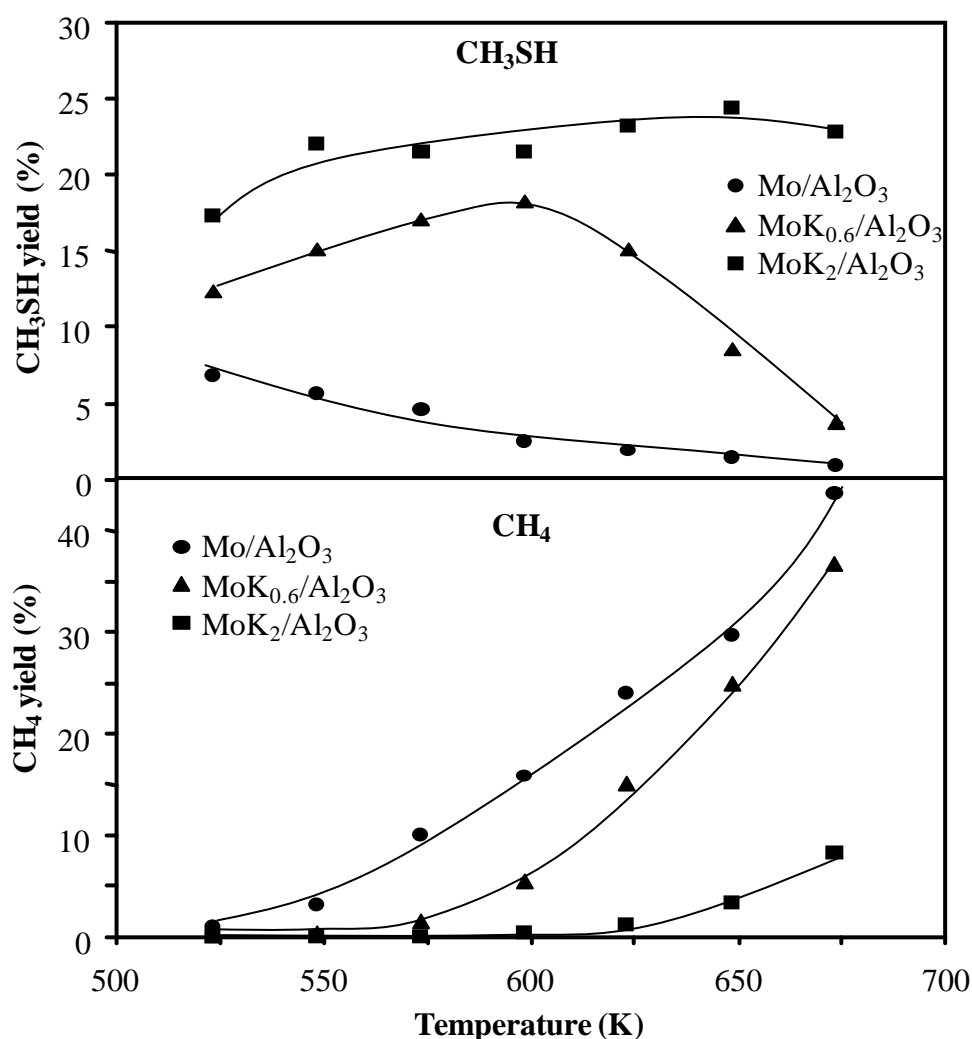
Figure 4.6: Yield of CH_3SH and CH_4 on Mo/Al_2O_3 (●), $MoK_{0.6}/Al_2O_3$ (▲), and MoK_2/Al_2O_3 (■). 30 MPa, 10 vol% COS, 20 vol% H_2S, 70 vol% H_2, 21 cm^3/min overall flow rate or GHSV=3024 h^{-1}.

4.3.7. Variation of the H_2/COS ratio

The conversion of COS obtained by varying the H_2/COS ratio are presented in Figure 4.7. The common trend is that an increasing H_2/COS ratio results in higher conversions. Furthermore, at given conditions, the Mo/Al_2O_3 catalyst exhibits a higher conversion of COS than the MoK_2/Al_2O_3 sample. For instance, at 543 K, the COS conversion is above 90% on Mo/Al_2O_3, but below 60% on MoK_2/Al_2O_3. The conversion of COS reaches values higher than 90% on both catalysts above 600 K for all tested H_2/COS ratios.
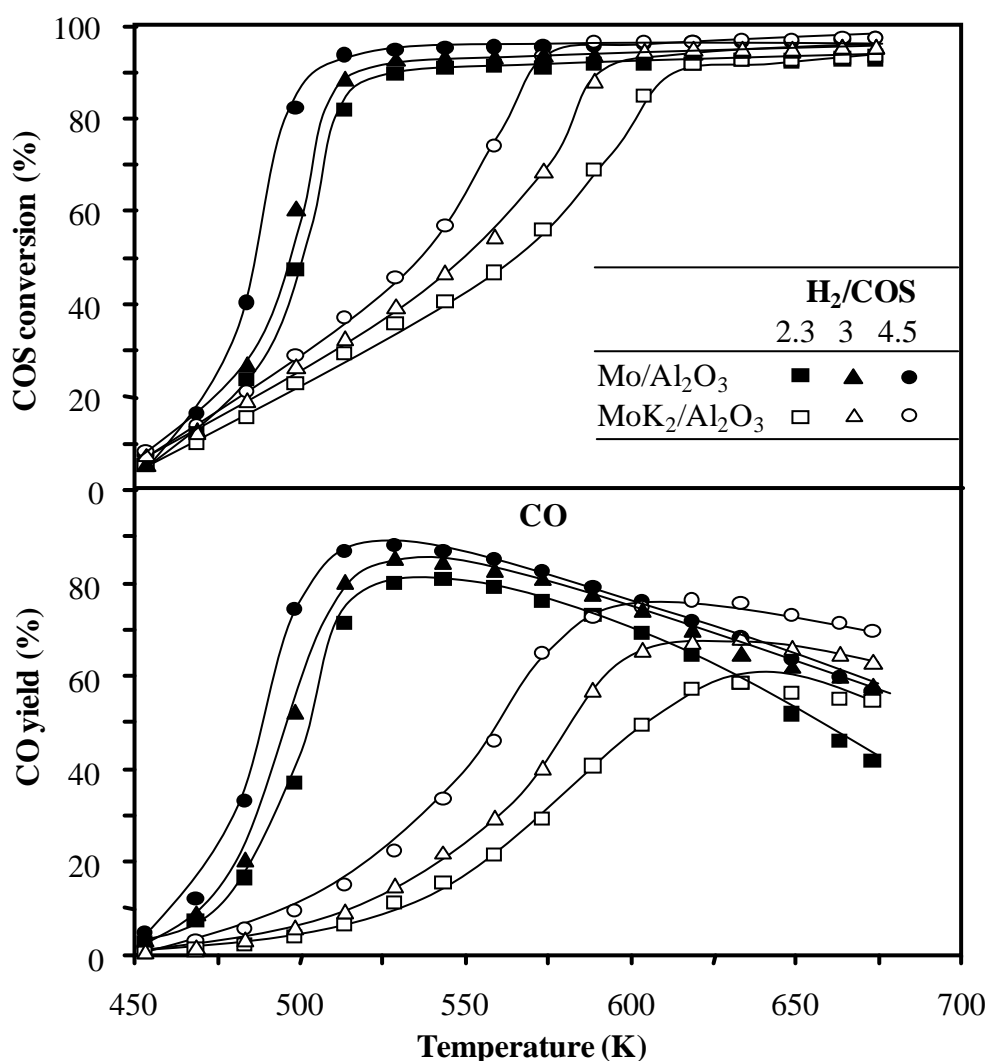
Figure 4.7: a) COS conversion and b) yield of CO at H_2/COS ratios of 2.3 (squares), 3 (triangles), and 4.5 (circles) on sulfided Mo/Al_2O_3 (black symbols) or MoK_2/Al_2O_3 (white symbols) at 30 MPa and 37 cm^3/min overall flow rate, corresponding to GHSV=5328 h^{-1}.

The product yields obtained over the Mo/Al_2O_3 and MoK_2/Al_2O_3 catalysts at different H_2/COS ratios and temperatures are shown in Figures 4.7-4.9. In the absence of potassium,

CO was the main product in all experiments. Maximum values for the yield of CO (79–88%) were observed at 528 K. Using the potassium containing catalyst, CO was the main product above 500 K for the ratios $H_2/COS=4.5$ and 3 and above 543 K for $H_2/COS=2.3$. The yield of CO on the MoK_2/Al_2O_3 catalyst, as shown in Figure 4.7, increased to 57-76% at 620 K and declined afterwards. The yield of CO_2 decreased with increasing H_2/COS ratio over pure Mo/Al_2O_3, as shown in Figure 4.8. Using the potassium-containing catalyst, the effect of the H_2/COS ratio on the yield of CO_2 greatly depended on the temperature. Below 573 K, the H_2/COS ratio did not affect the yield of CO_2, whereas above that temperature increasing the H_2/COS ratio reduced the yield of CO_2.
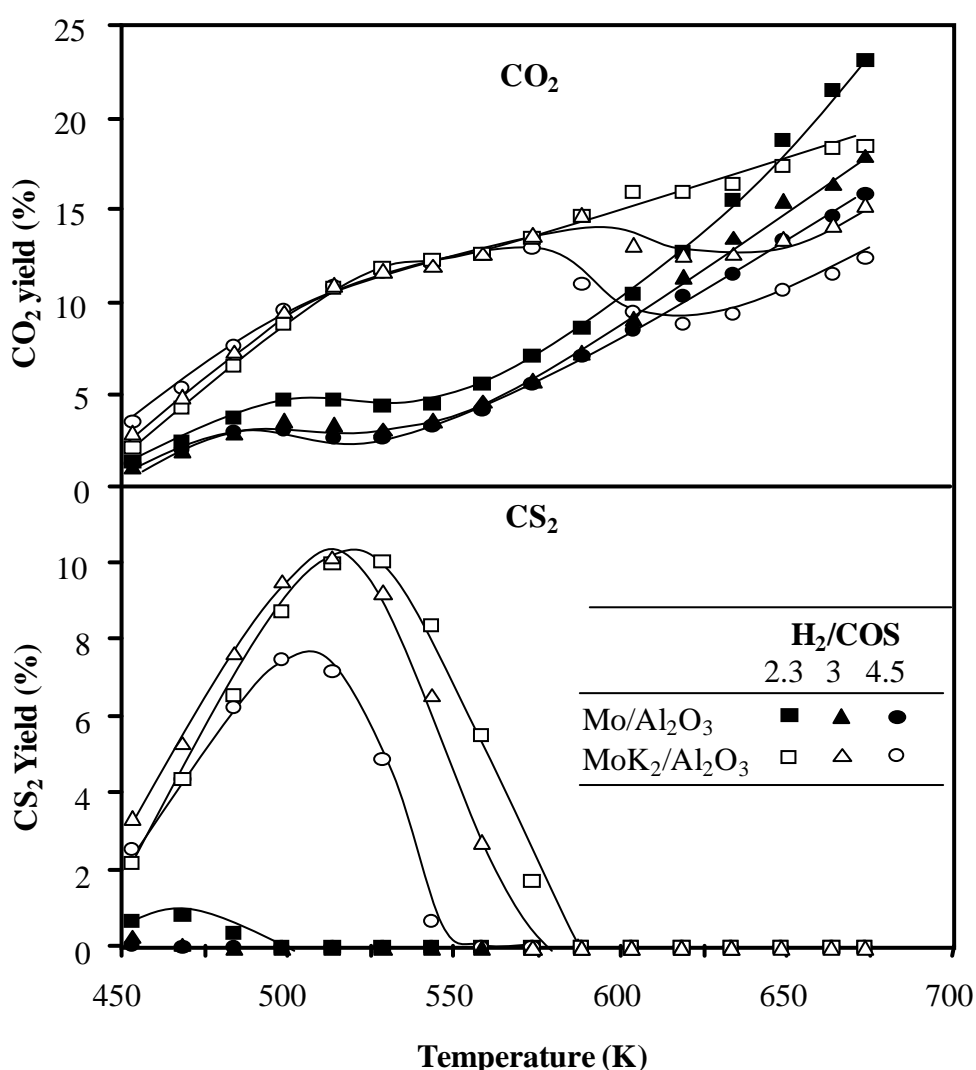
Figure 4.8: Yield of a) CO_2 and b) CS_2 at H_2/COS ratios of 2.3 (squares), 3 (triangles), and 4.5 (circles) on sulfided Mo/Al_2O_3 (black symbols) or MoK_2/Al_2O_3 (white symbols) at 30 MPa and 37 cm^3/min overall flow rate, corresponding to GHSV=5328 h^{-1}.

The yield of CS_2 is shown in Figure 4.8. Significantly larger amounts of CS_2 were formed using the potassium-containing catalyst than using Mo/Al_2O_3. Furthermore, the yield of CS_2 had a maximum at 503-513 K using MoK_2/Al_2O_3, whereas CS_2 was not detected on MoO_3/Al_2O_3 at 493 K or above. For both systems, the concentration of CS_2 decreased with increasing temperature or increasing H_2/COS ratio.

The yield of methanethiol increased until reaching a maximum on increasing the temperature (Figure 4.9). Below 553 K, the yield of CH_3SH was higher on the potassium-free catalyst than on MoK_2/Al_2O_3.
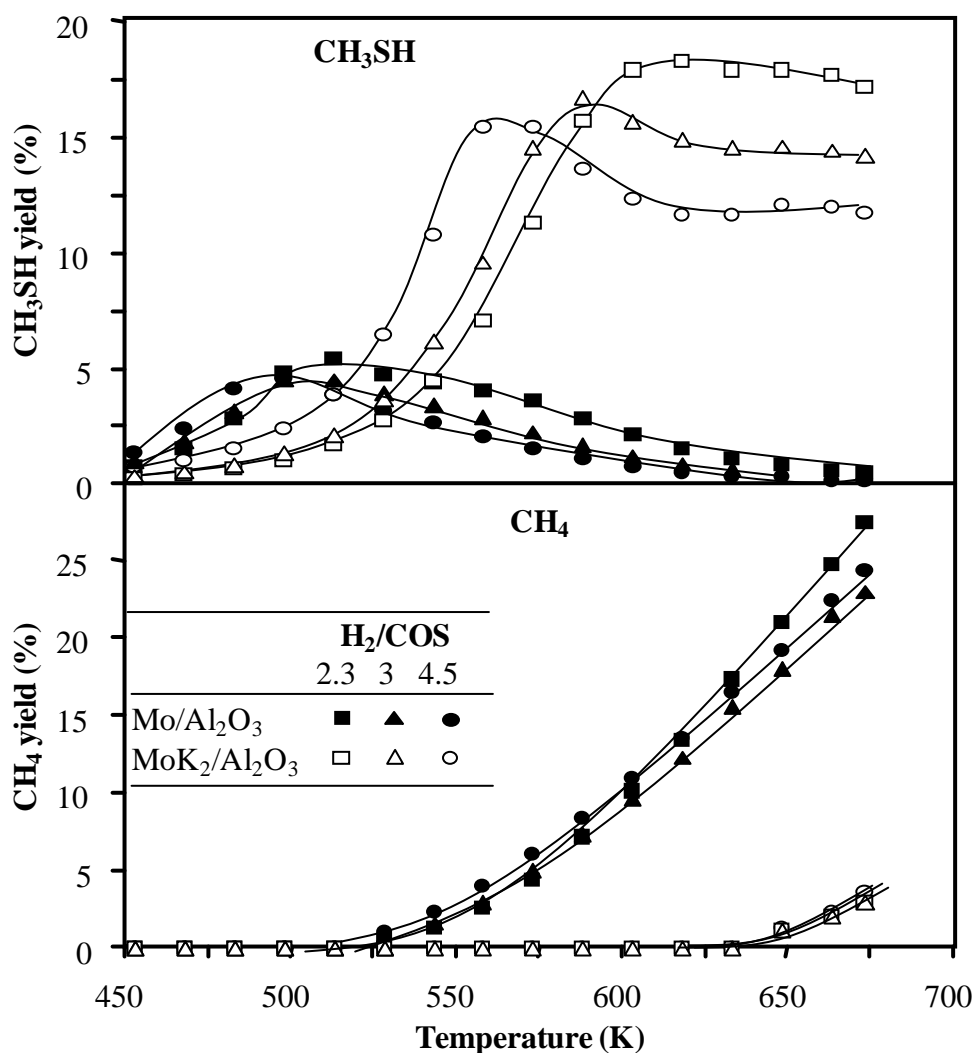
Figure 4.9: Yield of a) CH_3SH and b) CH_4 at H_2/COS ratios of 2.3 (squares), 3 (triangles), and 4.5 (circles) on sulfided Mo/Al_2O_3 (black symbols) or MoK_2/Al_2O_3 (white symbols) at 30 MPa and 37 cm^3/min overall flow rate, corresponding to GHSV=5328 h^{-1}.

The trend was reversed at higher temperatures, that is, on the potassium-free catalyst the yield of CH_3SH decreased with temperature, whereas on the potassium-containing catalyst the yield of CH_3SH was approximately 17% at 553 K and stable at higher temperatures. Significant influence of the H_2 partial pressure on the yield of CH_4 was not observed in both systems, as shown in Figure 4.9. The presence of potassium, however, suppressed the formation of CH_4 significantly. The yield of CH_4 was below 5% over potassium-containing catalysts even at 673 K, whereas on Mo/Al_2O_3 the yield of CH_4 was more than 25% at the same temperature.

4.4. Discussion

4.4.1. Reaction pathway

The yields of CO_2 and CS_2 are almost identical on Al_2O_3 and K-Al_2O_3 up to 520 K (Figure 4.2), indicating that both compounds are formed by disproportionation of COS [Eq. (1)]. The decrease of the yield of CO_2 after reaching the maximum at 540 K is accompanied by an increase in the yield of CO. This is attributed to the reverse water-gas shift reaction [Eq. (2)] and the consecutive reactions [Eqs. (3) and (4)]. The decrease in the yield of CS_2 in parallel with the formation of CH_3SH suggests that methanethiol is the product of CS_2 hydrogenation [Eq. (5)].

$$2\,COS \rightarrow CO_2 + CS_2 \qquad (1)$$

$$CO_2 + H_2 \rightleftharpoons CO + H_2O \qquad (2)$$

$$CO_2 + H_2S \rightleftharpoons COS + H_2O \qquad (3)$$

$$COS + H_2 \rightleftharpoons CO + H_2S \qquad (4)$$

$$CS_2 + 3\,H_2 \rightarrow CH_3SH + H_2S \qquad (5)$$

The main product was CO on MoO_3/Al_2O_3 even at low reaction temperatures (Figure 4.5), suggesting that COS preferentially decomposed to CO and H_2S according to Equation (4). At high temperatures, the decrease of the yield of methanethiol and the formation of CH_4 (Figure 4.6) imply that CH_4 is a product of the hydrogenolysis of methanethiol [Eq. (6)]. CS_2 was only found at low temperatures and low H_2 partial pressures (Figure 4.8), because it was rapidly hydrogenated to methanethiol at 30 MPa [19].

$$CH_3SH + H_2 \rightarrow CH_4 + H_2S \qquad (6)$$

Methanethiol is formed and consumed in hydrogen-consuming reactions, consequently, varying the H_2/COS ratio has two opposite effects. Higher H_2/COS ratios improve the yield of CH_3SH below 500 K on Mo/Al_2O_3 or 570 K on MoK_2/Al_2O_3 (Figure 4.9), but at higher temperatures the yield of CH_3SH decreases with increasing concentrations of H_2. This is in line with our previous study, in which the synthesis of CH_3SH from COS is postulated to occur on sulfided K_2MoO_4/SiO_2, as shown in Scheme 4.1 [19].
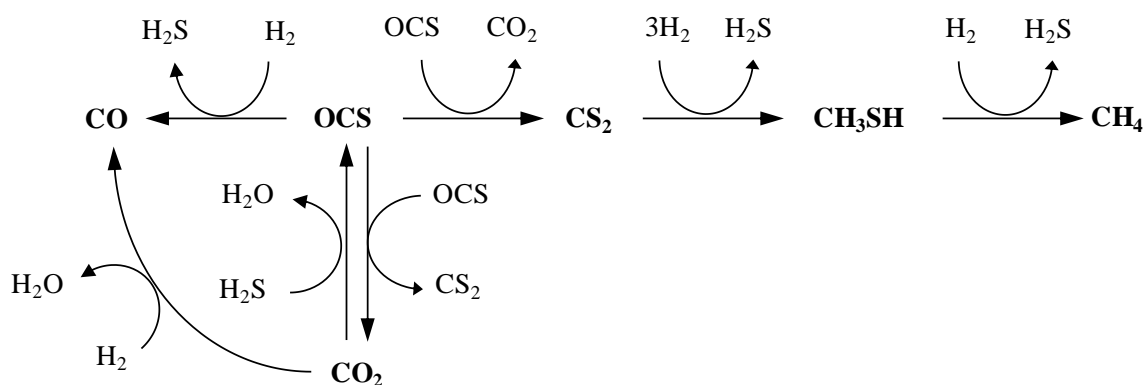
Scheme 4.1: Reaction pathway for the synthesis of CH_3SH from COS, H_2, and H_2S.

COS decomposes to CO and H_2S and disproportionates to CO_2 and CS_2, which is the precursor for methanethiol. At high temperatures, CO_2 is transformed to COS or to CO, whereas methanethiol is further hydrogenated to CH_4.

4.4.2. Effect of potassium during sulfidation

The effect of potassium is evident, when it is added to alumina. H_2S is not adsorbed on pure alumina, whereas on potassium-doped alumina a large amount of H_2S is consumed, releasing water as presented in Figure 4.10.

This can be explained on the basis of the work of Amenomiya et al.[21, 22]. The authors demonstrated that potassium weakens the bonds of oxygen atoms on the surface, that is, the concentration of reactive, mobile oxygen atoms increases. This implies that under a H_2S atmosphere, oxygen atoms on the surface of alumina are replaced by sulfur atoms, which results in H_2S adsorption without apparent H_2 consumption (Figure 4.10). The proposed mechanism for the O-S exchange on the surface of alumina is presented in Scheme 4.2.
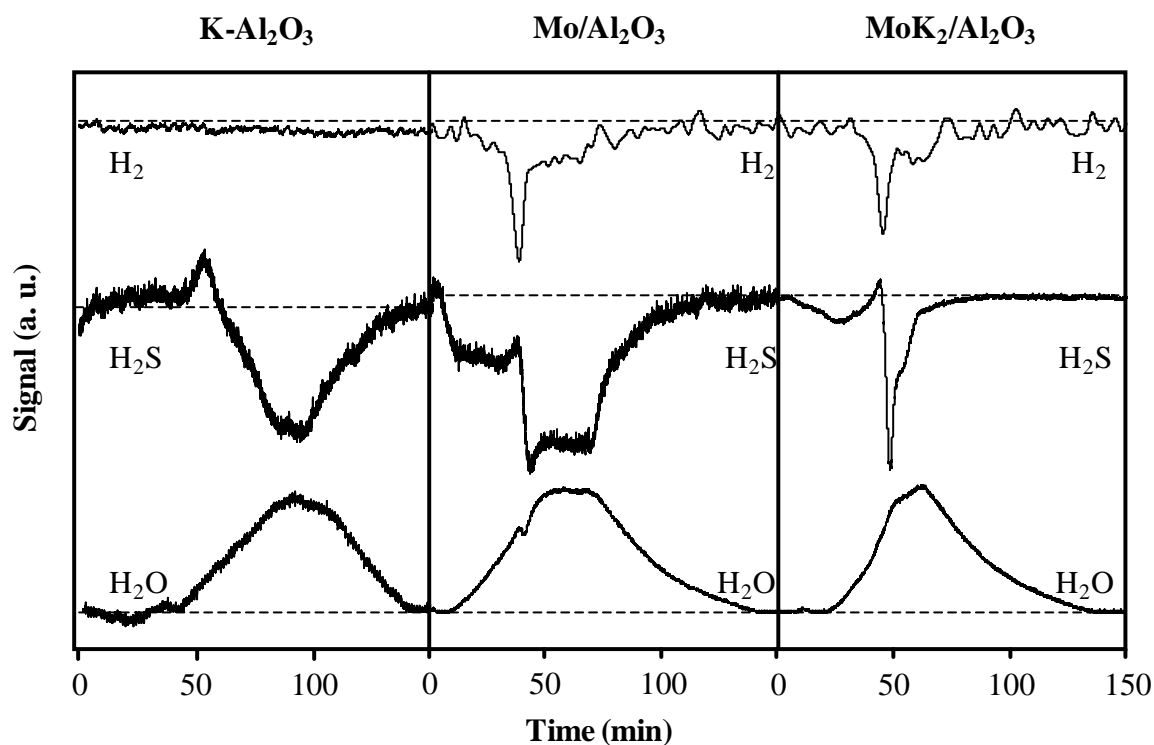
Figure 4.10: H_2, H_2S, and H_2O-evolution-consumption profiles of the TPS experiments of selected materials.
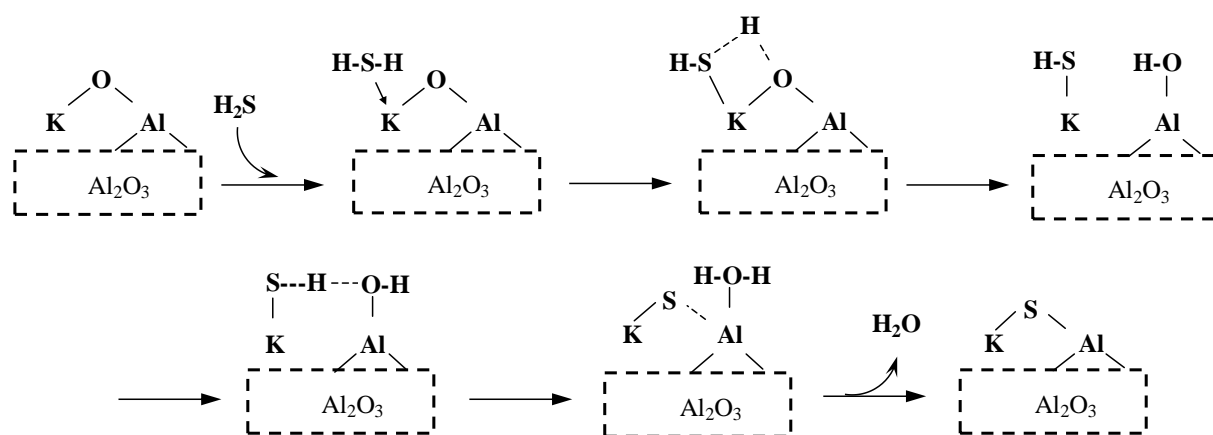
Scheme 4.2: Mechanism for the O-S exchange on the alumina surface.

The donation of electrons from H_2S to the potassium cations on the surface results in the creation of SH and OH groups. Then, the recombination of protons produces an adsorbed water molecule that desorbs, leaving a sulfur atom on the surface.

The temperature-programmed sulfidation (TPS) on alumina-supported molybdenum catalysts, as accepted in the literature, is described before discussing the TPS results of the

molybdenum-containing materials [23]. Sulfidation below 520 K occurs through oxygen-sulfur substitution according to Equation (7). In the same temperature interval, Mo^{6+} is reduced to Mo^{4+} through rupture of Mo-S bonds and formation of elemental sulfur. The sulfur adsorbs on the support and is reduced to H_2S in the presence of H_2 at 510–560 K, resulting in a H_2S production signal coupled with a strong H_2 adsorption in the TPS pattern. The H_2 consumption above 560 K is attributable to the reduction of Mo^{6+} to Mo^{4+}. It is believed that at 560 K, most of the molybdenum ions are already in the Mo^{4+} state because of reductive Mo-S bond breaking. Thus, the H_2S consumption at temperatures above 560 K is ascribed mainly to O-S exchange on Mo^{4+}.

$$Mo^{6+}\text{-}O^{2-} + H_2S \rightarrow Mo^{6+}\text{-}S^{2-} + H_2O \qquad (7)$$

The value for a monolayer of molybdenum-loading on Al_2O_3 is 5.7 atoms of molybdenum per nm^2 [24], whereas the catalysts used in this work have a molybdenum loading of more than 10 atoms of molybdenum per nm^2. Thus, crystalline phases are formed after the synthesis of the catalysts, as demonstrated by using XRD. As a consequence of the presence of agglomerated oxide and sulfide clusters, the steps of the TPS process are not well defined but overlapping. The TPS profile of the MoK_2/Al_2O_3 catalyst is the only one that exhibits a small H_2S release peak. For the other molybdenum-containing materials, there is a continuous and large H_2S adsorption (Figure 4.2). Instead of H_2S release, which appears in most of the H_2S profiles, is a local maximum or "shoulder" at approximately 550 K. We conclude, however, that this shoulder corresponds to the reduction of elemental sulfur, because a clear H_2-consumption peak appears at the same temperature in the TPS profiles as shown in Figure 4.10 for the Mo/Al_2O_3 and MoK_2/Al_2O_3 catalysts. Thus, the H_2S consumption region before the "shoulder" corresponds mainly to the O-S exchange of atoms bound to Mo^{6+}, whereas in the high temperature region it corresponds to the exchange of sulfur atoms for oxygen atoms on Mo^{4+} species.

The profiles of the Mo/Al_2O_3 and $MoK_{0.16}/Al_2O_3$ catalysts in Figure 4.2 are very similar, because the low potassium loading did not modify the sulfidation process significantly. The consumption of H_2S, however, decreases after the incorporation of potassium (K/Mo=0.16). This is attributed to the formation of molybdenum with a tetrahedral coordination, which negatively influences the reducibility of the materials [25]. At higher potassium loadings in the molybdenum-catalysts, it is obvious that by increasing the concentration of potassium the consumption of H_2S increases. Furthermore, for the catalyst with two-fold molar excess of

potassium, the H_2S-consumption line returns to the baseline faster than for other materials, suggesting that the available oxygen atoms are substituted by sulfur atoms earlier than on materials with lower potassium concentrations. Thus, according to the TPS process described before, potassium accelerates the O-S exchange on both Mo^{4+} and Mo^{6+}, as shown in general in Equation (8).

$$Mo^{n+}\text{-}O^{2-} + K^+ + H_2S \rightarrow Mo^{n+}\text{-}OH + K^+\text{-}SH \rightarrow Mo^{n+}\text{-}S^{2-} + K^+ + H_2O \qquad (8)$$

4.4.3. Effect of potassium during the reaction

Several indications are found in the kinetic results that potassium hinders the COS decomposition to CO and H_2S and enhances the disproportionation of COS. Clear evidence of the first effect is the series of experiments performed over Al_2O_3 and $K\text{-}Al_2O_3$. In those experiments, the addition of potassium results in a decrease in the COS conversion, which is associated with the blocking of its decomposition to CO. Concerning the molybdenum-containing catalysts, the yield of CO decreases, whereas the yield of CO_2 increases between 520 and 600 K with increasing potassium-loading (Figure 4.5). In the same temperature range, Figure 4.7 clearly reveals a considerably lower yield of CO on MoK_2/Al_2O_3 than on Mo/Al_2O_3. In Figure 4.8, the yields of CO_2 and CS_2, products of the COS disproportionation, are much higher on the potassium-containing catalyst than on Mo/Al_2O_3.

Potassium has the opposite effect above 600 K: it increases the yield of CO, but decreases the yield of CO_2 (Figure 4.5). This is attributed to the transformation of CO_2 to CO through the reverse water gas shift reaction [Eq. (2)] or through the consecutive reactions [Eqs. (3) and (4)]. An increase in the reaction rate for Equation (2), as confirmed by CO_2 and H_2 consumption, can be observed in Figure 4.8, in which the yield of CO_2 decreases at temperatures higher than 570 K on raising H_2/COS ratio, because more H_2 is available for the CO_2 consumption.

Another important effect of potassium can be seen in Figure 4.9. On the potassium-free catalyst, the yield of methanethiol reaches a maximum value (ca. 6%) below 520 K and then decreases steadily. On the potassium-containing catalyst, the maximum yield of CH_3SH (ca. 16%) shifts to temperatures higher than 550 K and remains constant afterwards. This indicates a strong reduction of the hydrogenation of CH_3SH to CH_4 in the presence of

potassium. This statement is confirmed by the results presented in Figures 4.6 and 4.9 that exhibit a reduced CH_4 formation in the presence of potassium.

4.4.4. Mechanism of the disproportionation of COS on alumina

For the disproportionation of COS on alumina, the Mars-van Krevelen mechanism, illustrated in Scheme 4.3, is proposed. COS (O=C=S) may bind to the adsorption site, depicted as squares, through the sulfur or the oxygen atoms (Scheme 4.3, A and B, respectively). In the former case, the CO fragment reacts with a nearby oxygen atom and desorbs as CO_2. In the second case, the CS fragment reacts with a sulfur atom and a CS_2 molecule desorbs.
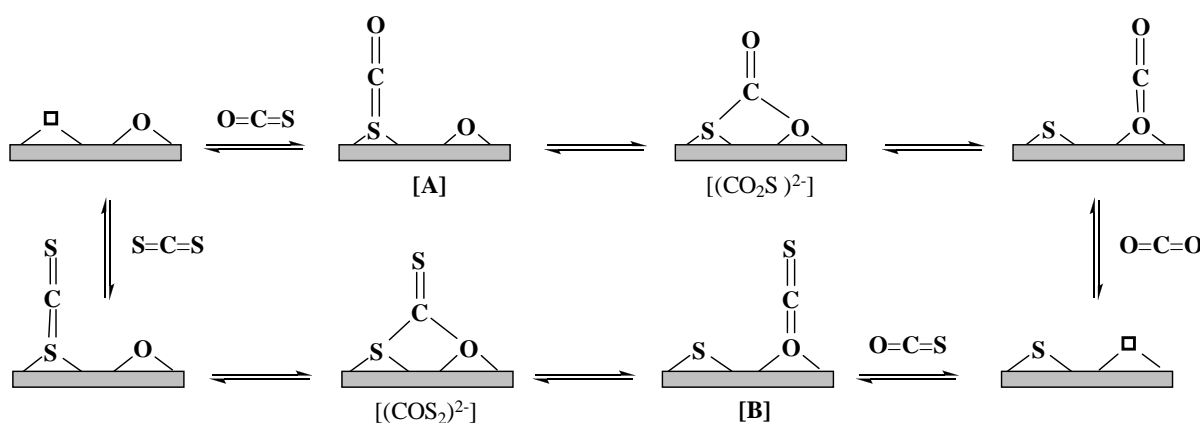
Scheme 4.3: Mechanism for the COS disproportionation to CS_2 and CO_2 over alumina or a partially oxidized MoS_2 phase.

From Scheme 4.3 it is clear that COS adsorption and the subsequent release of CO_2 or CS_2 requires two adsorbed intermediaries: dithiocarbonate $(COS_2)^{2-}$ and thiocarbonate $(CO_2S)^{2-}$. Both surface species have been observed on several oxides by means of infrared spectroscopy [26,27]. The effect of potassium on the disproportionation of COS is very limited on alumina (Figure 4.4), which means that the enhancement of the O-S exchange observed in TPS after potassium addition is not significant under reaction conditions. The reduction in the COS decomposition, evident on $K-Al_2O_3$, is attributed to the stabilization of COS molecules adsorbed on potassium cations, as detailed below.

4.4.5. Active phases in the molybdenum catalysts

It is likely that the formation of molybdenum species on alumina covers most of the active sites on the support, because of the high concentration of molybdenum precursors and the low area of the catalysts (Table 4.1). Accordingly, the performance of Al_2O_3 and Mo/Al_2O_3 are very different. For example, below 600 K, the rate of COS decomposition is much higher on Mo/Al_2O_3 than on alumina (compare Figures 4.4 and 4.5). The high rate of COS decomposition on Mo/Al_2O_3 coincides with our previous conclusion that the COS hydro-decomposition is catalyzed by the MoS_2 phase [19]. In the present work, small amounts of potassium in the catalysts do not influence the catalytic performance. However, at high concentrations or excess of potassium, the rate of COS disproportionation increases.

The increase of the COS disproportionation rate with increasing potassium-loading on the Mo/Al_2O_3 catalyst is a consequence of the creation of new disproportionation sites on the MoS_2 phase rather than improving the remaining sites on alumina. It is shown that potassium added to Al_2O_3 does not influence the disproportionation rate of COS. New disproportionation sites are located in a second active phase, potassium-decorated MoS_2, which is shown to promote the disproportionation of COS [19]. This assignment of catalytic properties to MoS_2 and K-MoS_2 is equivalent to what is known for the synthesis of mixed alcohols from synthesis gas over sulfided molybdenum catalysts, in that the potassium-promoted MoS_2 phase catalyzes the alcohol formation, whereas the unmodified MoS_2 phase is active for the formation of hydrocarbons [28,29]. This means that the C-O (or C-S) bond is preferably broken on pure MoS_2, but preserved in the presence of potassium.

As suggested by using Raman and X-ray photoelectron spectroscopy (XPS) characterization of the potassium-doped catalysts, potassium cations tend to disperse on the entire surface, that is, K^+ segregates from the MoS_2 phase either by migrating to the support or by forming crystalline, molybdenum-free species [17,19]. Therefore, the potassium-decorated MoS_2 can only be formed at high concentrations of potassium. In line with this statement, the addition of potassium facilitates the sulfidation of the molybdenum catalyst through Equation (8) only at high alkali loadings.

It is known that NO adsorbs on coordinatively unsaturated sites (CUS) at the edge of MoS_2. Thus, the concentration of NO adsorbed on sulfides is correlated with the concentration of CUS and the activity of the catalyst [30,31]. Accordingly, the adsorption of NO was correlated with the concentration of CUS available to complete the decomposition of COS [19]. In this work, the opposite trend is observed, that is, the amount of adsorbed NO increases with the loading of potassium, whereas the conversion of COS decreases

accordingly because of the hampering of the COS decomposition. This apparent contradiction is resolved by considering that NO does not absorb solely on exposed molybdenum atoms in MoS_2, but also on potassium cations, as indicated by several studies concerning the chemisorption of oxygen-containing compounds on alkali-doped MoS_2 [29,32,33]. This explains that NO adsorbs on potassium-doped MoS_2 even after flowing COS in the absence of H_2, which would block the Mo-CUS, as described elsewhere [19]. Furthermore, the assignment of potassium cations as adsorption centers implies that they can be part of the active sites responsible for the COS disproportionation, which is enhanced in the potassium-decorated MoS_2 phase.

4.4.6. Reaction mechanism for the COS disproportionation on the MoS_2 phases

The potassium-promoted molybdenum species have a much higher affinity for oxygen-containing compounds, as suggested by the TPS results and the adsorption of NO. In the TPS experiments, the presence of K^+ increases significantly the O-S exchange on Mo^{4+} and Mo^{6+}, whereas in the volumetric experiments the adsorption of NO correlates with the concentration of potassium. Unequivocal evidence of the O-S exchange is provided by Raman spectroscopy, which reveals formation of oxysulfide species after flowing pure COS over the sulfide catalyst doped with high concentrations of potassium. It is important to clarify that the formation of oxysulfide species occurs only on the surface and does not lead to bulk oxidation of the catalyst under reaction conditions (as illustrated by the XRD characterization of the used catalysts). We propose that the disproportionation of COS over the potassium-decorated MoS_2 phase proceeds according to Scheme 4.4.

Considering that potassium acts as adsorption center, a COS molecule binds to a potassium cation deposited on MoS_2, then a Mars-van Krevelen-type mechanism replaces the initial sulfur atom in the active site by an oxygen atom, thus releasing CS_2. As a result, the oxysulfide species found in the in situ Raman study are formed. Scheme 4.5a illustrates two different adsorption possibilities of a COS molecule on an active site. CS_2 is the product, if the oxygen-side of the molecule adsorbs on a sulfur-containing center, whereas CO_2 is produced, if the sulfur atom in the molecule adsorbs on an oxygen-containing site. Other possible combinations lead to desorption of COS. Note that the mechanism in Scheme 4.4 does not include CUS, which is in good agreement with the previous conclusion that CUS do not play an important role in the disproportionation reaction [19].
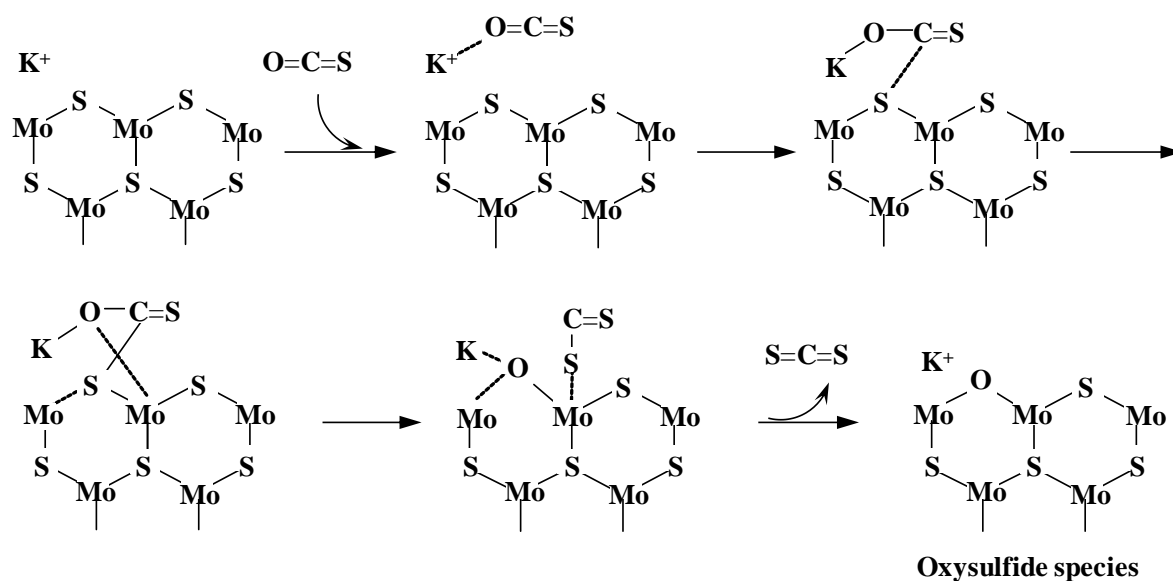
Scheme 4.4: Mechanism for the COS conversion to CS_2 over the potassium-decorated MoS_2 phase.

In the pure MoS_2 phase, the disproportionation would occur on the partially oxidized surface according to Scheme 4.3 with CUS as adsorption sites. However, the concentration of oxygen atoms on the surface in the MoS_2 phase must be very low, because oxysulfide species were not observed for catalysts with low potassium-loading in the Raman experiments.
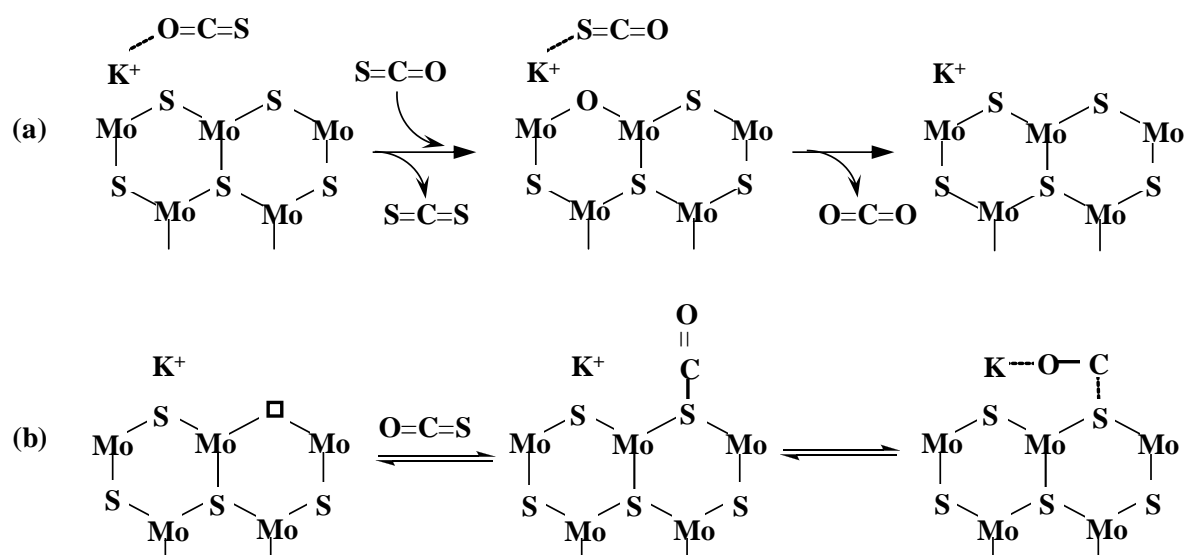
Scheme 4.5: (a) Possibilities for the adsorption of COS on the potassium promoted site that lead to the disproportionation to CS_2 and CO_2. (b) stabilizing effect of potassium on the adsorbed COS.

4.4.7. Other features of the potassium-decorated phase

It is proposed that K^+ can stabilize a COS molecule adsorbed on a CUS or the CO fragment on the surface for recombination with sulfur, thus hindering the decomposition as shown in Scheme 4.5b. The same stabilizing effect through CO-K bonding was attributed to potassium in the production of alcohols from syngas on molybdenum sulfide catalysts [34]. Potassium cations on the catalytic surface would also stabilize adsorbed CH_3SH. The CH_3S-fragments formed on K^+ centers would desorb again as methanethiol. Thus, the adsorption on CUS, which is more likely to result in further hydrogenolysis to CH_4, is hampered. The detailed analysis of the yield of CS_2 and CH_3SH on Mo/Al_2O_3 and K_2Mo/Al_2O_3 at low temperatures (Figures 4.8 and 4.9) suggests that the same stabilizing effect of K^+ occurs on the CS_2 molecules. The yield of CS_2 on Mo/Al_2O_3 is negligible at any H_2/COS ratio; the yield of CH_3SH, however, is higher on the same catalyst than on K_2Mo/Al_2O_3 below 525 K. This suggests that potassium slows down the hydrogenation of CS_2 as well as the other hydrogenation steps. Further evidence for the direct hydrogenation of CS_2 to CH_3SH will be provided in future communications. The mobility of surface oxygen atoms is improved by the addition of alkali salts to alumina, increasing the activity for the reverse water gas shift reaction at high temperatures [21]. Our results reveal that at high temperatures (above 590 K) the difference between the increasing yield of CO and the decreasing CO_2 yield widens with the potassium content, suggesting the same effect on the potassium-doped molybdenum catalysts. Thus, the oxygen-mobility present in the potassium-decorated MoS_2 phase also accelerates the formation of CO from CO_2.

4.5. Conclusions

A series of molybdenum catalysts supported on alumina and doped with potassium were synthesized and characterized in the oxide and sulfide form. Crystalline phases were formed in the oxide catalyst because of the high concentration of molybdenum. The nature of those crystalline phases depended on the concentration of potassium and the used precursors. In the sulfide form, however, only the MoS_2 phase was detected in all the catalysts. The synthesis of methanethiol from carbonyl sulfide (COS) and H_2 was explored on Al_2O_3 and the sulfided molybdenum catalysts doped with increasing amounts of potassium. The kinetic and characterization results allowed postulating the presence of two active phases, that is, pure MoS_2 and potassium-decorated MoS_2. The latter was formed only at high potassium concentrations because of the dispersion of potassium on the support. The main effect of

potassium was an increase in the mobility of the oxygen and sulfur atoms on the surface and the stabilization of adsorbed species. The improved O-S exchange increased the consumption of H_2S during sulfidation. In the sulfide catalysts, the oxygen and sulfur reactivity of the potassium-decorated MoS_2 phase increased the rate of COS disproportionation to CO_2 and CS_2 at low temperatures and the production of CO from CO_2 above 573 K. The stabilization of the surface species on exposed potassium cations, that is, adsorbed COS or CO fragments or adsorbed methanethiol, explained the hampering of COS decomposition and of the methanethiol hydrogenolysis to methane. A Mars-van Krevelen-type mechanism would allow for the disproportionation of COS on alumina or MoS_2. A reaction mechanism comprising the formation of oxysulfide species was proposed for the COS disproportionation on the potassium-decorated MoS_2 phase. The active center in this phase includes potassium cations instead of exposed molybdenum cations.

4.6. References

[1] Y. Yang, S. Dai, Y. Yuan, R. Lin, D. Tang, H. Zhang, Appl. Catal. A 2000, 192, 175-180.

[2] W. Hofen, W. Bock, S. Rautenberg, J. Sauer, D. Arntz, R. Goedecke, W. Taugner, R. Sonnenschein, European patent 0 850 922 (A1), 1998.

[3] J. Sauer, L. Von Hippel, D. Arntz, W. Bock, European patent 0 832 878 (A3), 1998.

[4] J. Olin, B. Buchholz, B. Loev, R. Goshorn, US patent 3 070632, 1962.

[5] M. Boulinguiez, C. Forquy, J. Barrault, US patent 4 665242, 1987.

[6] I. Wachs, US patent WO 98/54118, 1998.

[7] C. Ratcliffe, P. Tromp, US patent 4 668825, 1987.

[8] J. Barrault, M. Boulinguiez, C. Forquy, R. Maurel, Appl. Catal. 1987, 33, 309– 330.

[9] G. Mul, I. Wachs, A. Hirschon, Catal. Today 2003, 78, 327–337.

[10] B. Zhang, S. Taylor, G. Hutchings, Catal. Lett. 2003, 91, 181– 183.

[11] B. Zhang, S. Taylor, G. Hutchings, New J. Chem. 2004, 28, 471 –476.

[12] Y. Yang, Y. Yuan, S. Dai, B. Wang, H. Zhang, Catal. Lett. 1998, 54, 65– 68.

[13] S. Dai, Y. Yang, Y. Yuan, D. Tang, R. Lin, H. Zhang, Catal. Lett. 1999, 61, 157– 160.

[14] Y. Yang, H. Yang, Q. Wang, L. Yu, C. Wang, S. Dai, Y. Yuan, Catal. Lett. 2001, 74, 221– 225.

[15] A. Chen, Y. Wang, Y. Hao, W. Fang, Y. Yang, Catal. Lett. 2007, 118, 295– 299.

[16] A. Chen, Q. Wang, Y. Hao, W. Fang, Y. Yang, Catal. Lett. 2008, 121, 260 – 265.

[17] A. Chen, Q. Wang, Q. Li, Y. Hao, W. Fang, Y. Yang, J. Mol. Catal. A: Chem. 2008, 283, 69 –79.

[18] C. Kaufmann, O. Gutiérrez, Y. Zhu, J. Lercher, Res. Chem. Intermed. 2010, 36, 211 –225.

[19] O. Gutiérrez, C. Kaufmann, A. Hrabar, Y. Zhu, J. Lercher, J. Catal. 2011, 280, 264–273.

[20] G. Schrader, C. Cheng, J. Catal. 1983, 80, 369– 385.

[21] B. Krupay, Y. Amenomiya, J. Catal. 1981, 67, 362– 370.

[22] Y. Amenomiya, G. Pleizier, J. Catal. 1982, 76, 345 –353.

[23] P. Arnoldy, J. Van den Heijkant, G. De Bok, L. Moulijn, J. Catal. 1985, 92, 35–55.

[24] X. Wang, B. Zhao, D. Jiang, Y. Xie, Appl. Catal. A 1999, 188, 201 –209.

[25] N. Verbruggen, H. Knçzinger, Langmuir 1994, 10, 3148 –3155.

[26] A. Sahibed-Dine, A. Aboulayt, M. Bensitel, A. Saad, M. Daturi, J. Lavalley, J. Mol. Catal. A: Chem. 2000, 162, 125– 134.

[27] J. Lavalley, J. Travert, T. Chevreau, J. Lamotte, O. Saur, J. Chem. Soc. Chem. Commun. 1979, 146–148.

[28] M. Jiang, G. Bian, Y. Fu. , J. Catal. 1994, 146, 144 –154.

[29] N. Koizumi, G. Bian, K. Murai, T. Ozaki, M. Yamada, J. Mol. Catal. A: Chem. 2004, 207, 173– 182.

[30] Y. Okamoto, M. Kawano, T. Kubota, Chem. Commun. 2003, 1086– 1087.

[31] N. Topsøe, H. Topsøe, J. Catal. 1982, 77, 293– 296.

[32] M. Karolewski, R. Cavell, Surf. Sci. 1989, 219, 261 –276.

[33] K. Park, J. Kong, Top. Catal. 2002, 18, 175 –181.

[34] H. Woo, I. Nam, J. Lee, J. Chung, Y. Kim, J. Catal. 1993, 142, 672 –690.

Chapter 5

Synthesis of Methanethiol from Carbonyl Sulfide and Carbon Disulfide on (Co)K-Promoted Sulfide Mo/SiO$_2$ Catalysts

The catalytic properties of a series of (Co)K-promoted Mo sulfide catalysts supported on SiO$_2$ were explored in the synthesis of methanethiol from carbonyl sulfide (COS) and CS$_2$. MoS$_2$ was very active for the conversion of COS, but allowed only low yields of CH$_3$SH because of the parallel decomposition of COS to CO and H$_2$S and the reduction of CH$_3$SH to CH$_4$. CS$_2$, on the other hand, was completely converted to CH$_3$SH with high yield below 570 K on MoS$_2$. The formation of CH$_4$, however, dramatically decreased the yield of CH$_3$SH above 570 K. The addition of K$^+$ cations decreased the conversion of both reactants, but also reduced the rate of decomposition/reduction reactions. The doubly promoted CoK-Mo catalyst led to the highest conversions with moderate to high yields of methanethiol. We conclude that the addition of K$^+$ cations generates very weak adsorption sites, suppressing so the C-S bond cleavage. These sites catalyze, however, COS disproportionation. Accessible Co and Mo sites are part of the active sites for all reactions observed. All catalytically active sites are concluded to be situated on the edges of MoS$_2$ slabs.

5.1. Introduction

Methanethiol (methyl mercaptan, CH_3SH) is a key intermediate in the production of several important specialty chemicals such as methionine [1]. Thus, improving and developing new synthesis routes for methanethiol is of significant industrial interest. Large scale production of methanethiol is based on the thiolation of methanol [1,2]. However, it would be economically attractive to produce CH_3SH from less expensive reactants, such as carbon oxides, hydrogen sulfide, and hydrogen.

The synthesis of methanethiol from CO and CO_2 on transition metal sulfides supported on alumina was reported in the early work of Olin et al. [3], whereas Mn- and W-based sulfide catalysts promoted with alkali metals were applied later [4]. The formation of methanethiol from mixtures of CO and H_2S was subsequently investigated over group Vb metal oxides supported on TiO_2 and Al_2O_3 [5-7].

In recent years, the synthesis of methanethiol from H_2S-containing synthesis gas (H_2S-syngas) on a variety of sulfide materials has received significant attention again [8,9]. The outstanding CO conversion and CH_3SH selectivity set the K-promoted Mo-catalyst apart from other evaluated catalysts.

A two-stage process for the synthesis of methanethiol was devised as reported in refs 10,11. The first stage consists of the liquid-phase reaction of elemental sulfur with CO-H_2 mixtures to form carbonyl sulfide (COS) and H_2S. In the second stage, a plug-flow reactor is used to synthesize methanethiol from mixtures of COS, H_2S, and H_2. The reactions in the second stage were catalyzed by Mo-sulfide catalysts containing substantial concentrations of potassium and being supported on SiO_2 and Al_2O_3 [11,12].

The two-stage approach allows also to better understand how the H_2S-syngas mixture reacts to form CH_3SH. From the mechanistic investigations it is concluded that COS undergoes disproportionation to CO_2 and CS_2 and that the latter is hydrogenated to methanethiol. The addition of high concentrations of potassium leads to the formation of a "K-decorated" MoS_2 phase that enhances the COS disproportionation, but inhibits undesired reactions. However, the metal sulfide catalyzed synthesis of methanethiol from H_2S-containing synthesis gas is far from being optimized and completely understood. Stimulated by reports in the literature [13] we compare here the impact of double promotion, that is, K-Co, on the methanethiol synthesis using COS and CS_2 as reactants aiming to provide a knowledge basis to improve catalysts for the synthesis of methanethiol from H_2S-containing synthesis gas.

Cobalt was used as a second promoter because it is known to increase the reactivity of MoS_2 for hydrogenation [14]. Thus, a series of K- and CoK-promoted Mo catalysts supported on SiO_2 were synthesized, characterized, and explored with respect to the catalytic conversion of mixtures of COS or CS_2 with H_2S and H_2 to methanethiol.

5.2. Experimental

5.2.1. Catalyst Preparation

The oxide catalyst precursors were prepared by the incipient wetness impregnation of SiO_2 (AEROSIL 90, Degussa). Mo and K-Mo catalysts were prepared in a single impregnation step from aqueous solutions of ammonium heptamolybdate hexahydrate (($NH_4)_6Mo_7O_{24}\cdot6H_2O$, Aldrich, 99.9%) and potassium molybdate (K_2MoO_4, Sigma Aldrich, 98%), respectively. The resulting materials were dried at 353 K for 10 h and treated at 773 K in synthetic air for 12 h.

The Co-containing catalysts were prepared by the impregnation of the K-Mo oxide material with an aqueous solution of cobalt nitrate hexahydrate ($Co(NO_3)_2\cdot6H_2O$, Fluka, 98%) followed by the same thermal treatment as described above. The molybdenum loading was 1.17 mmol per gram of material, whereas in the promoted catalysts the molar K/Mo and Co/Mo ratios were 2 and 0.33 respectively. The equivalent nominal compositions were 11.3, 9.2, and 2.3 wt % in Mo, K, and Co respectively. The oxide catalyst precursors are denoted as Mo/SiO_2, KMo/SiO_2, and $CoKMo/SiO_2$.

5.2.2. Characterization of the Catalysts

5.2.2.1. Elemental Composition
The molybdenum, potassium, and cobalt content of the oxide precursors were determined by atomic absorption spectroscopy (AAS) using a UNICAM 939 spectrometer.

5.2.2.2. Textural Properties
The textural properties of the oxide precursors were determined by nitrogen adsorption-desorption using a PMI automated BET sorptometer. The samples were degassed in vacuum at 673 K for 2 h before adsorption.

5.2.2.3. X-ray Diffraction
The oxide precursors and the sulfide catalysts after activity tests were characterized by X-ray diffraction (XRD). Samples of the used catalysts were measured after cooling down the

reactor to room temperature in nitrogen flow. A Philips X'Pert Pro System (Cu Kα1-radiation, $\lambda = 0.154056$ nm) operating at 45 kV and 40 mA was used for recording XRD. Measurements were carried out using a step size of 0.017° (2θ) and 115 s as count time per step.

5.2.2.4. NO and CO_2 Adsorption

NO and CO_2 adsorption were determined by a pulse technique using a flow apparatus equipped with a mass spectrometer (QME 200, Pfeiffer Vacuum). A sample of 0.1 g of catalyst was loaded in a quartz reactor and activated in situ under 10 vol % H_2S/H_2 at 673 K for 3 h. After cooling to the adsorption temperature, that is, 300 K for NO and 358 K for CO_2, the reactor was flushed with high purity He for 5 h. Pulses of 10 vol % of NO or CO_2 in He were introduced every 30 min. The total concentration of gas adsorbed was calculated as the sum of the uptakes per pulse.

5.2.3. Kinetic Measurements

The synthesis of CH_3SH from COS or CS_2 was investigated with the sulfide form of Mo, K-Mo, and Co-K-Mo catalysts. In the following the sulfide catalysts are denoted simply as MoS_2/SiO_2, $KMoS/SiO_2$, and $CoKMoS/SiO_2$. Prior to the activity tests, samples of 0.5 g of the catalysts (particle size 250-500 μm) were sulfided in 10 vol % H_2S/H_2 at 3 MPa and 673 K for 12 h. Kinetic measurements were carried out in an experimental setup comprising a semibatch reactor and a plug-flow reactor in serial arrangement. Pure H_2 or CO-H_2 mixtures were bubbled through liquid sulfur in the semibatch reactor to generate either COS-H_2S or H_2-H_2S mixtures as previously reported [9,10]. These mixtures were diluted with the necessary concentrations of H_2, N_2, and/or CS_2 and introduced to the plug-flow reactor, where the synthesis of methanethiol was performed. CS_2 was introduced to the setup using a Shimadzu LC-20AT pump and vaporized at 423 K before mixing with the gas flow.

Using COS as starting reactant, the typical composition of the feed was 7.33 vol % COS, 3.08 vol % H_2S, and 17 vol % H_2 in N_2 (H_2/COS ratio of 2.4). The effect of the H_2/COS ratio (2.4, 3.2, and 5.2) was explored with a fixed COS concentration of 8 vol % and a H_2/H_2S ratio of 4.3. In the synthesis of CH_3SH from CS_2, the composition of the feed was 8.5 vol % CS_2, 18 vol % H_2S, 50 vol % H_2, and 23 vol % N_2 (H_2/CS_2 ratio of 5.9). These compositions referred to the gas mixture used in the plug-flow reactor. All reactions were performed at a constant pressure of 3 MPa and temperatures ranging from 420 to 673 K. The gas hourly space velocity (GHSV), defined as (volumetric flow rate)•(volume of the catalyst bed)$^{-1}$ was

kept constant at 89 min^{-1} in all experiments by diluting the reactant mixture in N$_2$. Absence of transport artifacts was confirmed in preliminary experiments with varying catalyst particle size and flow rates. Samples were taken after reaching steady state in steps of 15 K and analyzed by gas chromatography using a Shimadzu GC 2014 equipped with a packed Haysep Q and a packed molecular sieve (13X) column.

5.3. Results

5.3.1. Elemental Composition and Textural Properties

The metal concentration, surface area, and pore volume of the oxide catalysts are compiled in Table 5.1. The composition of metals in the oxide catalyst precursors is very similar to the metal concentration used in the precursor mixture during preparation. Table 5.1 shows that the surface area and pore volume of the materials decrease with the loading of metal oxides along with the increase in the density of the material. The Brunauer-Emmett Teller (BET) surface area and the pore volume of CoKMo/SiO$_2$ was lower than what was expected after incorporating 1.8 wt % of Co, which may suggest that some pores were blocked in the parent material during the preparation procedure.

Table 5.1: Nominal and experimental metal concentrations in the oxide materials[a].

Material	Co (wt. %) (nominal) experimental	K (wt. %) (nominal) experimental	Mo (wt. %) (nominal) experimental	BET surface area (m^2/g)	Pore volume (cm^3/g)
SiO$_2$	-	-	-	88	0.15
Mo/SiO$_2$	-	-	(11.3) 13.3	78	0.12
KMo/SiO$_2$	-	(9.2) 8.8	(11.3) 11.4	50	0.06
CoKMo/SiO$_2$	(2.3) 1.8	(9.2) 8.0	(11.3) 11,5	25	0.03

[a] BET surface area and pore volume determined by N$_2$ physisorption.

5.3.2. X-ray Diffraction Measurements

The X-ray diffractograms of the oxide precursors and the corresponding sulfide catalysts after the activity tests are shown in Figures 5.1a and 5.1b, respectively. The broad signal

between 15 and 35° (2θ) evidences the amorphous nature of the silica support. A crystalline structure of silica would produce the main reflection at around 26° (2θ) instead of a broad signal (see for instance quartz, PDF no. 01-074-0764). All other reflections in the diffractogram of Mo/SiO$_2$ are attributed to orthorhombic MoO$_3$ (PDF no. 00-001-0706). The oxidic KMo/SiO$_2$ catalyst shows a mixture of K$_2$MoO$_4$ (PDF no. 00-024-0880) and K$_2$Mo$_2$O$_7$ (PDF no. 00-036-0347). For the CoKMo/SiO$_2$ catalyst, the addition of Co modifies the proportion of K- and Mo-oxides. The fraction of K$_2$Mo$_2$O$_7$ increases while that of K$_2$MoO$_4$ decreases. However, slight shifts of the peak positions compared with the reference PDF data could indicate a mixture of potassium molybdenum oxides with different stoichiometries [15]. Evidence of crystalline Co-containing phases is not found in the diffraction patterns, probably because the concentration of cobalt is too low.
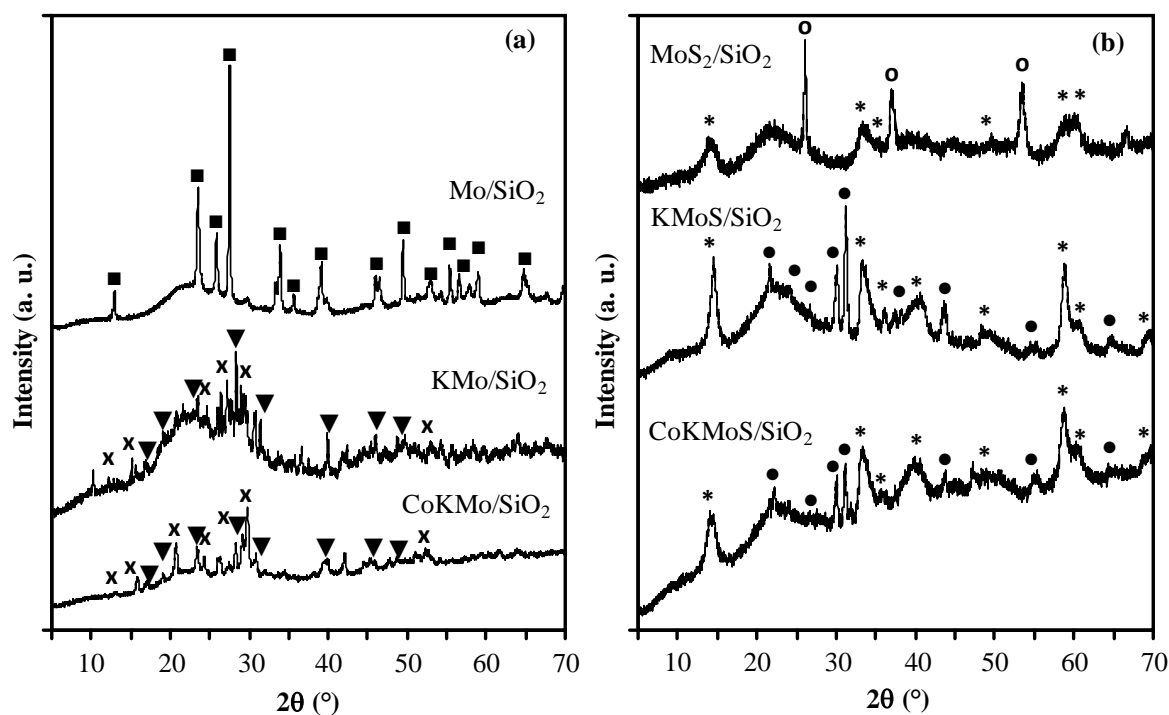
Figure 5.1: XRD diffractograms of the oxide precursors (a) and sulfide, used catalysts (b). MoO$_3$ (■), K$_2$MoO$_4$ (▼), and K$_2$Mo$_2$O$_7$ (x) in (a); MoS$_2$ (*), MoO$_2$ (O), and K$_2$SO$_4$ (●) in (b).

The XRD of the sulfide catalysts collected after the activity tests are shown in Figure 5.1b. Regardless of the oxide species present in the oxide precursor, all sulfided catalysts showed the presence of MoS$_2$ (PDF no. 00-024-0513) as the main crystalline phase. The diffractogram of the MoS$_2$/SiO$_2$ used catalyst showed some reflections corresponding to MoO$_2$ (PDF no. 00-033-0929) indicating incomplete sulfidation. In the sulfide and used KMoS/SiO$_2$ and

CoKMoS/SiO$_2$ catalysts, the K$_2$SO$_4$ phase (PDF no. 00-003-0608) was also detected. This Mo-free phase formed during the reaction as discussed in ref 11.

5.3.3. NO and CO$_2$ Adsorption Measurements

The active sites in the sulfide catalysts were characterized by means of NO and CO$_2$ adsorption because NO adsorbs on exposed cations of MoS$_2$, whereas CO$_2$ selectively adsorbs on basic sites [16,17]. The uptake of NO and CO$_2$ per pulse on sulfide MoS$_2$/SiO$_2$, KMoS/SiO$_2$, and CoKMoS/SiO$_2$ is presented in Figure 5.2.
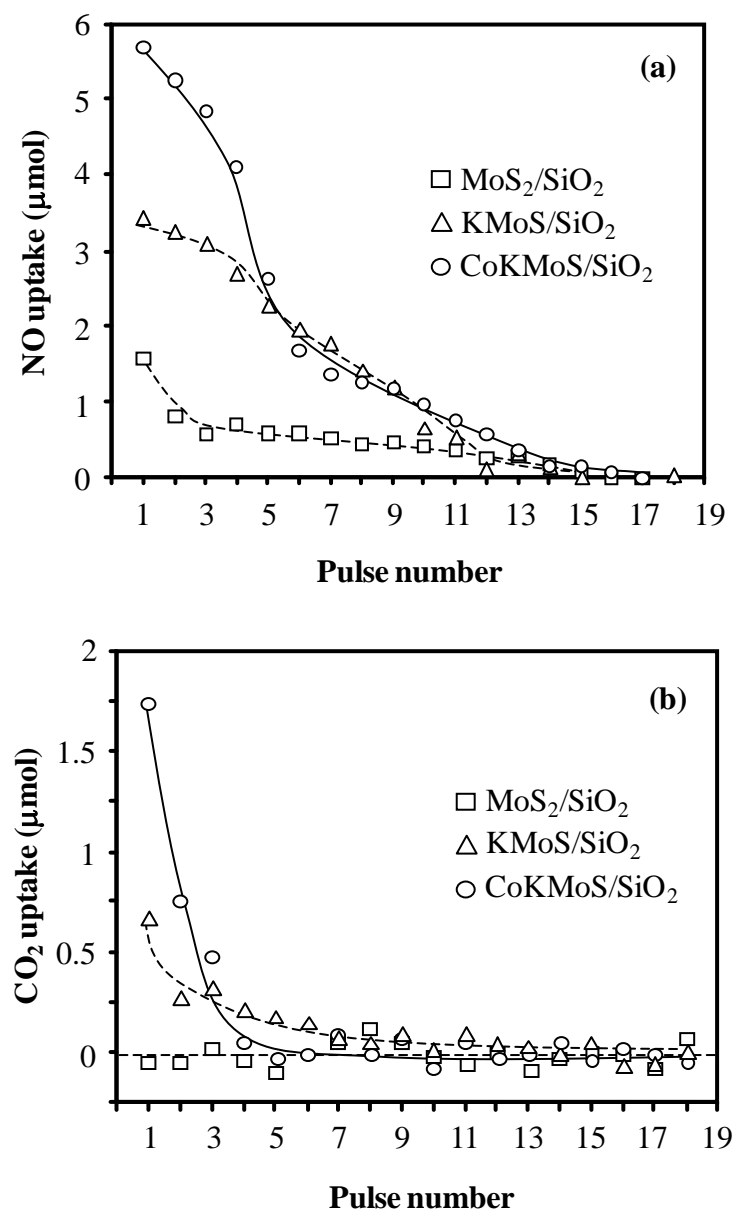
Figure 5.2: NO (a) and CO$_2$ (b) uptake at 300 and 358 K respectively on sulfided MoS$_2$/SiO$_2$ (□), KMoS/SiO$_2$ (Δ), and CoKMoS/SiO$_2$ (O).

Although there are marked differences in the starting uptakes of the samples, the uptake decreases to zero as the maximum adsorption capacity of the sample is reached. The NO uptake on the MoS_2/SiO_2 sample was rather low (69 µmol/g); however, the concentration of adsorbed NO increased significantly for the K-promoted catalyst (229 µmol/g) and was the highest for $CoKMoS/SiO_2$ (304 µmol/g). Only negligible concentrations of CO_2 were adsorbed on MoS_2/SiO_2, while 23 and 21 µmol/g of CO_2 were adsorbed on the $KMoS/SiO_2$ and $CoKMoS/SiO_2$ sulfide materials, respectively. Control experiments were also performed on pure SiO_2 after applying the same thermal treatment in H_2S/H_2 flow that was applied to the catalysts; adsorption of NO or CO_2 was not observed for pure SiO_2 carrier.

5.3.4. Comparison of Catalysts for the Synthesis of CH_3SH from COS

Previous studies of the synthesis of CH_3SH from COS implied that the reaction proceeds along the network presented in Figure 5.3 [11,12]. COS is transformed to CO and H_2S via decomposition and in parallel, to CO_2 and CS_2 via disproportionation. CS_2 is hydrogenated to CH_3SH, whereas the reverse water gas shift reaction transforms CO_2 into CO. The secondary reactions involving CH_3SH lead to CH_4 and CH_3SCH_3 as suggested by the results of this work discussed below.
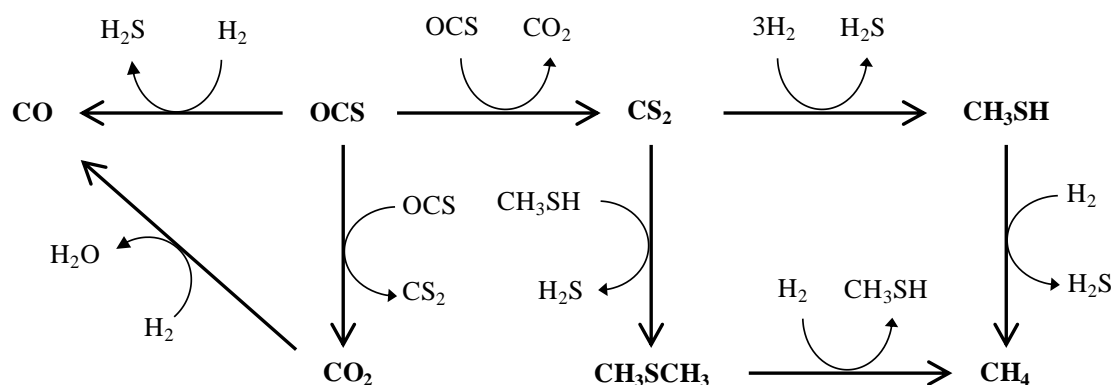
Figure 5.3: Reaction pathway for the production of CH_3SH from COS or CS_2. The main reaction steps are referred in the text as decomposition (1), disproportionation (2), and hydrogenation (3).

The synthesis of CH_3SH from COS was investigated over SiO_2-supported Mo, KMo, and CoKMo sulfide catalysts (see Figure 5.4a). With MoS_2/SiO_2 the conversion of COS increased rapidly from 12 to 80% between 473 and 508 K. With $KMoS/SiO_2$, the conversion of COS increased more slowly and did not reach the maximum value (>95%) until 623 K. The

addition of cobalt increased the conversion of COS leading to the most active catalyst between 423 and 498 K. At temperatures higher than 498 K the conversions achieved with MoS_2/SiO_2 and $CoKMoS/SiO_2$ were both above 95%. The highest yield of CO was obtained on MoS_2/SiO_2 as shown in Figure 5.4b.
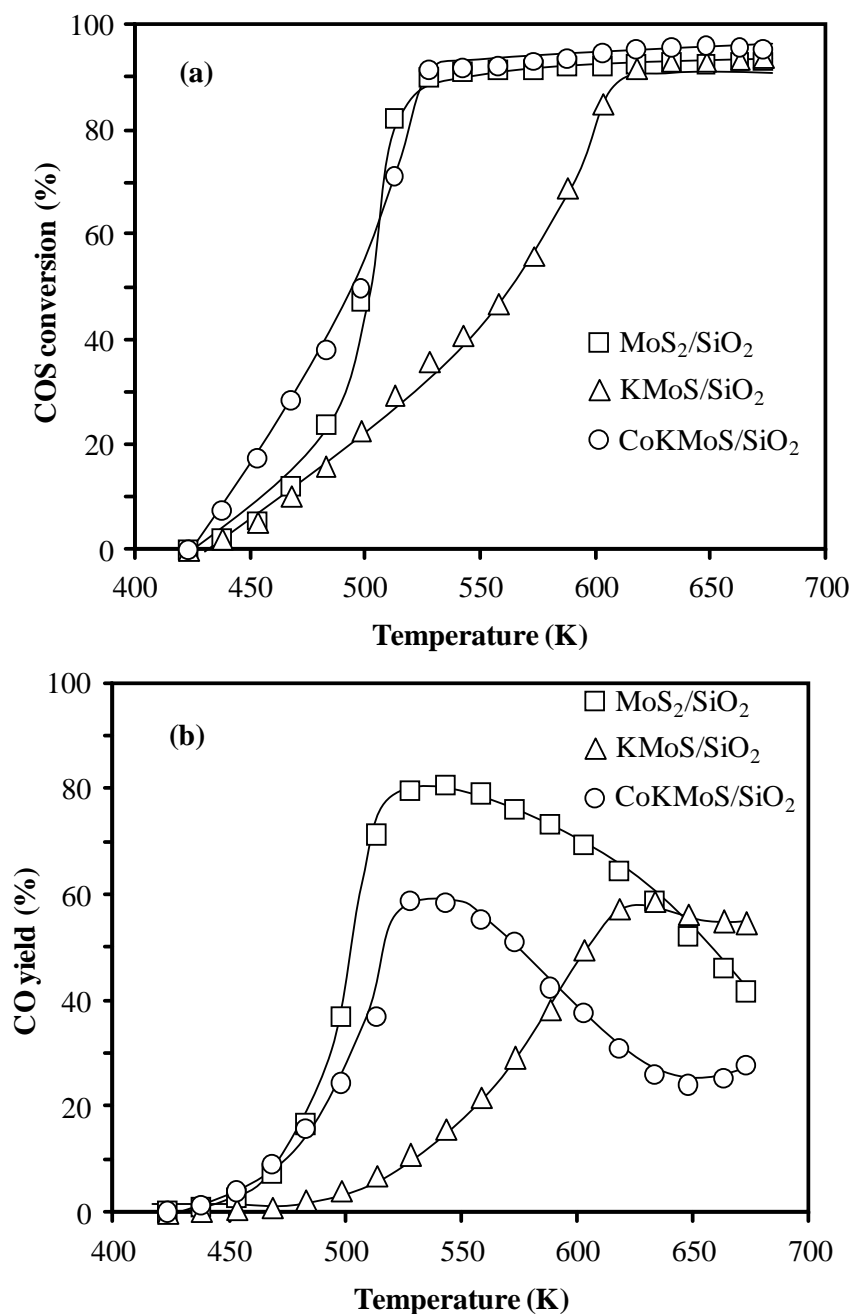
Figure 5.4: Conversion of COS (a) and yield of CO (b) on sulfided MoS_2/SiO_2 (□), $KMoS/SiO_2$ (Δ), and $CoKMoS/SiO_2$ (O). The feed contains 7.3 vol % COS and $H_2/COS = 2.4$ (3 MPa, GSHV = 89.2 min^{-1}).

Below 598 K, the yield of CO was higher on $CoKMoS/SiO_2$ than on $KMoS/SiO_2$ while the reverse was observed at higher temperature. On the three catalysts, the yield of CO

increased with temperature to a maximum value before declining. The temperature for the maximum yield of CO varied from 543 K with MoS_2/SiO_2, to 633 K with $KMoS/SiO_2$ and 528 K on $CoKMoS/SiO_2$.
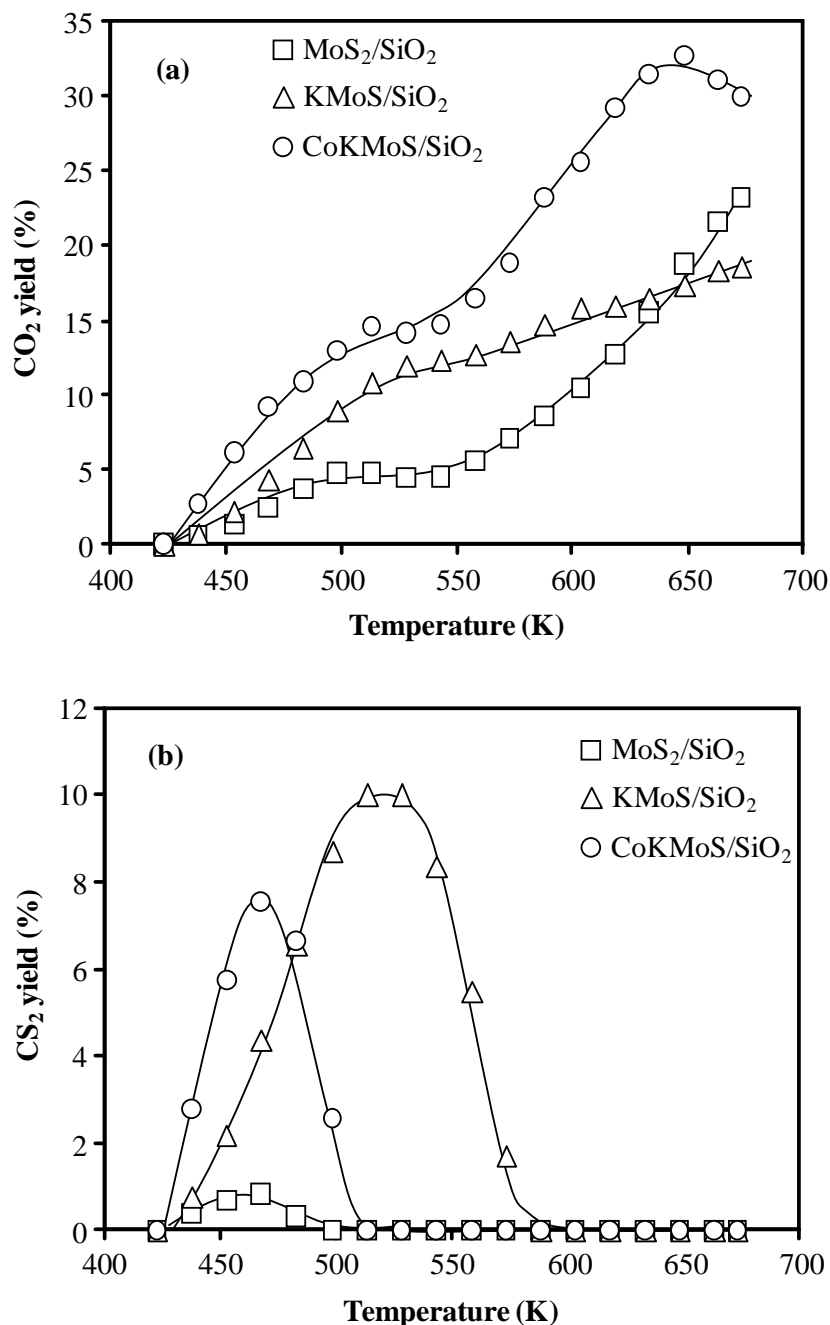
Figure 5.5: Yield of CO_2 (a) and CS_2 (b) on sulfided MoS_2/SiO_2 (□), $KMoS/SiO_2$ (Δ), and $CoKMoS/SiO_2$ (O). The feed contains 7.3 vol % COS and $H_2/COS = 2.4$ (3 MPa, GSHV = 89.2 min^{-1}).

The yield of CO_2 is shown in Figure 5.5a. The highest yield was observed with $CoKMoS/SiO_2$ in the whole temperature range. With $KMoS/SiO_2$ the CO_2 yield was the

second highest, whereas the lowest yield of CO_2 was observed with the unpromoted Mo sulfide catalyst. Three regions of the catalytic behavior can be distinguished in Figure 5.5a, that is, steady CO_2 yield increase (423-513 K), constant CO_2 yield (to 550 K), and finally CO_2 yield increase (>530 K).
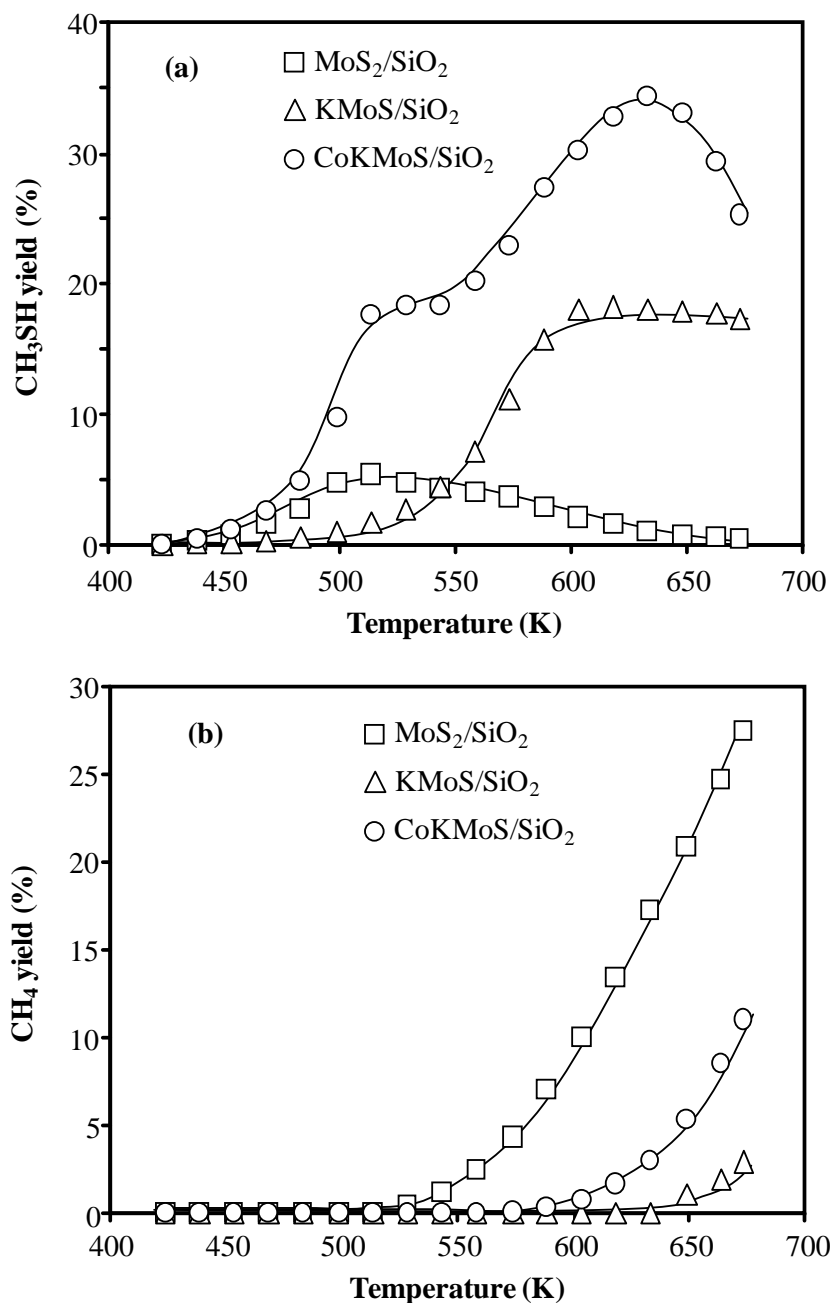
Figure 5.6: Yield of CH_3SH (a) and CH_4 (b) on sulfided MoS_2/SiO_2 (□), $KMoS/SiO_2$ (Δ), and $CoKMoS/SiO_2$ (O). The feed contains 7.3 vol % COS and $H_2/COS = 2.4$ (3 MPa, GSHV = 89.2 min^{-1}).

Very low yields of CS_2 were observed as shown in Figure 5.5b. The highest CS_2 yield (10%) was obtained with KMoS/SiO$_2$ at 523 K. Over the other systems, the maximum CS_2 yield was seen at 473 K, that is, 8% on CoKMoS/SiO$_2$ and just 1% on MoS$_2$/SiO$_2$.

A strong effect of the catalytic formulation was found on the yield of methanethiol (see Figure 5.6a). With MoS$_2$/SiO$_2$ the yield of methanethiol increased only to 7% at 518 K and then decreased again. With KMoS/SiO$_2$, the yield of methanethiol reached 18% at 603 K and did not significantly change with further increasing temperature. With CoKMoS/SiO$_2$, the yield of CH$_3$SH increased steeply from 423 to 513 K, then remained constant and increased again above 558 K reaching a maximum of 35% at 628 K. Figure 5.6b shows the yield of methane. The formation of CH$_4$ starts at 528 K on the unpromoted molybdenum catalyst, 633 K on KMoS/SiO$_2$, and 588 K on CoKMoS/SiO$_2$. In all cases, the yield of methane increased with reaction temperature.

5.3.5. Synthesis of CH$_3$SH from COS: Varying H$_2$/COS Ratio

Clearly, the CoKMoS/SiO$_2$ system showed the best performance with respect to the rate of COS conversion and the yield of methanethiol. Therefore, the effect of H$_2$/COS ratio was further studied on CoKMoS/SiO$_2$. Figure 5.7a shows that below 523 K, increasing the H$_2$/COS ratio leads to an increase in the conversion of COS. Above that temperature, the conversion of COS was higher than 90%, regardless of the H$_2$/COS ratio applied. Similarly, the yield of CO increased by increasing the H$_2$/COS ratio as shown in Figure 5.7b.

The yield of CO$_2$ (Figure 5.8a) was independent of the H$_2$/COS ratio up to 483 K. Above that temperature, raising the H$_2$/COS ratio lowered the yield of CO$_2$. Formation of CS$_2$ was detected only at temperatures between 423 and 525 K and clearly decreased with increasing H$_2$/COS ratio as shown in Figure 5.8b.

The yield of CH$_3$SH increased by raising the H$_2$/COS ratio in the range 423-500 K (Figure 5.9a). Above this temperature, however, a higher H$_2$/COS ratio led to lower yields of methanethiol. The yield of methane (Figure 5.9b) increased quickly above 598 K and was favored by increasing the H$_2$/COS ratio.
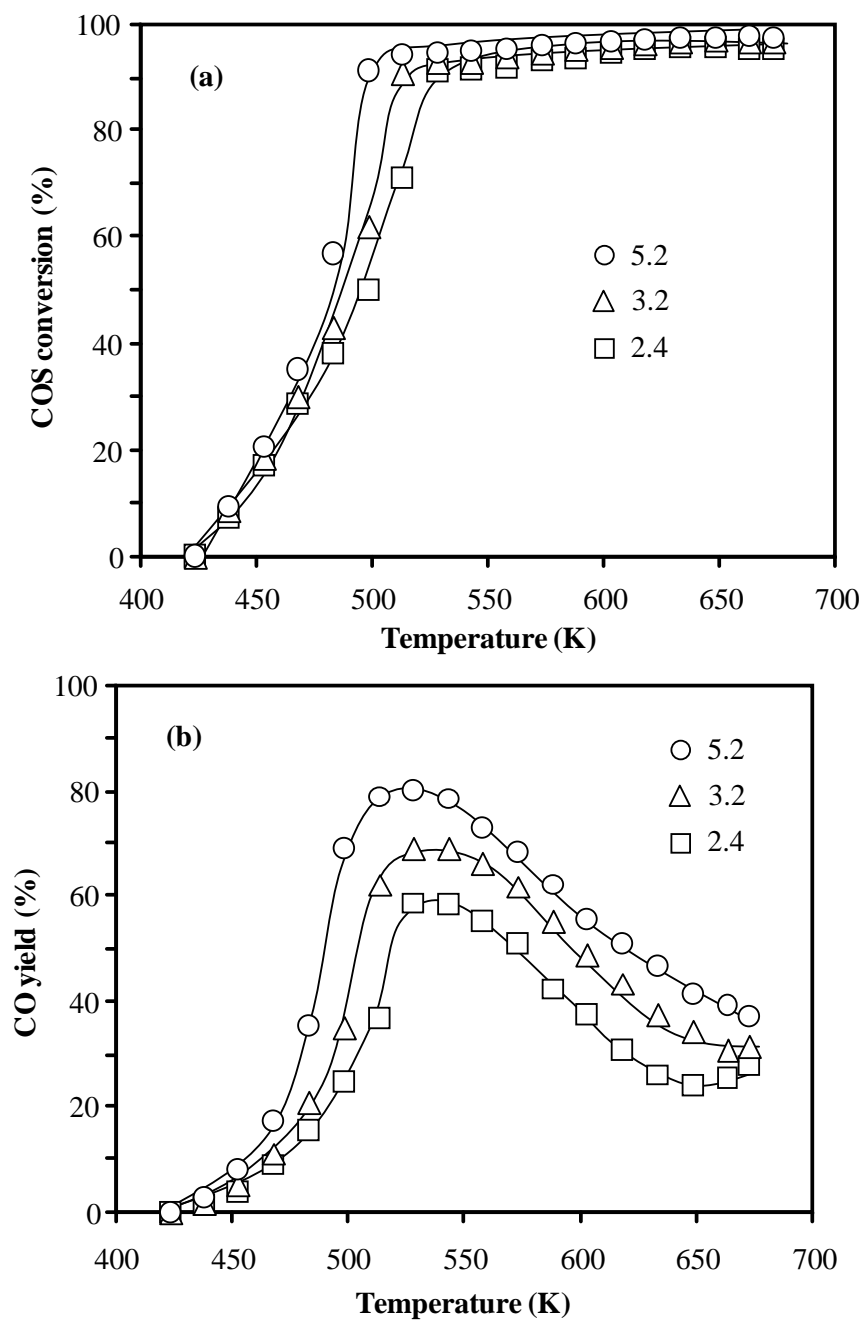
Figure 5.7: Conversion of COS (a) and yield of CO (b) on sulfided CoKMoS/SiO$_2$ at H$_2$/COS ratio of 5.2 (O), 3.2 (Δ), and 2.4 ($\square$). The feed contains 8 vol % COS and H$_2$/H$_2$S = 4.3 (3 MPa, GSHV = 89.2 min^{-1}).
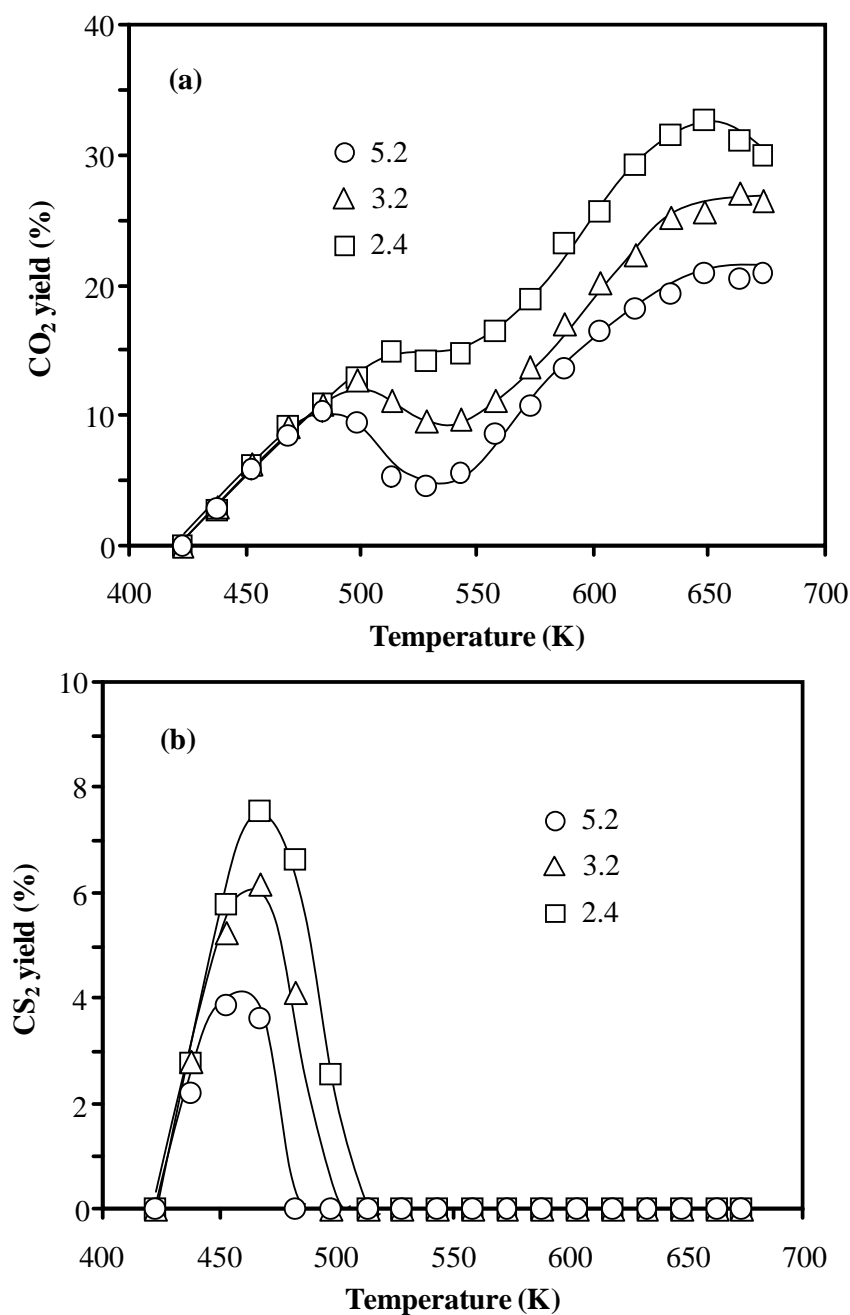
Figure 5.8: Yield of CO_2 (a) and CS_2 (b) on sulfided CoKMoS/SiO$_2$ at a H$_2$/COS ratio of 5.2 (O), 3.2 (Δ), and 2.4 (□). The feed contains 8 vol % COS and H$_2$/H$_2$S = 4.3 (3 MPa, GSHV = 89.2 min^{-1}).

121
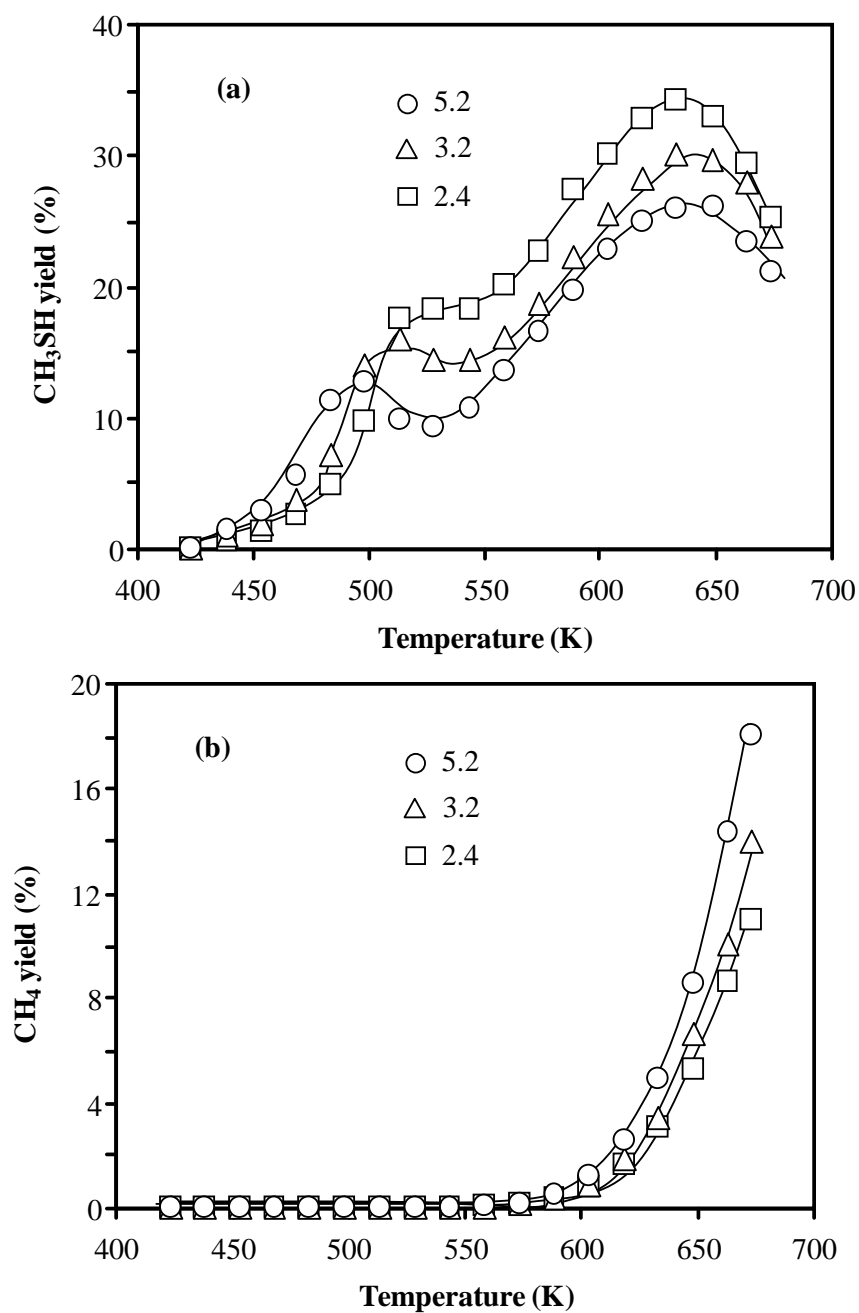
Figure 5.9: Yield of CH_3SH and CH_4 on sulfided $CoKMoS/SiO_2$ at a H_2/COS ratio of 5.2 (O), 3.2 (Δ), and 2.4 (□). The feed contains 8 vol % COS and $H_2/H_2S = 4.3$ (3 MPa, GSHV = 89.2 min^{-1}).

5.3.6. Synthesis of CH₃SH from CS₂

Full conversion of CS_2 was achieved at 573 K as presented in Figure 5.10a.
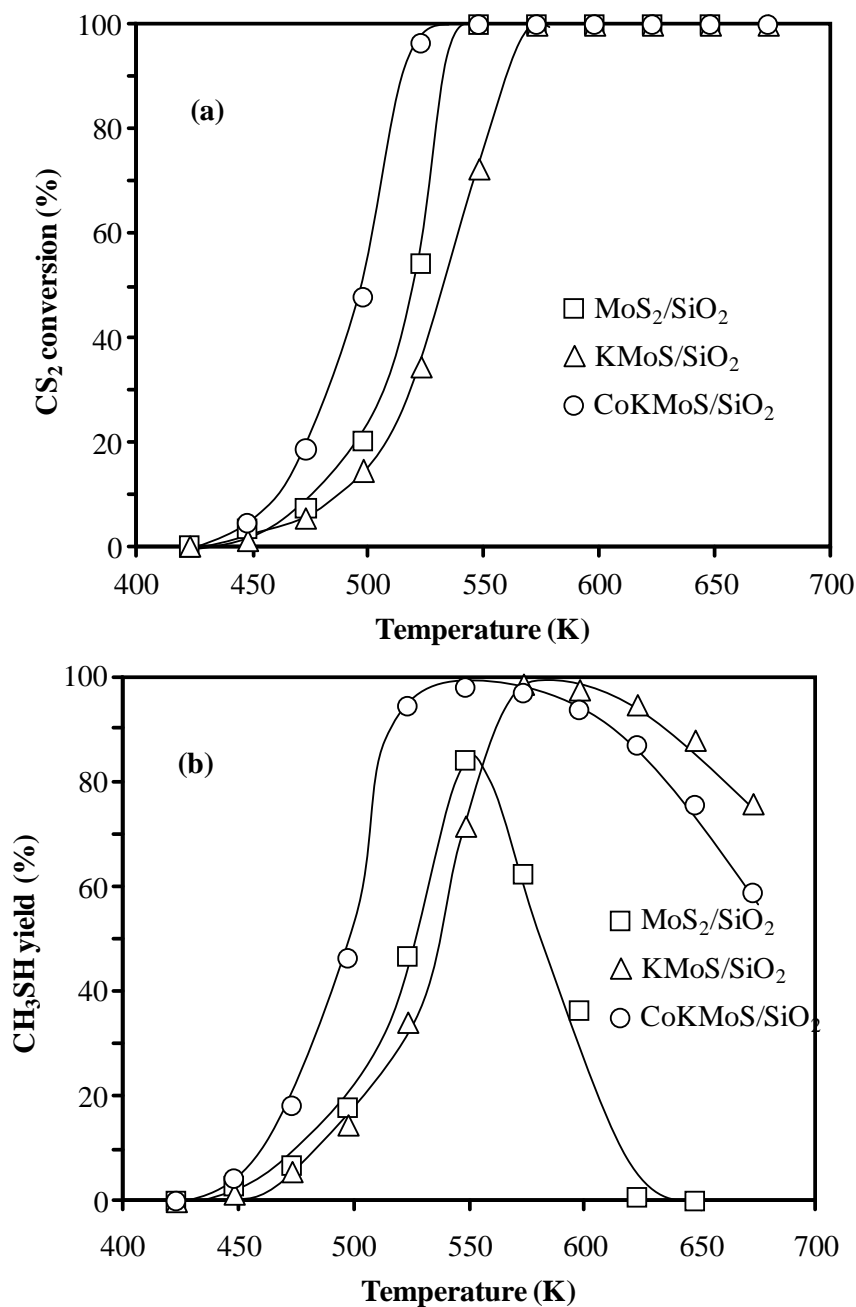
Figure 5.10: Conversion of CS_2 (a) and yield of CH_3SH (b) on sulfided MoS_2/SiO_2 (□), $KMoS/SiO_2$ (Δ), and $CoKMoS/SiO_2$ (O). The feed contains 8.5 vol % CS_2 and $H_2/CS_2 = 5.9$ (3 MPa, GSHV = 89.2 min⁻¹).

At lower temperatures, the highest CS_2 conversion was observed on $CoKMoS/SiO_2$ followed by the unpromoted catalyst, and the $KMoS/SiO_2$ system led to the lowest CS_2 conversion. Figure 5.10b shows that the yield of methanethiol rapidly increased at

temperatures above 573 K to a maximum value. On the unpromoted catalyst, the maximum yield of methanethiol was 84% at 548 K and then it decreased quickly to 0 at 623 K. On the K-containing catalyst the maximum CH_3SH yield of 98% was reached at 573 K followed by a steady decrease to 76% at 673 K. Using the $CoKMo/SiO_2$ catalyst, the maximum yield of CH_3SH (98%) was reached at 548 K, and it decreased to 58% at 673 K.
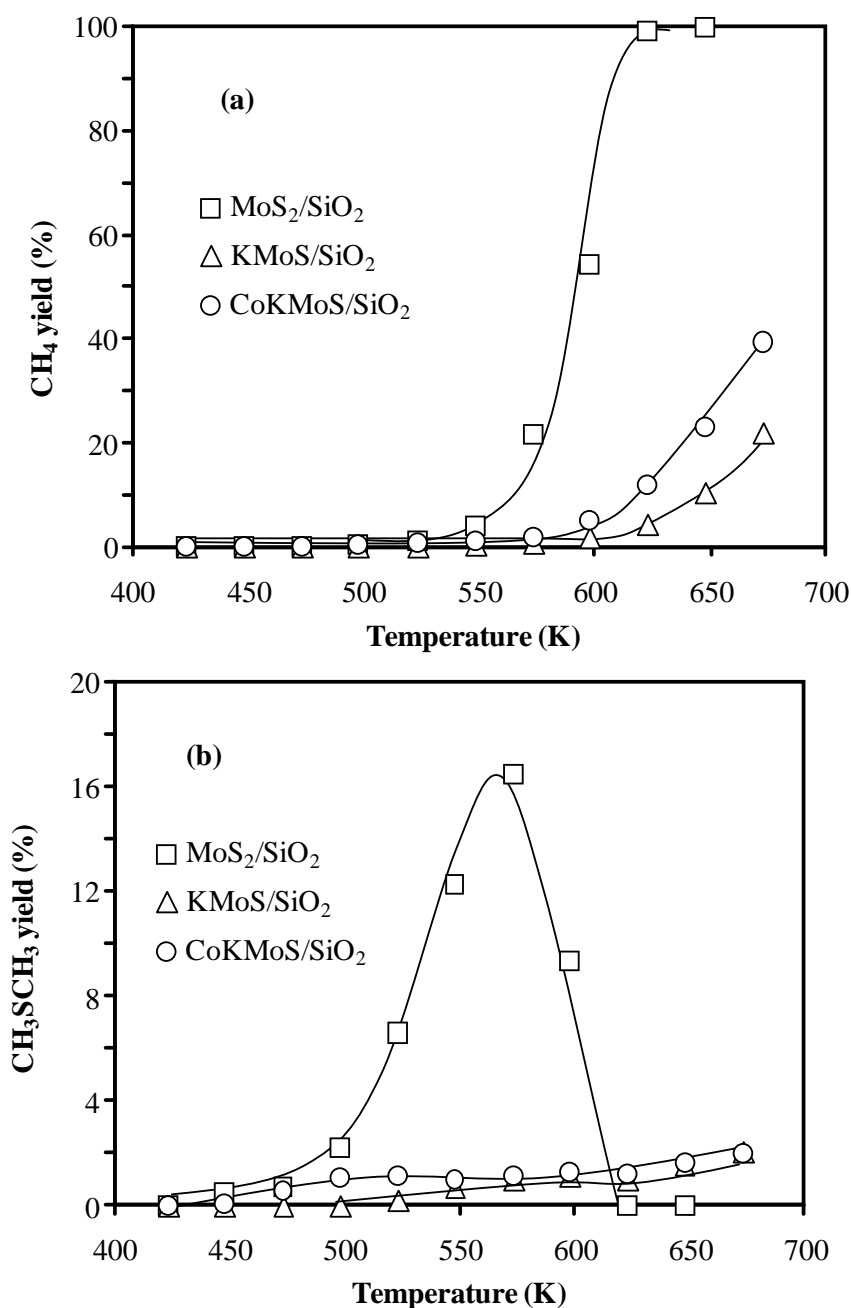
Figure 5.11: Yield of CH_4 (a) and CH_3SCH_3 (b) on sulfided MoS_2/SiO_2 (□), $KMoS/SiO_2$ (Δ), and $CoKMoS/SiO_2$ (O). The feed contains 8.5 vol % CS_2 and $H_2/CS_2 = 5.9$ (3 MPa, GSHV = 89.2 min^{-1}).

With all three catalysts, sulfided MoS_2/SiO_2, $KMoS/SiO_2$, and $CoKMoS/SiO_2$, only methane and dimethyl sulfide (CH_3SCH_3) were formed as byproducts in the synthesis of CH_3SH from CS_2. Figure 5.11a shows that for each catalyst the yield of CH_4 started increasing at the temperature corresponding to the decline in the yield of CH_3SH. Thus, the decrease in CH_3SH yield at temperatures higher than 548 K was due to CH_3SH reduction to methane. With MoS_2/SiO_2, the yield of methane increased rapidly above 548 K and reached almost 100% at 623 K. The formation of methane was significantly decreased by the presence of potassium in the $KMoS/SiO_2$ catalysts. The addition of Co to the $KMoS/SiO_2$ catalyst, however, slightly increased the formation of CH_4 again. This methane formation on both promoted catalysts started at 598 K and increased up to 673 K to a yield of 22 and 40% on $KMoS/SiO_2$ and $CoKMoS/SiO_2$, respectively. It is shown in Figure 5.11b that significant amounts of CH_3SCH_3 were observed only over MoS_2/SiO_2 where the CH_3SCH_3 yield increased up to 16.5% at 573 K and decreased at higher temperatures. Over the other systems the yield of CH_3SCH_3 was lower than 2% over the evaluated temperature range.

5.4. Discussion

5.4.1. Effect of the Catalytic Formulation on the Synthesis of CH₃SH from COS

Let us first analyze the activity observed with MoS_2/SiO_2 and then describe the effects of the K- or Co- and K-promotion. The conversion of COS which increases between 423 and 523 K is closely related to the yield of CO showing a parallel tendency. The yield of the other products, in contrast, remains rather low. This indicates that the decomposition of COS to CO has the highest reaction rate between 423 and 523 K on MoS_2/SiO_2. Relatively stable yields of CO and CO_2 were observed between 523 and 548 K suggesting that in this narrow temperature range, the relative rates of COS disproportionation and decomposition are constant. At higher temperatures the linearly increasing yield of CO_2 coupled with a decreasing CO yield indicates that the COS disproportionation becomes faster than the decomposition. Hence, we conclude that the disproportionation of COS has a higher activation energy than its decomposition. The yield of CS_2 is zero above 500 K, that is, it was consumed faster than formed. Thus, we conclude that CS_2 hydrogenation to CH_3SH is faster than COS disproportionation.

The addition of potassium to the catalyst decreases the conversion of COS, but it does not slow down all reaction steps equally. The much lower yield of CO observed with $KMoS/SiO_2$ than with MoS_2/SiO_2 below 623 K suggests that the decomposition of COS is drastically

reduced by potassium. The yield of CO_2, however, is much higher on the K-containing catalyst than on the unpromoted counterpart pointing to an increase in the rate of the COS disproportionation. In line with this statement, the yield of CS_2 is significantly higher with $KMoS/SiO_2$ than with MoS_2/SiO_2. The subsequent reactions are retarded by potassium to different extent. Note that the yield of CS_2 is negligible on MoS_2/SiO_2, whereas the yield of CH_3SH increases up to 5% at 500 K. This indicates that the hydrogenation of CS_2 to CH_3SH is fast. Interestingly, for the K-promoted catalysts the relatively high yield of CS_2 at 523 K is not accompanied by a high CH_3SH yield relative to the unpromoted system. Also, the formation of CH_4 ceased. Hence, the presence of potassium blocks or strongly retards the hydrogenation steps. The production of CH_3SH is less affected than its reduction to CH_4.

It is known that the reaction of syngas on MoS_2 yields hydrocarbons, whereas alcohols are selectively obtained on adding potassium to the catalytic formulation [18,19]. This observation seems to be analogous to the enhanced selectivity of H_2S-syngas to methanethiol on K-containing sulfides [9] as the carbon-heteroatom bonds are not cleaved in the presence of potassium. From another point of view, note that the hydrogenation of CS_2 to CH_3SH and the further reduction to CH_4 require the cleavage of C-S bonds. From this perspective, the decelerating effect of potassium on the C-S bond cleavage observed in this work is consistent with investigations addressing hydrodesulfurization (HDS). The results of those investigations indicate that potassium reduces the HDS activity of Mo-sulfide catalyst for model molecules and real oil feeds [20,21].

The formation of the $CoKMoS/SiO_2$ catalyst by adding cobalt increases the conversion of COS. Comparing the product yields observed with $KMoS/SiO_2$ and $CoKMoS/SiO_2$, the variation of the yields of CO, CS_2, and CO_2 shows that the increased rates are due to the acceleration of two parallel reactions, that is, the decomposition and the disproportionation of COS. Interestingly, the yield of CO, remains lower on $CoKMoS/SiO_2$ than on MoS_2/SiO_2 (the yield of CO is even the lowest and the CO_2 yield the highest on $CoKMo/SiO_2$ of all catalysts above 600 K) indicating that potassium blocks the decomposition pathway without cobalt reversing this blockage. The subsequent hydrogenation steps to CH_3SH and CH_4 are also accelerated by the cobalt promotion. In line with this accelerated disproportionation and subsequent hydrogenation, the yield of CS_2 reached a maximum value at lower temperatures than with other catalysts. In consequence, the yield of and the selectivity to CH_3SH is the highest with the double promoted MoS_2 catalyst. They decline slowly only above 650 K because of the enhanced reduction of CH_3SH to methane.

5.4.2. Effect of the Catalytic Formulation on the Synthesis of CH_3SH from CS_2

The reactions of CS_2 and H_2 on the unpromoted and the (Co)K-promoted catalysts confirm that the addition of potassium decreases the rate of CS_2 hydrogenation, whereas the presence of cobalt increases it, yielding only CH_3SH below 550 K. Above 550 K the CH_3SH yield drops with MoS_2/SiO_2 because of CH_4 formation. CH_3SH hydrogenation is nearly blocked with $KMoS/SiO_2$ indicating that the presence of K^+ cations blocks hydrogenation, while Co does hardly enhance CH_3SH hydrogenation, that is, it seems to remain less strongly adsorbed at the site of hydrogenation than on MoS_2/SiO_2. The significant formation of CH_3SCH_3 between 500 and 600 K with the latter catalyst and its disappearance in parallel to methane formation suggests that CH_4 is formed in a consecutive reaction from CH_3SCH_3 or as a parallel pathway (see Figure 5.3) on identical catalytic sites. The disappearance of these sites by addition of promoting atoms allows us to conclude that these sites are related to accessible Mo-cations.

5.4.3. Effect of the H_2/COS Ratio on the Synthesis of CH_3SH on $CoKMo/SiO_2$

Increasing the H_2/COS ratio led to the enhancement of the COS hydrodecomposition as seen from the increasing yield of CO, that is, $[COS + H_2 \rightarrow CO + H_2S]$. The increased rate of CO formation diminished the concentration of COS for the disproportionation reaction $[2\,COS \rightarrow CS_2 + CO_2]$. The positive influence of the hydrogen concentration suggests that all reactants are absorbed and that the two pathways follow the probability of finding a reaction partner on the sulfide surface.

Below 500 K higher partial pressures of H_2 enhanced the rate to CH_3SH $[CS_2 + 3H_2 \rightarrow CH_3SH + H_2S]$, while above 500 K accelerated rates of COS hydrodecomposition reduce the availability of CS_2, thereby reducing the rates to CH_3SH. It indicates that the energies of activation of the COS hydrodecomposition must be higher than that of CS_2 hydrogenation.

5.4.4. Role of the MoS_2 Phase and the Promoters

The X-ray diffractograms of the crystalline phases are reported for catalysts that were used in steady state operation after sulfidation of the oxide precursor. The catalytic experiments were also stopped to analyze the catalyst after different periods of reaction time, and the same XRD patterns for each catalyst were observed indicating the high stability of the investigated

catalytic materials. In the active sulfide state all catalysts showed the MoS_2 phase. In addition MoO_2 was also detected with MoS_2/SiO_2, and the formation of K_2SO_4 was observed on the K-containing catalysts.

The X-ray diffractograms of the oxide precursor suggest that relatively large crystals (average diameter of 93 nm) are formed upon supporting MoO_3 on SiO_2. After the sulfidation procedure, the molybdenum is effectively reduced to Mo^{4+}. The large crystals, however, are not completely sulfided, which resulted in a mixture of MoS_2 and MoO_2, the latter species having an average diameter slightly above 80 nm. Therefore, it is reasonable to assume that the MoS_2 formation starts from the surface and that the reduction of molybdenum is not correlated with the sulfide formation. While the presence of K_2SO_4 is startling at first it is highly unlikely that it catalyzes any of the reactions discussed here, because it is highly stable and difficult to reduce [22]. Indeed, it has been observed that the formation of surface sulfate species decreased the conversion of CS_2 in reactions carried out on Al_2O_3 or TiO_2 supports [23].

As the promoters, K or Co-K modify the behavior of the catalyst without changing the dominating MoS_2 phase, we conclude in agreement with the literature that K^+ cations do not occupy specific sites in the catalyst, but are randomly distributed on the surface of the support and the active sulfide phase [8,10]. Thus, some K^+ cations are associated with the sulfide and others are deposited on the support. It is also possible that not all supported MoS_2 is promoted by potassium. This random distribution of alkali promoter leads in consequence to the formation of two MoS_2 phases, that is, K-free and K-decorated MoS_2. K^+ cations not associated with MoS_2 agglomerate to form Mo-free crystalline species on silica, for example, K_2SO_4 as observed in this work. Interestingly, on Al_2O_3, K_2SO_4 does not form probably because of the stronger interaction of K^+ cations with alumina [12].

Different catalytic behaviors have been proposed for the two different phases [11,12]. The K-free MoS_2 catalyzes mainly the COS decomposition and the hydrogenation of CH_3SH, whereas the K-promoted phase hinders these two reactions and promotes the disproportionation of COS. These assignments are consistent with what is observed in this work. The origin of this effect has been explained by assigning the role of adsorption center to K^+ cations. Accordingly, the NO adsorption increases from 69 to 230 µmol/g by adding 8.8 wt % of potassium in the studied catalysts. This increase of adsorption sites concentration is neither reflected in the COS decomposition nor in the CS_2 hydrogenation. The only reaction enhanced with the K-promotion is the disproportionation of COS. This strongly suggests that the adsorption sites created by potassium differ from the Mo-coordinatively unsaturated sites

(Mo-CUS). The K-containing sites are active for disproportionation, but reduce the concentration of Mo-CUS and thereby limit reactions catalyzed by accessible Mo cations. For a detailed discussion of the nature of the K-containing active sites see ref 12.

On the other hand, Co is a very specific promoter of Mo sulfide. It is well-known that Co interacts with MoS_2 forming the CoMoS phase, in which a fraction of Mo sites at the edges of the MoS_2 slab is replaced by Co [24]. This Co-Mo-S association is favored at Co/Mo molar ratios of around 0.5, whereas Co-sulfides form at higher contents of promoter. In this work an amount of Co below the maximum Co/Mo ratio for the formation of the Co-Mo-S phase was added to the Mo catalyst. Thus, we can assume that in the $CoKMoS/SiO_2$ catalyst the Co-Mo-S phase is formed in agreement with the literature [25]. We cannot deduce from the present results whether or not Co incorporation occurs with preference on either MoS_2 or the K-decorated MoS_2. It is likely that cobalt decorates both MoS_2-like phases because all reaction steps are accelerated by Co promotion.

Considering that all reactions rates are accelerated and assuming that accessible Co is located at least in the nominal concentration at the edges of MoS_2 slabs, we deduce that all the reaction steps occur at the edges of MoS_2. To influence the catalytic performance of the MoS_2 phase, at least part of the K^+ cations must be located near the MoS_2 slab edges. Considering that K^+ enhances the O-S exchange [12], it is highly likely that the K^+ cations enhance the exchange on the edge of MoS_2 slabs because these sulfur atoms are much more labile than sulfur in the basal planes [26].

The influence of cobalt on MoS_2-based catalysts has been extensively studied for hydrotreating catalysts. Two main effects are attributed to Co-promotion, that is, increasing the concentration of CUS and facilitating the activation of H_2 [27]. For the catalysts studied in this work, NO adsorption shows that the addition of Co increases the adsorption of NO from 230 to 304 μmol/g. Thus, the enhanced activity of the $CoKMo/SiO_2$ catalyst can be related to the increase of CUS in the MoS_2 edges [16] as it has been done for the synthesis of alcohols from syngas on K-doped Mo sulfides [28].

A schematic view of the K^+- and Co-promoted MoS_2 slabs is presented in Figure 5.12. While we assume that the K^+ cations are distributed over the material surface, only those deposited near the slab edges are relevant for the catalytic performance. The K-containing adsorption sites without Mo-CUS (a) would catalyze the disproportionation of COS. The sites containing both Co and K^+ (b) in principle catalyze COS disproportionation and decomposition as well as hydrogenation steps. However, the K^+ cations would act as weak adsorption sites decreasing the rate of hydrogenation by adsorbing the reaction intermediates

more weakly. Finally, the MoS_2-CUS in the MoS_2 edge promoted only by Co would catalyze hydrogenation and C-S bond cleavage.
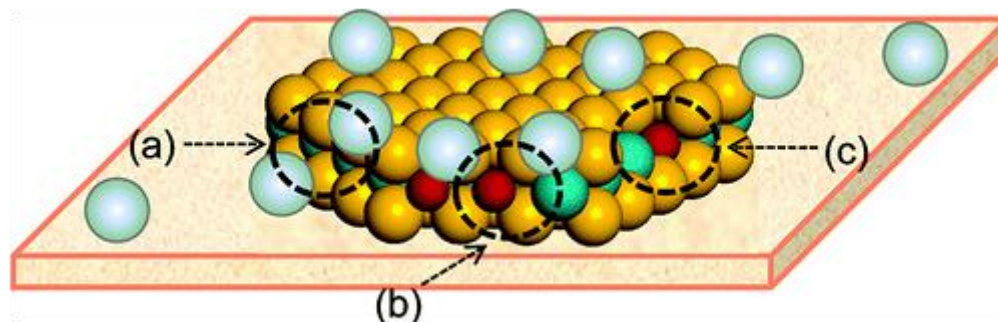
Figure 5.12: Schematic representation of a K- and Co-promoted MoS_2 slab. K^+ cations, Co, S, and Mo atoms are presented in light blue, red, yellow and green spheres, respectively. K^+-decorated site for COS disproportionation without Mo CUS (a); potential active sites for all reactions promoted with Co and K^+ (b); Co-promoted hydrogenation and hydrogenolysis sites (c).

The enhancing effect of cobalt in the hydrogenation and hydrogenolysis steps is not surprising because the same effect has been observed in hydrotreating applications. The promotion of the disproportionation step can be attributed to the increase of oxygen and sulfur mobility in line with the known Co effect of decreasing the binding energy between Mo and the heteroatom [29]. On the other hand, the formation of CH_3SCH_3 on MoS_2/SiO_2 implies that two CH_3S- fragments adsorbed on adjacent Mo-CUS combine before desorption. However, the hydrogenolysis to methane is faster than the recombination to CH_3SCH_3 above 573 K. On the K-containing catalysts, the occurrence of two Mo-CUS would be less probable because of the blocking of such sites by K^+. Readsorption of CH_3SH, however, cannot be ruled out as one of the critical steps leading to the formation of CH_3SCH_3. K^+ cations would in that case reduce the probability that CH_3SH reacts further.

Final evidence of the different adsorption abilities of Mo-CUS and K^+ cations is given by CO_2 adsorption. On MoS_2/SiO_2, the uptake of CO_2 is negligible in accordance with reports that CO_2 does not adsorb on MoS_2 [17]. In contrast, the sulfide KMo/Al_2O_3 catalyst adsorbs 23 μmol/g, which points to CO_2 adsorption involving the alkali atoms in agreement with ref 30. We speculate at present that such adsorption complexes have an sp^2 hybridized carbon atom. The adsorption of the same concentration of CO_2 on the sulfide $CoKMoS/Al_2O_3$ catalyst strongly suggests that the CO_2 interacts exclusively with K^+ cations, and not with CUS created by the incorporation of Co. The increased concentration of CUS on transition metals after Co-promotion is evidenced by the increase in the NO uptake by around 30%.

This value is consistent with the increase of CUS concentration of 25-33% found in Al_2O_3-supported MoS_2 after promotion with Ni reported in refs 31,32.

5.5. Conclusions

The CH_3SH synthesis was carried out starting from COS/H_2 and CS_2/H_2 mixtures catalyzed by Mo, K-Mo, and Co-K-Mo sulfide catalysts supported on SiO_2. On unpromoted MoS_2, the (undesired) COS decomposition leading to CO and the hydrogenation of CH_3SH to CH_4 are favored and are associated with the presence of the highly reactive accessible Mo cations. The promotion with K^+, decorating supported MoS_2 and CoMoS particles, accelerates the COS disproportionation by providing sites for a facile exchange of oxygen and sulfur (presumably via surface mixed carbonates containing also sulfur atoms) and thereby indirectly reduces the formation of CO by COS decomposition. Note that also the addition of the more Lewis acidic Co cation increases the rate of C-S bond cleavage, therefore, it does not seem to stabilize carbonate structures.

The promotion with potassium also retards all steps requiring hydrogen, thereby decreasing the formation of methane. However, the formation of CH_3SH is less affected leading to the optimum yield. Adding Co accelerates all individual steps in the reaction network. The CH_4 formation rate is only enhanced at higher temperatures hardly limiting the temperature window in which high yields of methanethiol are achievable. Minimizing the H_2 partial pressure allows further optimization of the CH_3SH selectivity.

5.6. References

[1]   Sauer, J.; Boeck W.; von Hippel, L.; Burkhardt, W.; Rautenberg, S.; Arntz, D.;
      Hofen, W. U.S. Patent 5 852 219, 1998.

[2]   Mashkin, V.; Kudenkov, V.; Mashkina, A. Ind. Eng. Chem. Res. 1995, 34, 2964–2970.

[3]   Olin, J.; Buchholz, B.; Loev, B.; Goshorn, R. U.S. Patent 3 070 632, 1962.

[4]   Haines, P. U.S. Patent 4 449 006, 1984.

[5]   Ratcliffe, C.; Tromp, P. U.S. Patent 4 668 825, 1987.

[6]   Ratcliffe, C.; Tromp, P.; Wachs, I. U.S. Patent 4 570 020, 1985.

[7]   Mul, G.; Wachs, I.; Hirschon, A. Catal. Today 2003, 78, 327–337.

[8]   Zhang, B.; Taylor, S.; Hutchings, J. New J. Chem. 2004, 28, 471–476.

[9]   Chen, A.; Wang, Q.; Li, Q.; Hao, Y.; Fang, W.; Yang, Y.
      J. Mol. Catal A: Chem. 2008, 283, 69–76.

[10] Kaufmann, C.; Gutiérrez, O.; Zhu, Y.; Lercher, J.
      Res. Chem. Intermed. 2010, 36, 211–225.

[11] Gutiérrez, O.; Kaufmann, C.; Hrabar, A.; Zhu, Y.; Lercher, J.
      J. Catal. 2011, 280, 264–273.

[12] Gutiérrez, O.; Kaufmann, C.; Lercher, J. ChemCatChem 2011, 3, 1480–1490.

[13] Chen, A.; Wang, Q.; Hao, Y.; Fang, W.; Yang, Y. Catal. Lett. 2007, 118, 295–299.

[14] Topsøe, H.; Clausen, B.; Massoth, F. Hydrotreating Catalysis Science and Technology;
      Springer-Verlag: New York, 1996.

[15] Bian, G.; Fu, Y.; Ma, Y. Catal. Today 1999, 51, 187–193.

[16] Topsøe, N.; Topsøe, H. J. Catal. 1982, 77, 293–296.

[17] Zmierczak, W.; Qader, Q.; Massoth, F. J. Catal. 1987, 106, 65–72.

[18] Lee, J.; Kim, S.; Lee, K.; Nam, I.; Chung, J.; Kim, Y.; Woo, H.
      Appl. Catal., A 1994, 110, 11–25.

[19] Surisetty, V.; Hu, Y.; Dalai, A.; Kozinski, J. Appl. Catal., A 2011, 392, 166–172.

[20] Kelly, J.; Ternan, M. Can. J. Chem. Eng. 1979, 57, 726–733.

[21] Verbruggen, N.; Knözinger, H. Langmuir 1994, 10, 3148–3155.

[22] Kasznoyi, A.; Hronec, M.; Delahay, G.; Ballivet-Tkatchenko, D.
      Appl. Catal., A 1999, 184, 103–113.

[23] Laperdrix, E.; Justin, I.; Costentin, G.; Saur, O.; Lavalley, J.; Aboulayt, A.; Ray, J.;
      Nédez, C. Appl. Catal., B 1998, 17, 167–173.

[24] Topsøe, N.; Topsøe, H. J. Catal. 1983, 84, 386–401.

[25] Iranmahboob, J.; Hill, D.; Toghiani, H. Appl. Catal., A 2002, 23, 99–108.

[26] Tauster, S.; Pecoraco, T.; Chianelli, R. J. Catal. 1980, 63, 515–519.

[27] Moses, P.; Hinnemann, B.; Topsøe, H.; Nørskov, J. J. Catal. 2009, 268, 201–208.

[28] Bao, J.; Fu, Y.; Bian, G. Catal. Lett. 2008, 121, 151–157.

[29] Byskov, L.; Nørskov, J.; Clausen, B.; Tøpsoe, H. Sulphur bonding in transition metal sulphides and MoS$_2$ based structures. In Transition Metal Sulphides - Chemistry and catalysis; Kluwer Academic Publishers: Dordrecht, Netherlands, 1998.

[30] Karolewski, M.; Cavell, R. Surf. Sci. 1989, 219, 261–276.

[31] Hrabar, A.; Hein, J.; Gutiérrez, O.; Lercher, J. J. Catal. 2011, 281, 325–338.

[32] Gutiérrez, O.; Klimova, T. J. Catal. 2011, 281, 50–62.

Chapter 6

Summary

6.1. Summary

Methyl mercaptan is a chemical feedstock employed in the synthesis of numerous products in the agricultural, plastics, rubber and chemical industries. Methyl mercaptan is predominantly produced by the reaction of methanol with hydrogen sulfide on an industrial scale. Owing to the fact that methanol is produced from synthesis gas, the idea to synthesize methyl mercaptan from synthesis gas directly, thereby omitting the methanol production step, is intriguing and has received considerable interest.

This thesis aimed at gaining insight into the formation of methyl mercaptan from H_2S-containing synthesis gas by devising a two-step approach consisting of the selective production of carbonyl sulfide as a first process step followed by the downstream synthesis of CH_3SH over promoted and unpromoted MoS_2 based catalysts in a subsequent reactor. This approach was chosen since it is commonly accepted in literature, that formation of methyl mercaptan from H_2S-containing synthesis gas proceeds via the formation of COS as a first step. However, the hydrogenation of COS over the described catalytic systems had not been investigated in detail prior to this thesis.

In Chapter 2 the formation of COS from CO, CO_2 and liquid sulfur in the presence and absence of H_2 was investigated. A reaction network for the formation of COS was elucidated based on the results obtained from various experiments at different reaction temperatures, pressures, residence times and reactant ratios. The presence of H_2 provides an alternative and complementary reaction route for the formation of COS from CO.

The formation of COS proceeds via the reverse water gas shift reaction when CO_2 is used as carbon source. CO is an intermediate that is further converted to COS by reacting with liquid sulfur or sulfanes - including H_2S. CO conversions of up to 95% leading to COS yields of 95% were achieved, which means quantitative conversion of CO to COS. All experimental results indicate, that the individual reactions depicted in the reaction network in Figure 6.1 mainly take place in the liquid sulfur phase.
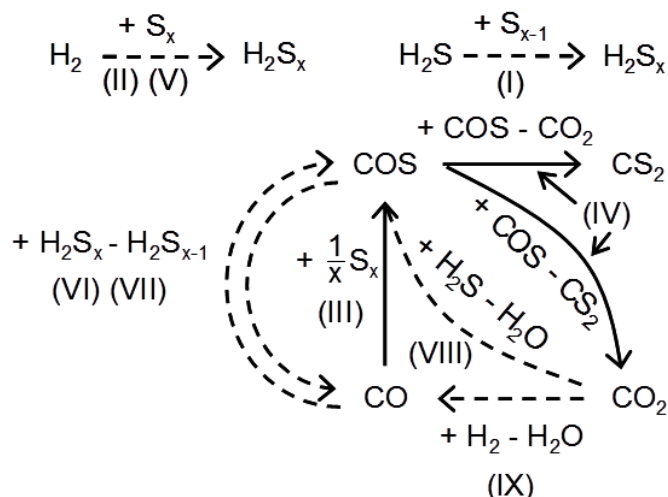
Figure 6.1: Reaction network of CO/CO_2 and sulfur in presence of H_2. The dashed lines correspond to the pathways created by the introduction of H_2 into the reaction system.

The highly efficient method for the formation of COS developed within the scope of Chapter 2 allowed the investigation of the second step, i.e. the formation of methyl mercaptan starting from COS as educt.

Chapter 3 of this thesis deals with the synthesis of methyl mercaptan from COS and H_2 in the presence of H_2S on K^+-promoted MoS_2 supported on silica. Combination of physicochemical characterization of the catalyst with detailed kinetic studies led to the conclusion that methyl mercaptan is solely formed by the hydrogenation of CS_2, as depicted in Figure 6.2, which is a disproportionation product of COS. This means that CS_2 is an additional intermediate in the hydrogenation of COS to methyl mercaptan. In addition, CO_2 found in the reaction mixture is produced by the disproportionation of carbonyl sulfide and not – as believed prior to this work – by the water-gas shift reaction between CO and H_2O.

Two catalytically active phases are present on the catalyst under the reaction conditions applied, MoS_2 and a K^+-decorated MoS_2 phase. Disproportionation of COS, as well as hydrodecomposition of COS were concluded to take place at coordinatively unsaturated sites. While hydrodecomposition of COS is favoured on the pure MoS_2 phase, disproportionation of COS to CO_2 and CS_2, which is hydrogenated to methyl mercaptan, is favored on the K^+-decorated MoS_2 phase.
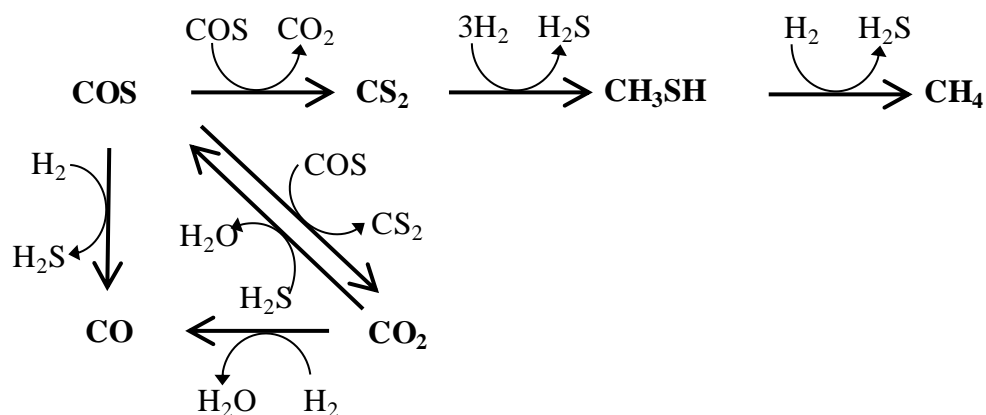
Figure 6.2: Reaction pathway for the hydrogenation of COS over sulfide K_2MoO_4/SiO_2.

The influence of potassium on the synthesis of methyl mercaptan from COS was investigated in more detail in Chapter 4. In order to understand the key role of the alkali metal in the formation of methanethiol, potassium-doped MoS_2 catalysts supported on alumina were tested in the synthesis of CH_3SH from COS and thoroughly characterized by means of atomic absorption spectroscopy, N_2 physisorption, NO adsorption, X-ray diffraction, temperature-programmed sulfidation and Raman spectroscopy. The results confirmed that two phases, pure MoS_2 and potassium-decorated MoS_2 were present in the active catalysts. The main effect of potassium during sulfidation and during the catalytic reaction was attributed to an increase in the mobility of surface oxygen and sulfur atoms, which promotes the disproportionation of COS to CO_2 and CS_2 and the production of CO from CO_2.
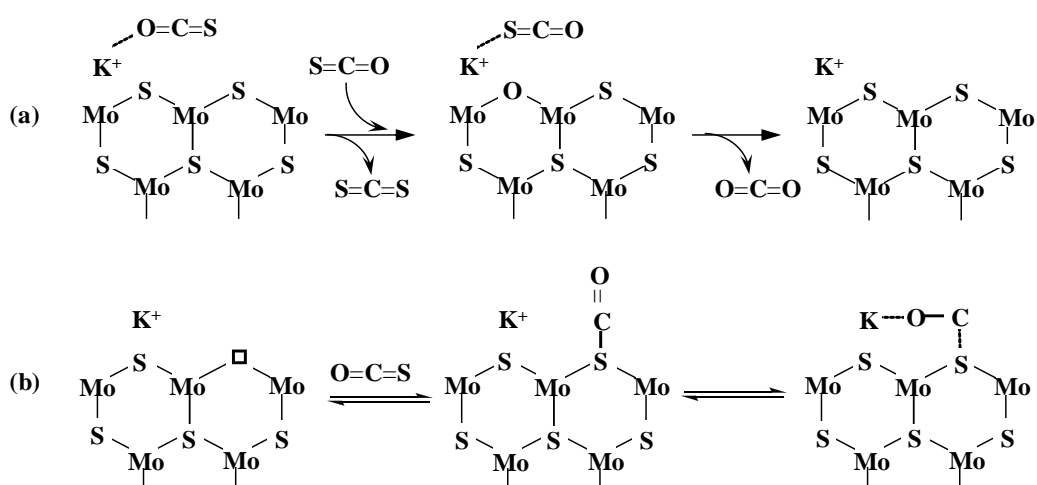
Figure 6.3: (a) Possibilities for the adsorption of COS on the potassium promoted site that lead to the disproportionation to CS_2 and CO_2. (b) Stabilizing effect of potassium on adsorbed COS.

137

Potassium cations were found to hinder the reductive decomposition of COS to CO and H_2S and the hydrogenolysis of methanethiol to methane. Mars-van Krevelen-type mechanisms are proposed to explain the disproportionation of COS on alumina and on K^+ decorated MoS_2 (Figure 6.3). The catalytically active site in the potassium-decorated MoS_2 phase is proposed to include a potassium cation as adsorption site.

Based on the finding that methyl mercaptan formation proceeds via the hydrogenation of CS_2, this route was explored within Chapter 5. Quantitative conversion of CS_2 to methanethiol in the presence of H_2 was achieved over potassium-promoted and cobalt-potassium double promoted MoS_2 catalysts. The doubly promoted catalyst was found to be superior to the potassium-promoted and pure MoS_2 catalysts with respect to methyl mercaptan formation from COS, which was also explored within the scope of Chapter 5. Adding Co accelerates all individual steps in the reaction network. The CH_4 formation rate is only enhanced at higher temperatures hardly limiting the temperature window in which high yields of methanethiol are achievable. Three different types of catalytically active sites are proposed, all of them located on the edges of MoS_2 slabs (promoted with K and/or Co) as depicted in Figure 6.4. K^+-decorated sites for COS disproportionation without Mo CUS (a); potential active sites for all reactions promoted with Co and K^+ (b) and Co-promoted hydrogenation and hydrogenolysis sites (c).
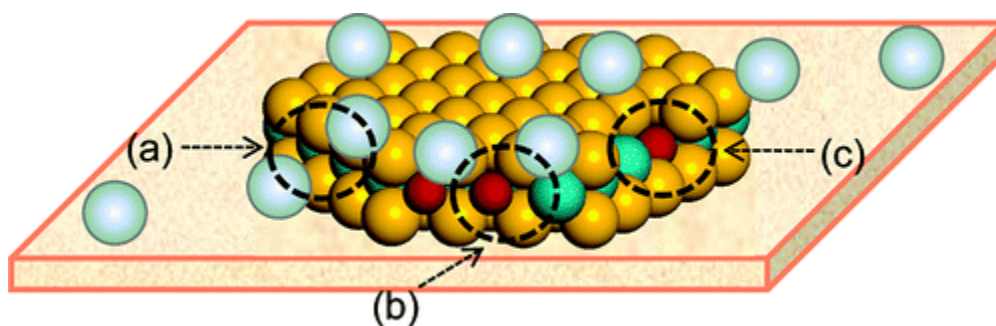
Figure 6.4: Schematic representation of a K- and Co-promoted MoS_2 slab. K^+ cations, Co, S, and Mo atoms are presented in light blue, red, yellow and green spheres, respectively.

The results of this thesis show that the synthesis of methyl mercaptan from COS/CS_2, and hence from H_2S-containing synthesis gas, can be tuned towards high yields and selectivities by choosing suitable promoters to influence the catalytic properties of supported molybdenum sulfide catalysts. Furthermore this thesis contributed to gain a more detailed understanding of

the reactions and their underlying mechanisms, which take place on MoS_2 catalysts. These results highlight the potential of these catalysts for their industrial application in the production and conversion of C1-compounds in presence of sulfur.

6.2. Zusammenfassung

Methylmercaptan ist ein Ausgangsstoff in der Synthese zahlreicher Produkte, die in der Landwirtschaft, der Kunststoff- und der chemischen Industrie zur Anwendung gelangen. Die großtechnische Darstellung von Methylmercaptan basiert vorwiegend auf der Reaktion von Methanol mit Schwefelwasserstoff. Da Methanol ausgehend von Synthesegas produziert wird, ist der Gedanke Methylmercaptan direkt aus Synthesegas unter Umgehung der Methanolsynthese darzustellen reizvoll und naheliegend und hat folglich in den letzten Jahrzehnten mehr und mehr Aufmerksamkeit erlangt.

Ziel der vorliegenden Arbeit war die Untersuchung der Bildung von Methylmercaptan aus mit Schwefelwasserstoff angereichertem Synthesegas. Dabei wurde ein zweistufiger Ansatz gewählt. In einem ersten Schritt wurde Carbonylsulfid dargestellt, welches in der Folge in einem nachgeschalteten Reaktor über promotierten und unpromotierten MoS_2-basierten Katalysatoren durch Hydrierung zu Methylmercaptan umgesetzt wurde. Dieser Ansatz wurde gewählt, da es in der Fachliteratur als gesichert angesehen wird, dass die Bildung von Methylmercaptan aus H_2S-enthaltendem Synthesegas über die Bildung von Carbonylsulfid in einem erstem Schritt erfolgt. Die darauf folgende Hydrierung des COS über den verwendeten Katalysatoren, auf deren Untersuchung das Hauptaugenmerk der vorliegenden Arbeit liegt, war zuvor nicht im Detail untersucht worden.

In Kapitel 2 wurde die Bildung von COS aus CO, CO_2 und flüssigem Schwefel in An- und Abwesenheit von Wasserstoff untersucht. Ergebnisse, die durch Experimente bei unterschiedlichen Reaktionstemperaturen und –drücken, sowie Verweilzeiten und Eduktzusammensetzungen gewonnen wurden, erlaubten die Ableitung eines Reaktionsnetzwerks. Durch die Anwesenheit von Wasserstoff eröffnet sich ein zusätzlicher und ergänzender Reaktionsweg für die Bildung von COS aus CO.

Die Bildung von COS erfolgt durch die Reaktion von CO mit flüssigem Schwefel oder Sulfanen – einschließlich H_2S. Wird CO_2 als Kohlenstoffquelle verwendet, so erfolgt in einem ersten Schritt die Bildung von CO über die umgekehrte Wassergas-Shift-Reaktion, welches dann weiter zu COS umgesetzt wird. CO-Umsätze von bis zu 95% bei COS-Ausbeuten von 95% konnten erzielt werden, was einer quantitativen Umsetzung von CO zu COS

gleichkommt. Sämtliche Ergebnisse legen nahe, dass die in Abbildung 6.1. dargestellten Reaktionsschritte hauptsächlich in der Phase des flüssigen Schwefels stattfinden.
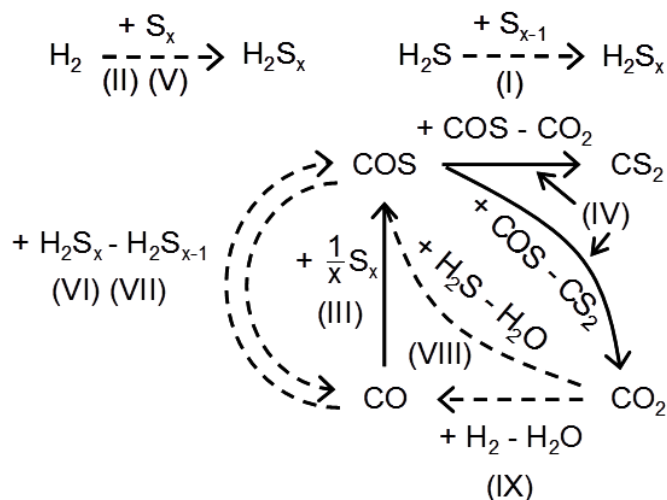
Abbildung 6.1: Reaktionsnetzwerk von CO/CO$_2$ mit Schwefel in Anwesenheit von Wasserstoff. Die gestrichelten Linien zeigen die durch die Anwesenheit von Wasserstoff zusätzlich möglichen Reaktionen.

Die in Kapitel 2 entwickelte, hocheffiziente Methode der Darstellung von COS erlaubte die gezielte Untersuchung der zweiten Stufe der Methylmercaptansynthese aus H$_2$S-enthaltendem Synthesegas, d.h. die isolierte Betrachtung der Bildung von Methylmercaptan aus COS.

Kapitel 3 beschäftigt sich mit der Synthese von Methylmercaptan aus COS und H$_2$ in der Gegenwart von H$_2$S über Silika-geträgerten, K$^+$-promotierten MoS$_2$-Katalysatoren. Die Kombination physikalisch-chemischer Charakterisierung der Katalysatoren in Verbindung mit detaillierten kinetischen Studien führte zu der Schlussfolgerung, dass Methylmercaptan ausschließlich, wie in Abbildung 6.2 dargestellt, durch die Hydrierung von CS$_2$ gebildet wird, welches ein Disproportionierungsprodukt von COS ist. Das heißt, dass CS$_2$ ein zusätzliches Intermediat in der Hydrierung von COS zu Methylmercaptan ist. Darüber hinaus handelt es sich bei dem als Reaktionsprodukt nachgewiesenen CO$_2$ ebenfalls um ein Disproportionierungsprodukt des COS und nicht - wie vor dieser Arbeit angenommen – um ein Produkt der Wassergas-Shift-Reaktion zwischen CO und Wasser.

Unter Reaktionsbedingungen existieren zwei katalytisch aktive Phasen, MoS$_2$ und eine K$^+$-dekorierte MoS$_2$-Phase. Sowohl die Disproportionierung von COS, als auch die Reduktion

von COS zu CO und H_2S erfolgen an koordinativ ungesättigten Zentren. Die Reduktion von COS findet bevorzugt an der reinen MoS_2-Phase statt, während die Disproportionierung von COS zu CO_2 und CS_2, welches in der Folge zu Methylmercaptan hydriert wird, bevorzugt an der K^+-dekorierten MoS_2-Phase stattfindet.
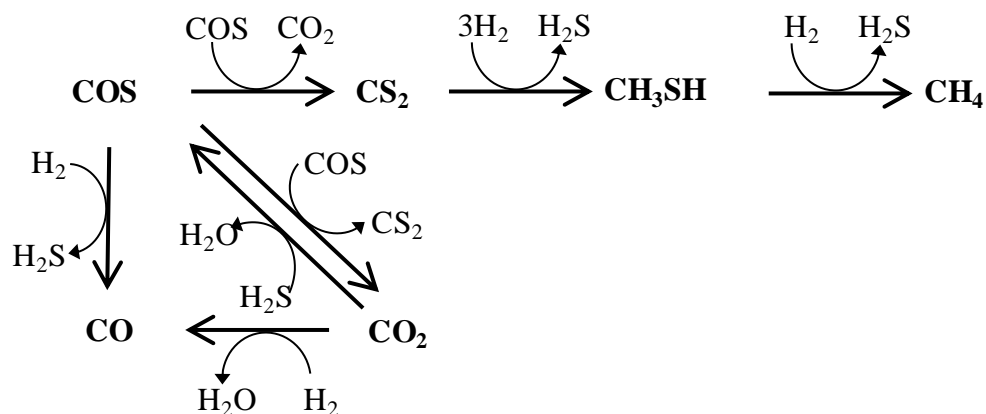
Abbildung 6.2: Reaktionnetzwerk der Hydrierung von COS über sulfidiertem K_2MoO_4/SiO_2.

Der Einfluss von Kalium auf die Synthese von Methylmercaptan aus COS war Gegenstand der Untersuchungen in Kapitel 4. Um die Schlüsselrolle des Alkalimetalls bei der Bildung von Methylmercaptan näher zu untersuchen, wurden Kalium-promotierte, auf Alumina geträgerte, MoS_2-Katalysatoren in der Synthese von Methylmercaptan aus COS getestet und via AAS, N_2-Physisorption, NO-Adsorption, XRD, TPS und Raman-Spektroskopie charakterisiert. Die Ergebnisse bestätigten, dass zwei Phasen, reines MoS_2 und K^+-dekoriertes MoS_2, im aktiven Katalysator vorliegen. Der Haupteinfluss des Kaliums während der Sulfidierung und während der katalytischen Reaktion konnte einer erhöhten Beweglichkeit von Oberflächen-Sauerstoff und -Schwefelatomen zugeschrieben werden, welche die Disproportionierung von COS zu CO_2 und CS_2 und die Bildung von CO aus CO_2 begünstigt. Die Reduktion von COS zu CO und H_2S, sowie die Hydrierung von Methylmercptan zu Methan, werden durch die Gegenwart von Kalium-Kationen behindert. Es wird vorgeschlagen, dass Reaktionsmechanismen vom Mars-van Krevelen-Typ für die Disproportionierung von COS über Alumina und über K^+-promotiertem MoS_2 verantwortlich sind (Abbildung 6.3). Weiterhin wird vorgeschlagen, dass das katalytisch aktive Zentrum in der K^+-dekorierten MoS_2-Phase ein Kalium-Kation als Adsorptionszentrum beinhaltet.
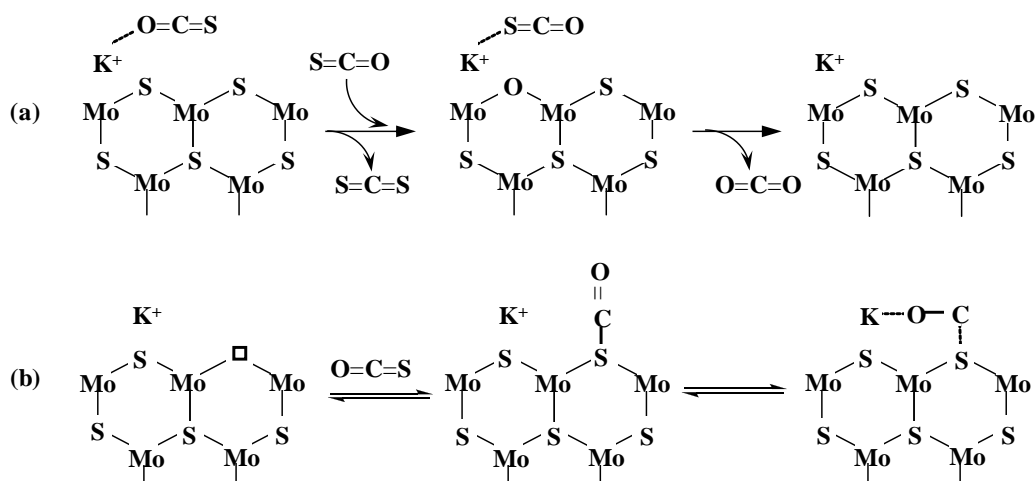
Abbildung 6.3: a) Möglichkeiten für die Adsorption von COS am Kalium-promotierten aktiven Zentrum, die zur Bildung von CS_2 und CO_2 durch Disproportionierung von COS führen. (b) Stabilisierender Effekt des Kaliums auf adsorbiertes COS.

Basierend auf der Erkenntnis, dass die Bildung von Methylmercaptan durch die Hydrierung von CS_2 erfolgt, wurde diese Route in Kapitel 5 näher untersucht. Quantitativer Umsatz von CS_2 zu Methylmercaptan konnte in der Gegenwart von Wasserstoff über Kalium- und Cobalt-Kalium-promotierten MoS_2-Katalysatoren erzielt werden. Bei der Bildung von Methylmercaptan aus COS, die ebenfalls im Rahmen von Kapitel 5 untersucht wurde, war der zweifach promotierte Katalysator dem Kalium-promotierten und dem unpromotierten MoS_2-Katalysator überlegen. Die Anwesenheit von Kobalt führt zu einer Beschleunigung aller individuellen Schritte des Reaktionsnetzwerks. Die Reaktionsrate der Bildung von Methan wird nur im oberen Temperaturbereich erhöht, wodurch das Temperaturfenster in dem hohe Ausbeuten von Methylmercaptan möglich sind kaum eingeschränkt wird. Wie in Abbildung 6.4. dargestellt, werden drei unterschiedliche Arten von katalytisch aktiven Zentren vorgeschlagen, wobei alle an den, gegebenenfalls mit Kalium und/oder Kobalt promotierten, Kanten der MoS_2-Kristallite lokalisiert sind. Dabei handelt es sich um K^+-dekorierte Zentren für die COS Disproportionierung ohne koordinativ ungesättigtes Mo (a), mit Kobalt und Kalium-Kationen promotierte aktive Zentren für alle stattfindenen Reaktionen (b), sowie Kobalt-promotierte Zentren an denen Hydrierung und reduktiver Zerfall von COS zu CO und H_2S stattfinden.
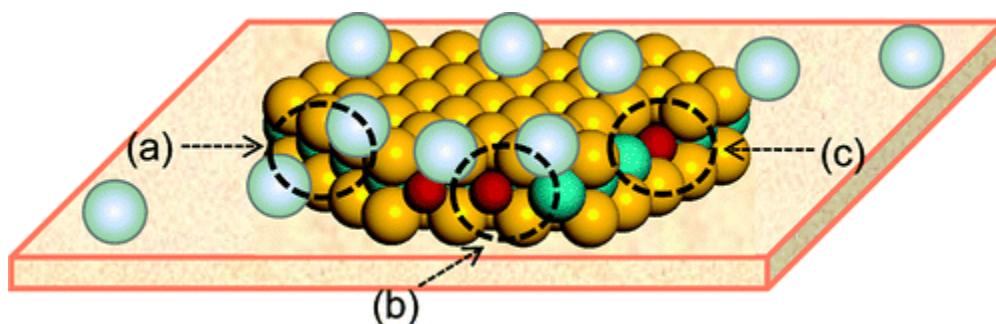
Abbildung 6.4: Schematische Darstellung eines Kalium- und Kobalt-promotierten MoS$_2$-Kristallits. Die Darstellung von K$^+$-Kationen, Co, S, und Mo Atomen erfolgt in hellblau, rot, gelb und grün.

Die Ergebnisse dieser Arbeit zeigen, dass für die Synthese von Methylmercaptan aus COS/CS$_2$, beziehungsweise aus H$_2$S-haltigem Synthesegas, durch die Wahl geeigneter Promotoren die katalytischen Eigenschaften von geträgerten MoS$_2$-Katalysatoren gezielt hinsichtlich hoher Ausbeuten und Selektivitäten beeinflusst werden können. Darüber hinaus hat diese Arbeit zur Vertiefung des Verständnisses der an MoS$_2$-Katalysatoren stattfindenden Reaktionen und der zugrunde liegenden Mechanismen beigetragen und damit das Potential dieser Katalysatoren für die industrielle Anwendung in der Darstellung und Umsetzung von C1-Bausteinen in Anwesenheit von Schwefel aufgezeigt.

7. Curriculum vitae

Christoph Rudolf Erwin Kaufmann was born on February 18th in 1976 in Munich, Germany. He attended the Aventinus-Gymnasium in Burghausen from 1986 to 1995 from which he graduated with the general qualification for university entrance (Abitur). After his military service he started studies at the Technical University of Munich. After four semesters of computer science he changed his field of study to chemistry. In 2005 he received his degree as "Diplom-Chemiker" after completing his studies and finishing his diploma thesis "Activation of Carbon-Carbon Single Bonds by Transition Metals of Group VI" at the chair of Prof. W.A. Hermann. He joined the group of Prof. Johannes A. Lercher as a PhD student, where he focused on alternative routes to methyl mercaptan from C1-compounds.

Since the beginning of 2009 he has been employed at Borealis Polymere GmbH, where he started as a process development engineer and is now working in the field of Advanced Process Control.

8. List of publications

Kaufmann, C., Gutiérrez, O. Y., Zhu, Y., Lercher, J. A.; „Effect of H_2 in the synthesis of COS using liquid sulfur" Res. Chem. Intermed., 2010, 36, 211–225. Available online, DOI; 10.1007/s11164-010-0131-8.

Gutiérrez, O. Y, Kaufmann, C., Hrabar, A., Zhu, Y., Lercher, J. A.; „Synthesis of methyl mercaptan from carbonyl sulfide over sulfide K_2MoO_4/SiO_2" J. Catal., 2011, 280, 264-273. Available online, DOI: 10.1016/j.jcat.2011.03.027.

Gutiérrez, O. Y., Kaufmann, C., Lercher, J. A.; „Influence of Potassium on the Synthesis of Methanethiol from Carbonyl Sulfide on Sulfided Mo/Al_2O_3 Catalyst" ChemCatChem 2011, 3, 1480–1490. Available online, DOI: 10.1002/cctc.201100124.

Gutiérrez, O. Y. , Kaufmann, C., Lercher, J. A.; „Synthesis of Methanethiol from Carbonyl Sulfide and Carbon Disulfide on (Co)K-Promoted Sulfide Mo/SiO2 Catalysts" ACS Catal., 2011, 1, 1595-1603. Available online, DOI: 10.1021/cs200455k.

Barth, J., Weckbecker, C, Redlingshöfer, H., Lercher, J., A., Kaufmann, C.; „Method for the production of methyl mercaptan from carbon-containing compounds, sulfur, and hydrogen" EP2456756 (A1).